The Role of Autophagy in the Maintenance of Mitochondrial Function and Adaptations to Contractile Activity

Alexandra Parousis

A Thesis submitted to the Faculty of Graduate Studies in Partial Fulfillment of the Requirements for the Degree of

Master of Science

Graduate Program in Kinesiology and Health Science

York University

Toronto, Ontario, Canada

April 23, 2014

Abstract

Autophagy is a critical survival mechanism facilitating protein turnover and pathogen defense in post-mitotic cells. More recently, mitophagy has been identified for the selective recognition and targeting of mitochondria for degradation. Mitochondrial availability is the net result of organelle catabolism via mitophagy and mitochondrial biogenesis. Although the latter process has been well described, mitophagy in skeletal muscle is less understood, and it is unknown how these two opposing mechanisms converge during contractile activity. We employed an *in vitro* model of chronic contractile activity (CCA) of myotubes in cell culture in the presence of autophagy inhibitor Bafilomycin A1 (BafA) and assessed the implications of defective autophagy on the adaptations to contractile activity. BafA lead to severe deficits to mitochondrial respiration and enhanced reactive oxygen species. CCA ameliorated this defective phenotype, reverting levels back towards untreated controls. Thus, contractile activity normalizes mitophagy flux and maintains a healthier mitochondrial profile during autophagy deregulation.

Acknowledgements

Sedit qui timuit ne non succederet.
He who feared he would not succeed sat still.
-Horace

Completing this Masters has given me a great lesson in resilience and determination. Although it was a difficult road, I cherish the experiences that have allowed me to grow as an individual and a researcher.

I would like to thank my partner Allan, who believed in me even when I did not. Thank you for the late night drives home from the lab, for your patience and support, and putting up with my crazy hours, I would not be here today without you. My sister Georgia, who was always there for encouragement, advice and a shoulder to lean on. Knowing you were only a phone call away, eased even the most trying moments. My parents, Alina and Kosta, who are the hardest working people I know, and have always provided me with endless support and never asked for anything in return. I love you all and hopefully one day I can repay the favor.

To my friends who stood by me even though I did not call or visit as often as I should have. I vow to be a better friend hereafter, and continue to value our friendship.

To my current and past lab members, each of you has a special place in my heart, I thank you all for your individual wisdom and am grateful to have meet all of you. I will take with me everything you have taught me and hope to be as good of mentor as you all have been to me.

To my Supervisor Dr. David Hood, thank you for your infinite wisdom, model organization and dedication to all of your students. You often went above and beyond your call of duty to make the graduate experience a memorable one. I will value your guidance always.

Table of Contents

List of Figures

Review of Literature

Mannuscript

Appendix B: Additional Data

List of Abbreviations

20S/26S	ribosomal subunit 20/26
3-MA	3-methyladenine
A.U.	Arbitrary units
AntA	Antimycin A
Acetyl CoA	Acetyl coenzyme A
ADP	Adenosine diphosphate
AIF	Apoptotic inducing factor
AMP	Adenosine monophosphate
AMPK	Adenosine monophosphate-activated protein kinase
AMPKα1	Adenosine monophosphate-activated protein kinase subunit alpha 1
ANOVA	Analysis of variance
ATG	Autophagy-related gene
ATP	Adenosine triphosphate
ATPase	ATP synthase
BafA	Bafilomycin A1
Bcl-2	B-cell lymphoma 2
Bcl-XL	B-cell lymhoma extra large
BNIP3L/NIX	BCL2/adenovirus E1B 19kDa interacting protein 3-like
CCA	Chronic contractile activity
CCCP	Carbonyl cyanide m-chlorophenyl hydrazone
Con	Control
COX	Cytochrome c oxidase
COXIV	Cytochrome c oxidase/ Complex IV
c-terminal	Carboxyl terminal
DCF	2',7'-dichlorodihydrofluorescein diacetate
DNA	Deoxyribonucleic acid
Drp1	Dynamin-related protein 1
E1/E2/E3	Enzyme 1/2/3
EPS	Electronic pulse stimulation
ERRα	Estrogen-related receptor alpha
ESR	Electron spin resonance
ETC	Electron transport chain
Fis1	Mitochondrial fission protein 1
GAPDH	Glyceraldehyde 3-phosphate dehydrogenase
Glut1	Glucose transporter 1
Glut4	Glucose transporter 4
GSH	Glutathione
GTPase	Guanosine triphosphatase

HSP70	Heat shock protein 70
IMM	Inner mitochondrial membrane
kDa	Kilodalton
LC3-I	Microtubule-associated protein 1 light chain 3, 18 kDA
LC3-II	Microtubule-associated protein 1 light chain 3, 14 kDA
LONP1	Lon peptidase 1
MELAS	Mitochondrial myopathy, encephalopathy, lactic-acidosis and stroke-like episodes
MERRF	Myoclonic epilepsy with ragged-red fibers
MFN1/2	Mammalian mitochondrial fusion protein 1/2
MIRO	Mitochondrial rho GTPase
MnSOD	Manganese superoxide dismutase
MPP	Mitochondrial processing peptidase
mPTP	Mitochondrial permiability transition pore
mRNA	Messenger RNA
mtDNA	Mitochondrial DNA
mTORC1	Mammalian target of rapamycin complex I
MUL1	Mitochondrial ubiquitin ligase activator of NF-κB
MURF-1	Muscle RING-finger protein 1
NAD^+	Nicotinamide adenine dinucleotide
$NADH+H^+$	NIcotinamide adenine dinucleotide hydrogen
NF-κB	Nuclear factor-kappa beta
NIX/BNIP3L	BCL2/adenovirus E1B 19kDa interacting protein 3-like
NRF1/2	Nuclear respiratory factor 1/2
N-terminal	Amino terminal
NUGEMPS	Nuclear-encoded mitochondrial genes of interest
OM	Outer membrane
OMM	Outer mitochondrial membrane
OXPHOS	Oxidative phosphorylation
p53	tumor supressor 53
p62	sequestosome 1 / protein 62
Park2	Parkin
PARL	Protease presenilin-associated rhomboid-like protein
PD	Parkinson's disease
PE	Phosphotidylethanolamine
PGC-1a	Peroxisome proliferator-activated receptor gamma coactivator 1-alpha
PI3K	Phosphotidylinositol-3-kinase
PINK1	PTEN-induced putative kinase 1 (Park6)
POLG	Polymerase γ

PP2A	Phosphatase 2A
PPARγ	Peroxisome proliferator gamma
RNA	Ribonucleic acid
ROS	Reactive oxygen species
SIRT1	Sirtuin-1
SIRT3	Sirtuin-3
SS31	Szeto-Schiller 31
TFAM	Mitochondrial transcription factor A
TIM	Translocase of the inner membrane
TNF-α	Tumor necrosis factor alpha
TOM	Translocase of the outer membrane
TRAP1	TNF receptor-associated protein
tRNA	Transfer ribonucleic acid
Trx	Thioredoxin
Ubiquitin	Ub
ULK1	unc-51 like autophagy activating kinase 1
UQ	Ubiquinone
V-ATPase	Vacuolar ATP synthase
VDAC	Voltage-dependent anion channel
Veh	Vehicle
VSP34	Class III phosphoinositide 3-kinase
ΔΨm	Membrane potential
ρ°	Rho negative

Review of Literature

1.0 Mitochondria

The evolutionary success of eukaryotes is attributed to the advent of aerobic respiration. The atmospheric availability of oxygen permitted the selection and adaptive success of organisms that utilized a strong oxidizing agent in the generation of chemical energy. Nearly all eukaryotes rely on mitochondria for the majority of their energy production, and thus survival. Mitochondria are dynamic, ovoid or reticular intracellular structures, comprised of outer and inner phospholipid bi-layers. Easily identified in electron micrographs, their characteristic inner membrane convolutions termed cristae run in a parallel formation, and function to significantly enhance the surface area of their constituent membranes. Early qualitative observations suggested that the complexity and abundance of cristae was correlated to the aerobic capacity of the tissue. Highly oxidative tissues such as heart, kidney and brain, are populated by mitochondria with a greater cristae density (37). The inner membrane houses enzyme complexes, collectively termed the electron transport chain (ETC), that allow for the generation of ATP, the core energy currency of the cell. Residing between the cristae is the inner-membrane space coined the matrix. Mitochondrial morphology is dictated by both physiological and pathological conditions, and their reticular formation was found to defend the organelle from degradation (144). In addition, it allows for a more efficient diffusion of metabolites and substrates, and is intricately coupled to the bioenergetics of the organelle (8). A distinctive feature of the mitochondrion is an inherent genome, resembling the

circular DNA of prokaryotes. The organelle is an assembly of proteins encoded by both nuclear DNA and mitochondrial DNA (mtDNA). The mitochondrial genome contains a total of 37 genes, encoding proteins of 2 ribosomal subunits, 22 transfer RNAs and 13 mitochondrial proteins. These complex organelles are made up of in excess of a thousand total proteins, the majority of which are nuclear-encoded, and rely on import for their concerted integration. Mitochondrial transcription factor A (TFAM) regulates the transcription of mtDNA, while peroxisome proliferator-activated receptor gamma co-activator (PGC-1α) allows for the coordinated expression of both genomes.

1.1 Mitochondrial Biogenesis

Mitochondrial biogenesis is the neosynthesis of organelles, involving the activation of a collective transcriptional program in response to their systemic environment. Expansion of mitochondrial mass is paralleled by enhanced enzymatic activity and often a more networked reticulum. This process is finely synchronized to physiological stimuli, and in the case of skeletal muscle, the foremost effector is the presence or absence of contractile activity (59, 141). Endurance exercise has long been known to induce favorable molecular adaptations, including an increased inclination for aerobic metabolism (57). Takahashi and Hood (161) demonstrated that chronic low frequency stimulation of the tibialis anterior in rodents gave rise to significant increments in mitochondrially-derived enzymes. Citrate synthase and succinate dehydrogenase increased in tandem, along with a substantial increase in the unique mitochondrial membrane phospholipid cardiolipin. These adaptations to chronic contractile activity

(CCA), demonstrate that the expansion of the mitochondrial membrane coincides with an enhanced enzymatic inclination, and an overall improvement to the bioenergetic profile of muscle. The synchronous increases to such biochemical markers formally define mitochondrial biogenesis.

1.1.1 Regulators of biogenesis : PGC-1α

During bouts of submaximal exercise, the hydrolysis of ATP at the myosin ATPase site of muscle is paralleled by the accumulation of ADP (118). Phosphotransferases such as adenylate kinase interconvert ADPs to ATP and AMP, when a high [ADP] favors the forward-reaction. The ensuing accretion of AMP results in the activation of AMPK, an energy sensing kinase responsive to states of energy depletion. AMPK acts upstream of the activation of peroxisome proliferator-activated receptor gamma co-activator 1-alpha (PGC-1α), a known regulator of mitochondrial biogenesis. Another biogenesis signaling mechanism involves the co-enzymes nicotinamide adenine dinucleotides, NAD^+ and $NADH+H^+$, which provide the electrons fuelling the redox reactions of the ETC. Exercise perturbs the NAD/NADH ratio, and incites the signaling pathways preceding the mitochondrial adaptations to exercise. The deacetylase SIRT1 consumes NAD^+, and is also receptive to the exercise-induced fluctuations of the substrate. SIRT1 has been proposed as an important modulator of exercise-mediated mitochondrial adaptations. A decrease in $NADH+H^+$, and subsequent increase in NAD^+, especially during prolonged low-moderate intensity exercise, results in the activation of SIRT1 and family member SIRT3. Both have been proposed to invoke mitochondrial

biogenesis, with SIRT1 de-acetylating the transcriptional co-activator PGC-1α (88). PGC-1α, identified as a nuclear receptor co-activator, was found to induce the gene expression of ETC subunits, mtDNA transcription factors (183) and total mtDNA (140). PGC-1α does not bind DNA directly but docks onto transcription factors, exerting expressional control over a large subset of metabolic genes (101). The PGC-1α isoform is enriched in skeletal muscle, and to the highest degree in oxidative type I fibres (102). Further, transgenic expression driven by a muscle-specific creatine kinase promoter in mice, resulted in a phenotypic shift to a more oxidative profile of glycolytic fiber types. In muscle, the protein induces a broad expression of nuclear-encoded mitochondrial genes of interest, including (NUGEMPs) PPARγ, NRF1 and NRF2, ERRα and TFAM (63). Transgenic expression in C2C12 myotubes was found to increase maximal rates of respiration by 1.9-fold, revealing a positive regulatory effect on ETC proteins by enhancing mitochondrial biogenesis (140). In humans, acute contractile activity induced robust 25-fold increases in PGC-1α mRNA in biopsied vastus lateralis muscle. Transcript levels peaked at 2 hours following activity, and corresponded to an increase in total mRNA at a later time point (138). Exogenous expression of the protein in cardiac muscle brought on "uncontrolled proliferation" of mitochondria (93), demonstrating the potent regulatory control on organelle synthesis. Knockdown of PGC-1α was found to blunt the adaptive responses to chronic contractile activity (CCA) in skeletal muscle cells (171), and helped establish PGC-1α as a central player to the exercise-induced mitochondrial adaptations. The local supply of ATP at the myosin ATPase site of muscle, must be continually replenished during extended bouts of submaximal intensity

exercise. By modulating oxidative capacity through regulators such as PGC-1α, muscle displays an amazing propensity to adapt to physiological demands.

1.1.2 C2C12 myotubes as a model of CCA

C2C12 cells are a murine derived cell line that has been extensively used in the tissue culture studies of skeletal muscle. Easily differentiated into excitable muscle cells, they are a valuable tool in the study of muscle activity. The contractile activity accountable for musculoskeletal adaptations is mimicked in the *in vitro* model through the application of a controlled voltage. It has been demonstrated that the molecular alterations seen in the trained mouse model are highly reproduced in the cell culture model of C2C12 stimulation (3, 125). Contractile activity-induced changes to the transcriptional profile of *in vitro* myotubes matched those of a trained mouse model (125). The authors compared low frequency 24 hour electronic pulse stimulation (EPS) of cultured myotubes to a 6 week treadmill training regimen in mice. The PGC-1α transcript was found to increase by 2.9-fold in the cell culture model versus an analogous 2-fold increase in trained mice (18). In addition to PGC-1α upregulation, Burch et. al found a similar upregulation in the expression of TFAM (transcription factor of mitochondria) as well as genes of oxidative phosphorylation (OXPHOS), including ubiquinol oxidase and Complex I (NADH-ubiquinion subunit 5). We have previously demonstrated that the *in vitro* model of chronic contractile activity to induce mitochondrial biogenesis as evidenced by enhanced enzymatic cytochrome oxidase (COX) activity and OXPHOS protein expression (24, 119, 171). This *in vitro* model is

thus a valuable tool, permitting the controlled study of molecular adaptations to "exercise".

1.2 Oxidative phosphorylation

Cellular survival depends on a steady supply of adenosine triphosphate (ATP), generated by a sequence of energy coupling reactions in the ETC, located at the inner mitochondrial membrane (IMM). In eukaryotes, the mitochondrial respiratory chain exists as a series of electron-shuttling cytochromes, accepting high energy electrons from the pyridine nucleotide NADH, and succinate, in a process termed oxidative phosphorylation (OXPHOS). The glycolysis product pyruvate, and the β-oxidation of fatty acids, yields Acetyl CoA, proceeding to Krebs cycle for the indispensable production of co-enzymes NADH and $FADH_2$. The co-enzymes represent the electron donor pool for ATP production at the ETC, ultimately reducing molecular oxygen (158). Five multi-protein complexes span the IMM, complexes I through V. The first enzyme in the chain, Complex I (NADH: ubiquinone oxidoreductase), transfers electrons donated from NADH to reduce the electron carrier ubiquinone (UQ), embedded in the membrane between Complex I and II (7). Protons are successively transferred from the matrix and accumulate in the inter-membrane space, generating a chemiosmotic gradient. UQ provides a point of entry for succinate derived electrons, which are transferred to Complex II (succinate dehydrogenase). Complex III (cytochrome bc1 complex), which can both oxidize reduced UQ and accept electrons from Complex I, eventually shuttling electrons to Complex IV (Ubiquinol oxidase). Like Complex I, Complexes III and IV

transport matrix protons into the inter-membrane space against their electro-chemical gradient, establishing the mitochondrial membrane potential ($\Delta\Psi m$) between the outer and inner membranes. The maintenance of $\Delta\Psi m$ is critical to the bioenergetics of the organelle and facilitates to the proton-motive force exploited by the F_OF_1 ATP synthase (Complex V) (180). This trans-membrane enzyme contains an ion channel permitting the flow of protons back into the matrix, coupled with an ATP synthase. Harvesting the free energy released as H^+ flow back into the matrix, down their electro-chemical gradient, Complex V enables the phosphorylation of ADP into ATP. The complex IV-mediated reduction of oxygen, acting as the terminal electron acceptor, combines with H atoms and condenses to water, and hence, the oxygen consuming pathway is termed oxidative phosphorylation (56) (OXPHOS).

1.2.1 States of respiration

Cellular respiration is defined as the oxygen consumption of intact cells (27), although largely attributed to both the quantity and functional capacity of mitochondria (15), other cellular compartments may also consume oxygen (12) and confound results. Unlike mitochondrial respiration, cellular respiration cannot be normalized to mitochondrial content making it impossible to delineate conclusions on organelle quality (15). It is therefore necessary, when attempting to gain insight on the discrete respiratory quality of the mitochondrial population, to perform measures on fractions of isolated mitochondria while correcting for protein content. In 1955, Chance and Williams revealed an effective assay allowing for the quantification of oxidative respiration of

isolated mitochondria. The consumption of oxygen in the process of OXPHOS, and the reliance on ADP, were used to deduce the rates of respiration using a known concentration of the dinucleotide (27). Using a platinum electrode inserted into a cuvette, the authors were able to monitor oxygen consumption of isolated organelles in response to the addition of energy substrates. A slope correlating to the kinetics of oxygen consumption was determined, and when dissolved substrates or oxygen were exhausted, the slope was equivalent to zero. When mitochondria are removed from their local cellular environment in the process of isolation, they are likewise removed from the milieu of substrates allowing for functional respiration. Exogenous administration of substrates into the suspension medium is therefore necessary to evaluate respiratory control. Healthy, intact mitochondria exhibit a tight coupling of ETC reduction reactions, to the complex IV-mediated reduction of oxygen, so the utilization of O_2 is consequently an effective indicator of respiratory control. Different states of respiration have been defined for the *in vitro* analysis of mitochondria: State IV respiration is oxygen consumption on a particular substrate in the absence of ADP, while State III is defined as the oxygen consumption in the presence of ADP.

1.3 Reactive Oxygen species

Reactive Oxygen Species are a normal byproduct of OXPHOS. They are generated when high energy electrons fail to complete the ETC and inadvertently result in the partial reduction of oxygen. Mitochondrial superoxide ($O_2^{\bullet -}$) is produced as a result of the addition of a single electron to molecular oxygen, and is an important source

of intracellular ROS. Complexes I and III (16) are seen as the canonical sites of ROS generation, though recently Complex II has also been implicated (142), depositing the oxidizing agents into both the matrix and intermembrane space. Since the matrix contains inherent antioxidant defense systems, matrix-bound ROS are readily quenched under model conditions. Manganese superoxide dismutase (MnSOD) catalyzes the reduction of $O_2^{\bullet -}$ into H_2O_2, to be further reduced by glutathione (GSH) and thioredoxin (Trx) into water (5). ROS deposited into the intermembrane space may evade this defense and escape through porins into the cytoplasm. When H_2O_2 levels are high, and in the presence of reduced iron (Fe^{2++}) or copper (Cu^{+}), the molecule engages in Fenton's reaction, producing hydroxyl radicals (•OH), the most volatile class of ROS (167). Oxidative stress results when ROS production exceeds the inherent buffering capacity of the organelle. Estimates place ROS generation at 0.2-2% of total oxygen consumption during OXPHOS (114). While the majority of the literature identifies the organelle as the primary effector (30, 98, 115, 190), it has been contested for lack of evidence (17). The heterogeneity of intracellular ROS production undoubtedly confounds the determination of the organelles relative contribution to cellular oxidants. Boveris et al. quantified H_2O_2 production on isolated fractions of cellular organelles and found that peroxisomes generated a maximal 16.4 nmol/min per mg of protein, compared to 0.5 nmol in the mitochondrial fraction during state IV respiration (12). Perhaps the most conclusive evidence combined flow cytometry, electron spin resonance (ESR), and fluorescent probes with models of cellular stress to evaluate ROS production (86). Unpaired electrons can be effectively detected through ESR using both permeable and

impermeable probes. Intact cells incubated with antimycin A (AntA), a potent complex III inhibitor, were found to undergo a 2-fold increase to intracellular ROS. Further, impermeable ESR probes could not detect $O_2^{\bullet -}$ emission from control isolated mitochondria, but AntA treatment resulted in the significant increase of both intra-mitochondrial and emitted ROS. This evidence corresponded to the whole cell analysis under ROS-inducing conditions, using the fluorescent probe, 2'7'dichlorofluorescein (DCF) which detects H_2O_2 preferentially, thus disclosing that under basal conditions, mitochondria are not significant sources of intracellular ROS. Conversely, under circumstances of OXPHOS disruption and cellular stress, they become prominent cellular ROS effectors (86).

1.3.1 Inherent antioxidant system: MnSOD

Aerobic metabolism has the potential to introduce highly reactive oxidants to the cellular environment. Excess unbuffered ROS can lead to nuclear and mtDNA damage, the oxidation of proteins, membrane disruption, and can mediate cell death pathways through tumor necrosis factor alpha (TNF-α) (129). Mitochondria possess high efficiency inherent oxidant buffering systems. MnSOD is a nuclear-encoded enzyme localized to the matrix, and is the principle quencher of mitochondrial ROS. Mammalian MnSOD exists in tetrameric formation containing a manganese (Mn) core and an N-terminal mitochondria-targeting sequence. The transition between Mn^{3+} and Mn^{2+} at the active site allows for the protonation of $O_2^{\bullet -}$ into hydrogen peroxide (1). The activity of MnSOD is positively influenced by de-acetylation via SIRT3 in response to cellular stress (163). MnSOD knockout mice die before 3 weeks of age, and knockdowns reveal

autophagosome accretion (LC3-II), with enhanced mitochondrial content (citrate synthase activity) (134). Further, lack of gene function has been purported to deregulate autophagy (123), potentially signifying a phenotypic autophagy defect. A sustained reduction in MnSOD was linked to elevated deoxyguanosine, a biomarker of DNA oxidation, in both nuclear and mitochondrial DNA, and an upregulation in tumor frequency (146). MnSOD levels may rise as a cytoprotective response to cellular aerobic stress (21), and as an adaptive mechanism during endurance training (147).

1.3.2 Role in pathology

As a potential therapeutic target, ROS toxicity has become a study of interest, found to participate in the pathogenesis of chronic conditions such as diabetes (62, 127), cardiovascular (66), neurodegenerative diseases (39), and even cancer (20, 97, 149, 150). Excess ROS production is a characteristic of ETC insufficiency (69), and conditions of oxygen tension such as hypoxia (108). mtDNA mutations linked to ROS are a common feature of tumor cells, and ROS have been found to contribute to metastatic potential (69). Ischemic and failing hearts display augmented ROS production (91, 145). The etiology of neurodegenerative diseases provides conclusive evidence that ROS are a partial contributor to neuronal attrition (44, 74).

1.4 Fusion and fission

The distribution and availability of mitochondria in post-mitotic cells is contingent on fission and fusion events, critical for the propagation of mtDNA, organelle biogenesis and segregation for selective autophagy. Fusion is a process culminating in

the amalgamation of inner and outer mitochondrial membranes, while fission defines the reverse phenomenon. Chronic contractile activity like endurance training, is known to lead to adaptive responses in the mitochondrial network, namely the expansion and elongation of the mitochondrial reticulum in skeletal muscle (67, 84). Mammalian mitochondrial fusion is mediated by the proteins Mfn1/2 and OPA1, while fission is primarily governed by two key polypeptides, dynamin related protein 1 (Drp1) (47), and mitochondrial fission protein 1 (Fis1) (177). Localized to the OMM (47), these proteins dynamically regulate mitochondrial morphology by facilitating dissociation from the reticulum. The opposing mechanism of fusion involves the transmembrane GTPase Mfn1, when constitutively overexpressed results in hyper-clustered, perinuclear mitochondria (148). Opa1 promotes the association of inner membranes during fusion (36), by operating in conjunction with Mfn1. Alterations in the ratios of these fusion and fission proteins reveal which system is prevailing. Chronic muscle use was found to lead to an increased ratio of fusion: fission proteins, while chronic disuse increased the prevalence of fragmented mitochondria and shifted the ratio toward fission (67). Electron micrographs of denervated muscle revealed smaller, more fragmented organelles within 24 hours (120), communicating the malleable nature of the mitochondrial landscape. This remodeling process is highly responsive to the cellular milieu and bioenergetic demand, allowing for maximal cellular efficiency.

1.5 Mitochondrial protein import

Import is vital to the functional integrity of the organelle, and the mitochondrial membranes contain discrete modes of entry for substrates and integral proteins. Porins, located on the outer mitochondrial membrane (OMM), facilitate the transport of molecules of less than 5 kDa in size, while transport complexes allow for the active transport of larger proteins. The outer and inner membranes contain distinct translocase systems, the TOM and TIM complexes respectively, working in a coordinated fashion to facilitate the import of newly-translated proteins. The TOM complex is a collection of 9 known subunits spanning the outer membrane, individually identified by a unique name corresponding to their specific molecular weights (TOM20,TOM40 etc.). These subunits comprise cytosolic receptor domains, and include peptides and proteins that construct the import channel (137). Nuclear-encoded proteins destined for mitochondria are translated in the cytoplasm as precursors, and undergo unfolding to achieve their import-ready state (99). These pre-proteins contain positively charged amino-targeting sequences recognized by the cytosolic chaperone, heat shock protein 70 (HSP70), and the receptor complexes TOM20 and TOM22. HSP70 mediates the unfolding of pre-proteins in preparation for translocation, and is established to be critical for the active transport process (100). Although TOM20/TOM22-mediated import is contingent on an N-terminal pre-sequence, other proteins containing inherent target sequences can be imported through other members of the TOM machinery (TOM37,TOM70). Facilitating delivery across the inner membrane, the TIM complexes TIM23 and TIM17 dimerize upon the presence of a sufficient membrane potential. The impending translocation of

proteins into the mitochondrion is contingent on ΔΨm (42). Additional TIM components interact with a matrix HSP70 (mtHSP70) allowing for the final transition of the pre-protein into the mitochondrial matrix driven by ATP hydrolysis. Before the newly imported pre-protein can be folded into its mature protein conformation, the targeting sequence is cleaved by the mitochondrial processing peptidase (MPP). Mitochondrial proteases, including LONP1, degrade polypeptides that fail to achieve their tertiary conformation (131).

1.6 Apoptotic signaling: mPTP opening

The maintenance of mitochondrial membrane potential (ΔΨm) is critical to the bioenergetics of the organelle and overall cellular viability. Dissipation of ΔΨm can result in the initiation of a cell death program known as apoptosis. Mitochondria play an integral role in the regulation of cellular survival by manipulating the translocation of inter-membrane mitochondrial proteins into the cytosol. Kroemer and colleagues identified a key apoptotic protein released upon the disruption of ΔΨm, termed the apoptotic inducing factor (AIF). AIF travels to the nucleus where it induces structural modifications to chromatin and DNA fragmentation, biomarkers of apoptosis (160). The mitochondrial permeability transition pore (mPTP) is a crucial mediator of cellular survival. By modifying membrane permeability, the pore is able to facilitate the escape of pro-apoptotic factors, cytochrome c, AIF and a number of caspases (109). Bcl-2 and Bcl-XL are key pro-survival polypeptides, with Bcl-XL preferentially expressed in long-lived cells (11), while pro-apoptotic proteins Bax and Bak (107) moderate mPTP

opening. Although a consensus has not been reached on the precise mechanisms of apoptotic regulation, the two most accepted arguments involve the heterodimerization of Bax with Bcl-2/Bcl-XL thus inhibiting the formation of pro-apoptotic Bax homodimers, conversely, Bcl-2/Bcl-XL may suppress cell death in the absence of heterodimerization with Bax/Bak (113). ROS has been found to play a role in apoptotic signal transduction when levels exceed the buffering capacity of the organelle (45). Mitochondrial calcium overload is a known inducer of mPTP. It fosters apoptosis when matrix Ca^{++} is elevated (54) through poorly defined mechanisms. In some cell types Ca^{++} chelation attenuated ROS-induced apoptosis (48), suggesting that the two conditions converge to impede cellular survival.

1.7 Mitochondrial DNA mutations

Mitochondria divide and transmit their genetic information through the process of binary fission, with each organelle inheriting multiple copies of a circular genome. Though the mitochondrion is equipped with a proof-reading enzyme, the mutation rate is estimated to be at least 10-15 times that of nuclear DNA (38, 53). Polymerase γ (POLG) is the sole DNA polymerase found in mitochondria, and participates in both the synthesis and base-excision repair process of mtDNA (111). Unlike nuclear DNA, mtDNA is not endowed with the same repair capacity and lacks protective histones (23), leaving it more vulnerable to damage. mtDNA mutations occur in heteroplasmy (133), as a result of heterogeneous clonal expansion. The most prevalent ETC deficiency occurs at Complex I, a feature of Leigh syndrome, and presents with severe anomalies in the CNS causing fatality in most cases before the age of 5 (50, 65). Exercise intolerance is a hallmark of

mitochondrial myopathies, caused by mutations resulting in ETC insufficiency (164). Mitochondrial myopathy, encephalopathy, lactic-acidosis and stroke-like episodes, (MELAS syndrome in short), was characterized in 1985 by Pavlakis et. al, who clustered the symptoms as a distinct clinical syndrome (136). This severe malady includes mental retardation and profoundly decreased life expectancy. An interesting feature of the syndrome is the presence of "ragged red fibres" in skeletal muscle as a result of ETC defects. Gene sequencing later revealed that an A to G mutation of the tRNA at position 3243 (A3243G) of mtDNA is a common feature of MELAS, and maternally inherented diabetes and deafness (MIDD) syndrome (133). The molecular features of MELAS include severe enzymatic deficiencies in complexes I and IV with milder impairments to complexes III and V (186), systemically distributed among all tissue types. Some evidence suggests that the A3243G mutation disproportionately affects skeletal muscle (32). Since the reliance on oxidative phosphorylation and thus ATP varies considerably by tissue type, the manifestation of disease varies accordingly. Interestingly, the majority of mtDNA point mutations encompassing defects of oxidative phosphorylation involve mitochondrial tRNAs (124). Such disorders include the aforementioned Leigh syndrome, MERRF, skeletal and cardiomyopathy. Patients are typically exercise intolerant and present with progressive myopathy (89), and episodic symptoms (124). Although undiagnosed at the time, it has been proposed that Charles Darwin was afflicted with a mitochondrial syndrome caused by a mutation in A3243G, which would explain his variable and peculiar symptoms including nausea, muscle-spasms and lethargy.

Family lineage studies confirmed maternally-linked symptoms, characteristic of mtDNA mutations (55).

2.0 Degradation / Quality Control Pathways

2.1 Ubiquitin and p62

Autophagy is a catabolic process that involves a series of events commencing with the irreparable step of identification, and subsequent degradation of proteins (9). Ubiquitin (Ub), an 8.5 kDa protein (152), identified to be a critical component of the proteolytic pathway, is highly conserved and expressed in most cell types (179). Ubiquitination is a tightly regulated, ATP-dependent process, involving activation and conjugation of the peptide to the amino-terminus of lysine residues of target substrates (179), often forming poly-Ub chains at several sites. In 1996, Vadlamudi et. al identified p62/SQSTM1 as a novel Ub-binding protein associating with multiple Ub-chains (174). E3-ligases are the terminal enzymes in the Ub pathway, requiring the activity of E1-activating, and E2-conjugation enzymes. The conjugation culminates in the covalent addition of Ub to substrate proteins, effectively tagging them for proteasomal degradation. p62 functions to sequester and consolidate target substrates into bodies for degradation by autophagy. Inadequate clearance resulting in the accrual of protein aggregates are the hallmark of many degenerative diseases including Alzheimer's, Parkinson's and some forms of steatohepatitis (188), and coincide with the build-up of p62, in addition to other stress-responsive proteins. The myofibrillar myopathies myotilinopathies and desminopathies, resulting from the mutations of genes encoding

contractile proteins, are also characterized by abnormal protein aggregates in muscle co-localizing with p62 (73). Free radical-induced oxidation of aggregates further reduces the availability of these aggregates to proteolytic digestion (73), and may explain the degenerative propensity of the disease.

2.2 Proteasome system

An important component of the protein degradation machinery in eukaryotic cells is the proteasome. The catalytic complex was found to be integral to the Ub-conjugated proteolysis pathway (117), and present in all mammalian cells. Two populations of proteasomes exist, a larger ATP-dependent 26s proteasome and its smaller 20s ATP-independent counterpart (61). It is the 26s proteasome that preferentially targets Ub-tagged substrates. The Ub-proteasome and autophagy are two often intersecting cellular mechanisms of protein catabolism.

2.3 Autophagy proteins and pathway

Autophagy is a process involving the bulk sequestration and degradation of cytoplasmic material in response to cellular stress, metabolic status and pathogen infiltration. Considered a cytoprotective mechanism, inhibition of the process has been found to trigger apoptosis (14). Early evidence of autophagy included the glucagon or hypoxia-stimulated encapsulation of cytoplasmic material by a double-membraned vesicle, now known as the autophagosome (43). Ultrastructural studies revealed that the autophagosome contained whole organelles and fused to pre-existing lysosomes (43), which deliver the digestive enzymes. Microtubule-associated protein 1 light chain 3

(LC3), the mammalian orthologue to the Atg8 protein first documented in yeast (83), was established to play an essential role in autophagosome formation. It was revealed that LC3 was distributed in the cytosol under steady-state conditions, and largely responsive to starvation, at which time it rapidly associated with the autophagic membrane. This upregulation of autophagy in response to conditions of nutrient-starvation, was shown to improve cellular viability (170) by repurposing nutrients for essential cellular processes. The identification of LC3 in mammalian cells, and the protein's interaction with the autophagosome membrane (77), provided novel insights into a largely uncharacterized mechanism. Kabeya et al. (78) conveyed evidence for two distinct forms of the protein, LC3-1 and LC3-II, resulting from sequential post translational modifications. Initially, the LC3 precursor undergoes a cleavage of 22 amino acids from its c-terminus producing LC3-I, and in this form maintains a cytosolic distribution. LC3-I is converted to LC3-II through conjugation with phosphotidylethanolamine (PE) (78), an indispensable lipidation event which facilitates hydrophobic membrane incorporation. LC3-I and LC3-II migrate as discrete bands in immunoblot SDS gels, representing the cytosolic and membranous forms respectively. Increments to autophagy coincide with enhanced p62 clearance, whereas the opposite is true for p62 accretion. Serum starvation gave rise to elevated protein expression of LC3-II, and was determined to correspond to enhanced autophagy. Autophagy proceeds sequentially through phases of induction, nucleation, elongation and termination. Upon receipt of the necessary autophagy stimuli, initiation events ensue and include the complexing of ULK1, Beclin1 and VPS34 (class III phosphoinositide 3-kinase), assisting in early autophagosome formation in the nucleation

phase (95). The proceeding elongation stage encompasses a series of ubiquitin-like conjugations, Atg5 conjugates to Atg12, partaking in E3-enzymatic activity, and binding Atg16L1 to form a trimeric complex. Atg16L1 is able to localize the complex with the autophagosome membrane, while Atg5-Atg12 interacts with the E2-enzyme Atg3 (132), which further conjugates the E1-ligase, Atg7. The terminal step of autophagy involves the Atg3-Atg7 dependent conjugation of Atg8 (LC3) with PE, allowing the membrane stabilization of LC3-II and enclosure of the autophagosome membrane. The mature autophagosome is free to bind the lysosome to facilitate the final proteolytic process.

2.3.1 Autophagy signaling

The mammalian target of rapamycin complex I (mTORC1) is the main mediator of autophagy in mammals, and when active, exerts an inhibitory effect on the catabolic process. Adenosine monophosphate-activated protein kinase (AMPK) embodies an opposing signaling cascade. AMPK is a key activator of autophagy (82), and this metabolic-sensing kinase, is itself phosphorylated on threonine^{172}, mediated by an increased ratio of AMP:ATP, subsequent to energy depletion. The nutrient-stress signaling of AMPK, results in the targeted phosphorylation of raptor at serine$^{722/792}$, which exerts an inhibitory effect on mTORC1. This complex is a critical check-point in the initiation and sustainment of anabolic processes such as protein translation, the expression of translation machinery, and cell-cycle progression (22), thereby ensuring that the current metabolic status meets the requirements for growth. Proliferative events are impeded by mTORC1 inhibition, allowing mammals to systemically modulate growth

and non-essential cellular processes in response to poor energy-status. In this way, multi-level cellular regulation is fine-tuned to changing physiological and environmental conditions, and favors survival. Another cytoprotective response to transient and sustained energy-deprivation is the catabolic process of autophagy. The dependence of macroautophagy on nutrient availability was illustrated by the studies of Hutson and Mortimore, who recognized that the loss of amino acids was a potent catabolic stimulus upregulating the autophagic localization of cytosolic aggregates (64). Rapamycin, an mTORC1 inhibitor, inactivates the complex and mimics the effect of nutrient depletion by enhancing autophagy (182). During nutrient sufficiency, mTORC1 is active and exerts inhibitory control on downstream regulators to block autophagy. Despite the fact that nutrient depletion was identified as a potent stimulator of autophagy nearly half a century ago, the precise mechanisms modulating the canonical nutrient sensing pathways remain obscure. One model proposes that the activated mTORC1 phosphorylates TAP42, causing association of the protein with PP2A (phosphatase 2A) (185). Bound to TAP42, the activity of PP2A is sequestered, impeding the de-phosphorylation of its target, Atg13 (187). The resulting hyper-phosphorylated state of Atg13 prevents its localization to ULK1 and the initiation of autophagic events (116). Upon nutrient duress, PP2A action is re-instated, the hypo-phosphorylated Atg13 can interact with ULK1, and autophagy inhibition is lifted. Thus, the phosphorylation status of Atg13 is mediated by the metabolic signaling through mTORC1, and regulates the catabolic pathway. Alternatively, AMPK can directly activate ULK1 at two phosphorylation sites, while active mTORC1 can exert an inhibitory phosphorylation on ULK1 (82). The mammalian

homologue to the *S. cerevisiae* protein Atg1, ULK1, is at a pivotal interrogation point to the suppression or commencement of autophagy and characterizes the induction phase. Nuclear factor-kappa B (NF-κB), a pro-survival transcription factor with an expansive range of gene targets including those of apoptosis, proliferation and differentiation (169), was found to be a negative regulator of autophagy by repressing TNF-α (40). In contrast, constitutive expression of TNF-α, a pro-apoptotic cytokine, resulted in a drastic increment in autophagy in human myocytes (81). Muscle wasting in models of disuse was found to enhance muscle ubiquitination, through increased expression of the muscle RING-finger protein-1 (MURF-1). This effect was blocked by targeted antioxidant administration (162), implicating ROS in disuse-mediated autophagy. Contractile activity, like exercise, can mimic the metabolic signaling of nutrient disparity, and has been found to activate autophagy in skeletal muscle (51, 71, 105).

2.3.2 ROS-mediated autophagy

Emerging evidence suggests ROS as key mediators of skeletal muscle autophagy. C2C12 cells were subjected to well-established inducers of autophagy, nutrient deprivation and rapamycin, and acute treatment resulted in elevations in ROS and LC3 lipidation. Incubation with both mitochondrial-specific antioxidants and NAC pointedly reduced LC3-II, and reduced the expression of autophagy proteins. This evidence successfully validated ROS as a critical upstream autophagy effector (143). Similarly, exogenous H_2O_2 administration resulted in a heightened autophagic response (40, 92), and enhanced p62 degradation (92), whereas antioxidant treatment diminished basal

autophagy (172). ROS are dominant inducers of AMPK activation (34, 68, 143, 168, 181), and genetic ablation of the kinase compromised autophagy in a ULK1 dependent manner (41). The Atg1 homologue was identified to be an AMPK substrate containing four phosphorylation sites including the conserved sites $Ser^{555,574}$. ULK1 phosphorylation at Ser^{555} was induced by both phenformin-mediated complex I inhibition and constitutively active AMPKα1 expression (a subunit of AMPK) (41), indicating the AMPK-mediated phosphorylation of ULK1 is responsive to mitochondrial respiratory distress. Further, ROS stimulated AMPK activity can exert its canonical influence through mTORC1 inhibition (29), providing an additional mode of autophagy control.

2.4 Autophagy flux

Autophagy is a dynamic process which fulfills the essential role of organelle and protein turnover within the cell. When autophagy is elevated, LC3-II incorporation into the autophagosome is likewise enhanced, and eventually subjected to proteolysis alongside autophagosome cargo, consequently resulting in the rapid decomposition of LC3-II under normal conditions. During pathological states ensuing in autophagy deficits, or when the requirement for autophagy overwhelms cellular capacity, LC3-II levels can accrue. Thus, an increase in LC3-II can paradoxically reflect an upregulation of the process, or a decrement in its clearance, presenting a challenge in generating inferences on this dynamic process (122). Autophagasome substrate delivery to the lysosome, including upstream events, is herein referred to as autophagic flux. The study of mammalian autophagy has been aided by the development of approaches that decipher

the limitations in assessing autophagic flux. Reliable studies often include multiple approaches in flux valuation including fluorescent visualization of the LC3 expression vector (77), and chemical interventions that arrest autophagic flux are required to accurately gauge its progression. Pharmacological inhibition of autophagic flux can be compared across conditions, if an arrest in degradation confers an additive response to LC3-II, this is translated to elevations in flux (122). Downstream inhibitors of autophagy such as lysosomal pH neutralizers BafA and chloroquine, are commonly used to determine flux (25). The Ub-scaffold protein p62 co-localizes with protein aggregates, and must be assessed in corroboration with LC3 to accurately gauge autophagic flux. The protein which allows for the sequestration of LC3, is degraded alongside autophagic substrates, and reduced levels are reflective of enhanced clearance and vice versa.

2.4.1 Autophagy inhibition

Pharmacological and genetic approaches have both been described that effectively inhibit autophagy through a variety of mechanisms. Autophagy inhibitors that target the lysosome include bafilomycin A1 (BafA) and chloroquine. Both agents result in an increased lysosomal pH. BafA inhibits the vacuolar type H^+ ATPase (V-ATPase) shuttle that allows for the translocation of protons into the lysosome, while chloroquine diffuses directly into the lysosome and consumes H^+ through oxidation. Since the fusion of autophagosome and lysosome are pH dependent (80), these agents exert their effects by thwarting a critical phase of autophagy. The compounds 3-methyladenine (3-MA)

and wortmannin inhibit phosphotidylinositol-3-kinase (PI3K), required for autophagosome formation (70), and inhibit early autophagy.

2.4.2 Bafilomycin A1 alternate effects

Bafilomycin A1 is an antibiotic derived from *Streptomyces*. It was determined to be a highly specific inhibitor of V-ATPases, and exerts no effect on the mitochondrial F_OF_1 ATP ase (13). This macrolide averts the acidification of lysosomes, a prerequisite for the fusion and formation of autolysosomes (184). At high concentrations (>150 nM), BafA has been reported to exert K^+ ionophoric effects, contingent on K^+ availability of the incubation media. The resulting potassium influx permits a mild swelling of mitochondria. In addition, decrements to $\Delta\Psi m$ were observed in a dose-dependent manner and only when concentrations exceeded 150 nM, and attenuated mitochondrial respiration (166). Concentrations $\geq$10 nM exerted an inhibition of cell growth and survival (58). At extreme concentrations (10 μM), the agent resulted in significant acidification of the cytosol (10). In adipocytes, BafA (400-800 nM) stimulated Glut4 and Glut1 translocation through the activation of PI3K (33). Some studies suggest the compound exerts a cytoprotective response against chloroquine-mediated apoptosis (154). Most off-target BafA effects are reported at concentrations exceeding 100nM and transpire in a dose-dependent manner. The compound remains a potent, widely used, and specific inhibitor of autophagy at lower concentrations.

2.5 Mitophagy

Mitochondrial degradation and turnover is termed mitophagy, involving the selective identification and targeting of the organelle for lysosomal proteolysis. Mitophagy is an integral process allowing for the clearance of compromised and senescent mitochondria, and critical for conservation of cellular energetics and survival. Selective autophagy is a fairly recent proposal; it was long believed that autophagy was a non-specific macro process involving the bulk degradation of cytoplasmic components. The first evidence for the selective autophagy of mitochondria was the extensive loss of the organelle in the maturation of erythroid cells (153). Schweers et. al, provided novel evidence for the discrimination of targets in autophagic pathways. Pulse-chase experiments involving the sequential incorporation of ^{14}C estimate the half-life of mitochondria at 1.8-3 days in liver cells (104, 121). Mitochondrial clearance and regeneration rate are known to be responsive to biochemical and physiological perturbations. Classical studies reveal that the availability of mitochondria in tissue is highly volatile, rapidly responding to physiological stimuli (4). Dietary restriction was found to reduce the half-life by 60% (121). Likewise, cold acclimation enhances metabolic rate and elicited enhanced organelle turnover. Mitophagy-evoking stimuli include organelle injury, mtDNA damage (156) and depletion (112), hypoxia (106), and perhaps the most potent is the loss of $\Delta\Psi_m$ (178). This quality control mechanism is integral to the fitness of clonal mitochondrial progeny, since the organelles divide and transmit their genome through binary fission. Mild oxidative stress was found to trigger mitophagy, independently of macro-autophagy, implicating mitochondrial dysfunction as

the driving-force for clearance (46). It is suggested that by sequestering defective and senescent organelles, such as those emitting excess ROS, mitophagy can curtail the deleterious oxidation of proteins, lipid membranes, nuclear and mtDNA.

2.5.1 Evidence for selective mitophagy

The Bcl-2-related protein, NIX, was first described for its critical role in the purging of mitochondria from reticulocytes, which in the process of maturation undergo a complete loss of the organelle. The precise mechanism by which NIX arbitrates mitophagy has yet to be defined, however, genetic ablation was found to prevent mitochondrial localization to the autophagosome (153) thereby mediating mitochondrial clearance. Nix strongly co-precipitates with the key autophagosome protein LC3 when cells are treated with the mitochondrial uncoupler CCCP (128), demonstrating that the protein promotes mitophagy in an LC3-dependant manner. NIX contains a C-terminal mitochondrial-targeting sequence (28), and an LC3-binding motif (128), corroborating a role in the cargo-selection of mitochondria to the autophagosome.

2.5.2 Mitophagy proteins: PINK1 and Parkin

Originally identified as a tumor suppressor, PTEN-induced putative kinase 1 (PINK1) levels are down-regulated in ovarian tumors (173). Genome mapping has since identified PINK1 to be mutated in homozygous early onset hereditary Parkinson's disease (PD) (175). PD is characterized by neural degeneration in the post-mitotic cells of the substantia nigra. The pathogenesis of PD is far from clear-cut, though it has been linked to mitochondrial dysfunction through mild Complex I and ubiquinone deficiency

(151), together with elevated markers of oxidative stress (189). The progressive course of the disease suggests the gradual accumulation of metabolic disturbances. PINK1 is a mitochondrial serine/threonine kinase, with a dense expressional profile in brain, muscle and testes (165). Normally, the 66 kDa full length PINK1 ($PINK1_{FL}$) is imported into the mitochondrion where it undergoes rapid proteolytic cleavage by rhomboid protease presenilin-associated rhomboid-like protein (PARL), a matrix protease, yielding a 51 kDa fragment ($PINK1_{\Delta 1}$) (75). However, upon the dissipation of $\Delta\Psi_m$, PINK1 stabilizes on the outer mitochondrial membrane (OMM) (85), where it forms a complex with TOM70 (90). Pulse-chase studies depict the half-life of $PINK1_{FL}$ at 27 min. The cleaved $PINK1_{\Delta 1}$ was detected within 3 min, with a half-life of 30 min, which was markedly reduced following mitochondrial uncoupling. Co-immunoprecipitation of $PINK1_{\Delta 1}$ with the matrix chaperone HSP90 was similarly diminished with OXPHOS uncoupling. A concomitant increase in the stability of $PINK1_{FL}$ was observed (103), signifying a shift in the localization of the protein in response to the functional status of the organelle. The OMM localization of $PINK1_{FL}$ in conditions of mitochondrial duress allows the protein to exert its biochemical phosphorylation activity. The kinase has a number of known mitochondrial targets including TRAP1 (139), Parkin (155), MIRO (6), and Mfn2 (31), with ensuing downstream mitophagy events. In the absence of PINK1, mitophagy inactivation arises, leading to increased apoptotic cell death in the face of mitochondrial stress (94). During elevated oxidative stress, PINK1 suppresses the release of cytochrome c, averting apoptotic stimuli and conferring a cytoprotective role (139), further illustrating that mitophagy is a critical process mediating overall cellular

homeostasis. This effect was found to be directed by the phosphorylation of the TNF-receptor protein (TRAP1/Hsp75) (139). Interestingly, PINK1$^{-/-}$ animals fail to develop appreciable levels of neurodegeneration and CNS disturbances as seen in PD. However, they do display impaired pre-protein (OTC) import, severe mitochondrial respiration deficits and diminished body weight (49). Advancing age exacerbated mitochondrial dysfunction, and PD-like symptoms developed in the absence of neural atrophy (49). Loss of PINK1 gene-function was linked to diminished mtDNA levels, swollen vacuous mitochondria, and coincided with drastic reductions in ATP content (135). PINK1 mutants are more vulnerable to oxidative stress-induced apoptosis than their wild-type counterparts (139), and display defects in Complex I and IV (52). Interestingly, the kinase is believed to function as a mitophagy sensor, arbitrating a multi-tiered mitochondrial quality control mechanism, through import, mitophagy, and fission (35). PINK1 accretion on the OMM is required for the enlistment of Parkin and Beclin-1 (94). Parkin is recruited by PINK1, in part through an association with Fbxo7 (19), and is subsequently phosphorylated on serine^{65} (85). It has been proposed that the voltage-dependent ion channels located on the OMM (VDACs 1-3) constitute a Parkin docking site on compromised organelles (159). Parkin directs the post translational modifications of protein stability through E3-ubiquitin ligase activity. Mitochondrial ubiquitin ligase activator of NFKB 1 (MUL1), was identified in muscle and exerts a similar mitophagy-promoting mechanism (110). Although an interaction between PINK1/Parkin and Nix has yet to be characterized, Nix-dependent mitophagy was preceded by necessary Ub-conjugation events (153). The integrated mitochondrial network or reticulum is protected

from autophagy (144), and orchestrated by the fusion proteins, Mfn1/2. Mitochondrial injury and OXPHOS failure, heightens the proteolysis of the OMM fusion proteins, in a Parkin-dependent manner (52). Dissociation from the mitochondrial reticulum, and sequestration of the organelle are obligatory phenomena preceding the autophagy cascade. To such a degree, OMM remodeling imparts a potent stimulus for mitophagy (26, 94, 191). In addition, PINK1/Parkin may regulate selective ETC protein turnover autonomously of mitophagy. Vincow et. al, demonstrated that both $PINK^{-/-}$ and $Parkin^{-/-}$ animals presented decreased turnover rates of ETC subunits, and to a greater extent than autophagy Atg $7^{-/-}$ mice (176). Thus, these findings suggest the proteins play a supplementary role in the maintenance of ETC components independent of mitophagy. Recently, Youle and colleagues reported a novel stimulus for the induction of mitophagy, that of mitochondrial unfolded protein aggregation. Activation of the PINK1 Parkin pathway worked to enhance mitophagy and reduce the protein load irrespective of $\Delta\Psi_m$ (76). In light of the evidence, mitophagy discloses a critical mechanism in mediating cellular energetics and survival.

2.5.3 Mitophagy signaling

Forfeit of mitochondrial $\Delta\Psi_m$ is a potent initiator of the mitophagy cascade (87, 178). The pharmacological ionophore carbonyl cyanide m-chlorophenylhydrazone (CCCP) disrupts OXPHOS and $\Delta\Psi_m$, and is universally used to induce mitochondrial uncoupling. CCCP was demonstrated to drive mitophagy through an inhibition of mTORC1, in an AMPK-independent manner (87). ROS are another stimulator of the

quality-control pathway. Over-expression of MnSOD blocked the onset of mitophagy (178). In the presence of mitochondrial-specific antioxidants SS31 and mito-tempol, rapamycin and nutrient deprivation of C2C12 myotubes fail to initiate autophagy (143). ETC deficient ρ° cells exhibit low levels of endogenous ROS and in response to starvation, fail to commence mitophagy (96). ROS was found to activate AMPK and inhibit mTORC1 (95, 142), elucidating the mechanisms of autophagy induction. Accordingly, ROS are materializing as significant modulators of mitophagy.

2.5.3.1 Skeletal muscle and contractile activity

Muscle is primarily comprised of long-lived post-mitotic cells. Since the intracellular components such as mitochondria and contractile proteins are relatively short-lived, quality control mechanisms dictate their turnover. The responsiveness of mitophagy to metabolic state is a fairly recent area of study, due in part to its recognition as a selective process and the identification of mitophagy-specific proteins. The NAD^+/NAD^+H^+ ratio is an indicator of cellular energy status, and energy depleting conditions like exercise lead to a relative increase in NAD^+ levels. Cells treated with 5 mM of the metabolite exhibited LC3 punctae and enhanced mitochondrial fragmentation, suggesting an upregulation of mitophagy in response to metabolic status through activation of SIRT1 (72).

2.5.3.1.1 Muscle wasting

Mitophagy initiation is enhanced following denervation, an experimental model of muscle wasting (130). This activation is thought to be secondary to mitochondrial functional decrements (State III and State IV respiration), hindered import, increased ROS production (157), and fragmentation (67). When mitochondrial elimination occurs in the absence of organelle synthesis, as is in the case of disuse, there is a net loss of the organelle (2, 130) and mtDNA (79). Suppression of the mitochondrial ubiquitin ligase MUL1 was found to attenuate muscle wasting in response to disuse (110), providing evidence that deregulated mitophagy can contribute to pathological muscle atrophy.

2.5.4 Mitophagy in pathology

The cytoprotective properties of mitophagy involve elimination of dysfunctional organelles from the mitochondrial pool. An upregulation of mitophagy is seen in patients with Choline kinase β mutations (CKB). The condition results in congenital muscular dystrophy, progressive muscle wasting and enlarged mitochondria lacking enzymatic capacity. CKB patients exhibited enhanced expression of PINK1 and Parkin, alongside autophagy transcripts LC3 and p62 (126). Mitophagy appears to be a compensatory mechanism for curbing mitochondrial dysfunction, but may become deregulated in pathophysiological conditions. Mitophagy decrements proceed induced pressure-overload in models of the failing heart (4), and may underlie organelle dysfunction in cardiovascular disease. Mitophagy depression is seen in both senescent animals and in pharmacologically-induced heart failure, and has been ascribed to the activity of tumor-

suppressing p53. Cytosolic p53 was recently found to sequester Parkin, impeding its mitophagic activity and organelle clearance. $p53^{-/-}$ displayed resistance to mitophagy inhibition and displayed a preservation of cardiac functions relative to controls (60). The evolutionary-conserved process of mitophagy is a critical mechanism mediating the both the quality of the mitochondrial pool and global cellular survival.

Study Objectives

The mechanisms and regulators of mitochondrial biogenesis in muscle have been well recognized and defined. Conversely, little is known about the processes that govern organelle degradation, mitophagy, in skeletal muscle. In light of the fact that mitophagy and biogenesis interplay to mediate mitochondrial turnover, we set out to determine how the two divergent processes interplay. Applying an *in vitro* model of mitochondrial biogenesis, chronic contractile activity (CCA) (24, 171), our goal was to assess the role of mitophagy in shaping the integrity and overall content of the mitochondrial pool. In other words, to illuminate the role of autophagy in regulating mitochondrial quality in muscle cells. Through the use of lysosomal inhibitors to perturb mitochondrial clearance, we sought to investigate mitophagy as a determinant of mitochondrial integrity during CCA. Multiple biochemical measures of mitochondrial activity and quality were used to gain insight into the functional consequences of mitophagy inhibition. Fluorescence microscopy was employed to validate the autophagy protein data, and provide insight into mitochondrial morphology. Further our goal was to investigate the molecular

mechanisms governing this quality control pathway in muscle cells, by evaluating the expression of mitophagy-related genes. By performing comprehensive assessments of mitochondrial quality, we hope to gain novel data on the mechanistic role of mitophagy during contractile-induced biogenesis in skeletal muscle. We hypothesized that autophagy would be upregulated in skeletal muscle following contractile activity, as a result of enhanced protein turnover indispensible for muscle remodeling. In addition to an enhanced state of autophagy, we hypothesized a similar increase in the process of mitophagy, coinciding with mitochondrial biogenesis. By impairing mitophagy through lysosomal inhibition, we predicted an ensuing accumulation of superfluous organelles with diminished respiratory capacity, an effect we expect to moderate with CCA.

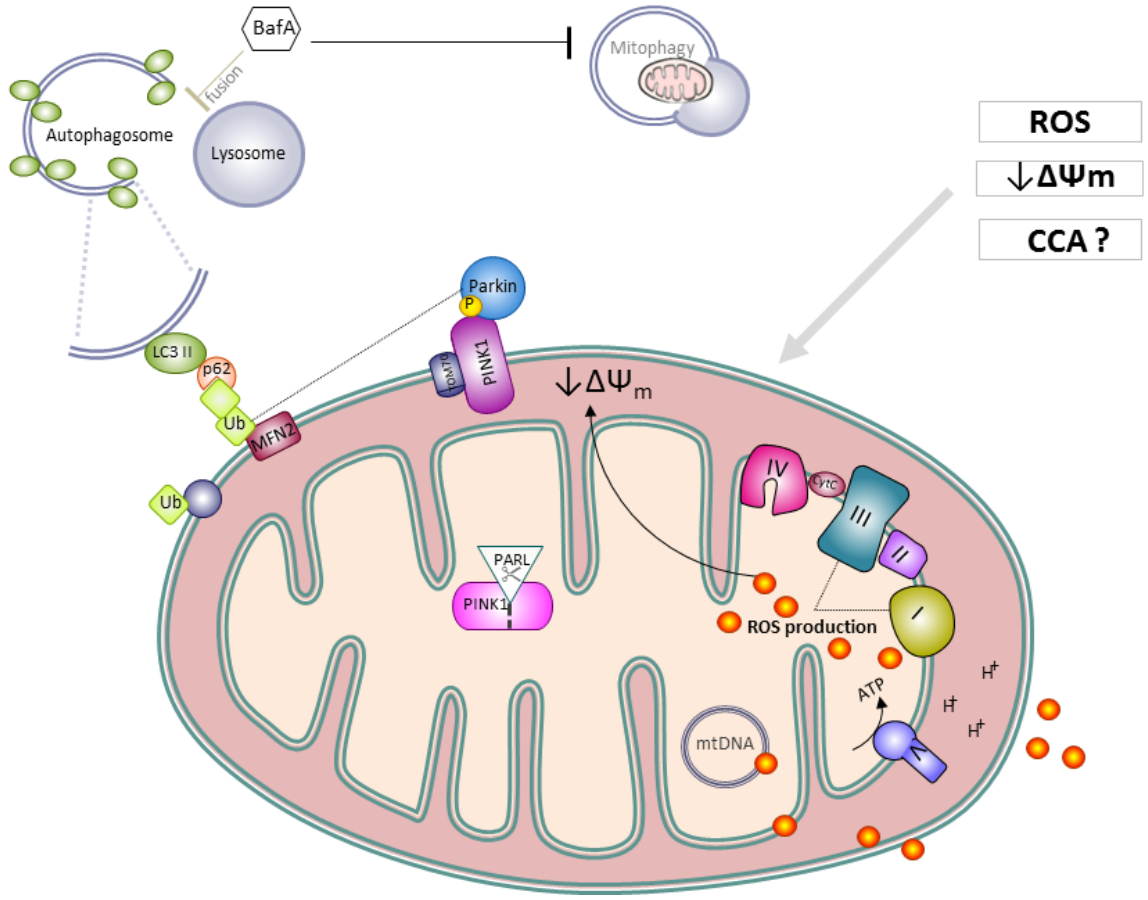

Fig. 1: *Mitophagy protein interactions on the outer mitochondrial membrane (OMM).* Mitochondria participate in a multifaceted quality control mechanism, mediating the turnover of senescent and aberrant organelles. Organelle dysfunction coincides with excessive reactive oxygen species (ROS) production as a result of electron transport chain insufficiency. Elevated ROS contribute to pathology through oxidative damage and potentiate further loss of $\Delta\Psi_m$. Outer-membrane proteins play an integral role in the initiation and commitment to a mitophagy signaling cascade. Normally, PINK1 is imported into the inner membrane for PARL-dependent cleavage. Upon the loss of membrane potential ($\Delta\Psi_m$), PINK1 accumulates on the OMM recruiting Parkin by an unknown mechanism. PINK1 phosphorylates TRAP1, suppressing mPTP opening and apoptosis under mitochondrial stress. Parkin, an E3-ubiquitin ligase, targets OMM proteins for degradation via the proteasome. Proteasomal degradation of OMM protein results in the remodeling of the outer membrane identifying organelles for mitophagy. LC3-II contributes to the elongation pre-autophagosome membrane in early mitophagy and bulk autophagy, and p62 and BNIP3L participate in cargo-selection and recruitment of LC3-II. Mitochondria destined for proteolysis are enveloped in a double-membrane autophagosome and proceed to lysosomal degradation in the final steps of mitophagy. BafA treatment inhibits lysosomal activity and thus, prevents autophagy. CCA induces mitochondrial biogenesis and may restore autophagic flux with autophagy inhibition.

Reference List

1. **Abreu IA, Cabelli DE**. Superoxide dismutases-a review of the metal-associated mechanistic variations. *Biochim. Biophys. Acta* 1804: 263–74, 2010.
2. **Adhihetty PJ, O'Leary MFN, Chabi B, Wicks KL, Hood DA**. Effect of denervation on mitochondrially mediated apoptosis in skeletal muscle. *J. Appl. Physiol.* 102: 1143–51, 2007.
3. **Ahadian S, Ostrovidov S, Hosseini V, Kaji H, Ramalingam M, Bae H, Khademhosseini A**. Electrical stimulation as a biomimicry tool for regulating muscle cell behavior. *Organogenesis* 9: 87–92, 2013.
4. **Albin R, Dowell RT, Zak R, Rabinowitz M**. Synthesis and degradation of mitochondrial components in hypertrophied rat heart. *Biochem. J.* 136: 629–37, 1973.
5. **Aon MA, Stanley BA, Sivakumaran V, Kembro JM, O'Rourke B, Paolocci N, Cortassa S**. Glutathione/thioredoxin systems modulate mitochondrial H2O2 emission: an experimental-computational study. *J. Gen. Physiol.* 139: 479–91, 2012.
6. **Ashrafi G, Schwarz TL**. The pathways of mitophagy for quality control and clearance of mitochondria. *Cell Death Differ.* 20: 31–42, 2013.
7. **Baltscheffsky H, Baltscheffsky M**. Electron transport phosphorylation. *Annu. Rev. Biochem.* 43: 871–97, 1974.
8. **Benard G, Rossignol R**. Ultrastructure of the mitochondrion and its bearing on function and bioenergetics. *Antioxid. Redox Signal.* 10: 1313–42, 2008.
9. **Beynon RJ, Bond JS**. Catabolism of intracellular protein: molecular aspects. *Am. J. Physiol.* 251: C141–52, 1986.
10. **Bidani A, Heming TA**. Effects of bafilomycin A1 on functional capabilities of LPS-activated alveolar macrophages. *J. Leukoc. Biol.* 57: 275–81, 1995.
11. **Boise LH, González-García M, Postema CE, Ding L, Lindsten T, Turka LA, Mao X, Nuñez G, Thompson CB**. bcl-x, a bcl-2-related gene that functions as a dominant regulator of apoptotic cell death. *Cell* 74: 597–608, 1993.
12. **Boveris A, Oshino N, Chance B**. The cellular production of hydrogen peroxide. *Biochem. J.* 128: 617–30, 1972.
13. **Bowman EJ, Siebers A, Altendorf K**. Bafilomycins: a class of inhibitors of membrane ATPases from microorganisms, animal cells, and plant cells. *Proc. Natl. Acad. Sci. U. S. A.* 85: 7972–6, 1988.
14. **Boya P, González-Polo R-A, Casares N, Perfettini J-L, Dessen P, Larochette N, Métivier D, Meley D, Souquere S, Yoshimori T, Pierron G, Codogno P, Kroemer G**. Inhibition of macroautophagy triggers apoptosis. *Mol. Cell. Biol.* 25: 1025–40, 2005.
15. **Brand MD, Nicholls DG**. Assessing mitochondrial dysfunction in cells. *Biochem. J.* 435: 297–312, 2011.
16. **Brand MD**. The sites and topology of mitochondrial superoxide production. *Exp. Gerontol.* 45: 466–72, 2010.

17. **Brown GC, Borutaite V**. There is no evidence that mitochondria are the main source of reactive oxygen species in mammalian cells. *Mitochondrion* 12: 1–4, 2012.
18. **Burch N, Arnold A-S, Item F, Summermatter S, Brochmann Santana Santos G, Christe M, Boutellier U, Toigo M, Handschin C**. Electric pulse stimulation of cultured murine muscle cells reproduces gene expression changes of trained mouse muscle. *PLoS One* 5: e10970, 2010.
19. **Burchell VS, Nelson DE, Sanchez-Martinez A, Delgado-Camprubi M, Ivatt RM, Pogson JH, Randle SJ, Wray S, Lewis PA, Houlden H, Abramov AY, Hardy J, Wood NW, Whitworth AJ, Laman H, Plun-Favreau H**. The Parkinson's disease-linked proteins Fbxo7 and Parkin interact to mediate mitophagy. *Nat. Neurosci.* 16: 1257–65, 2013.
20. **Campian JL, Qian M, Gao X, Eaton JW**. Oxygen tolerance and coupling of mitochondrial electron transport. *J. Biol. Chem.* 279: 46580–7, 2004.
21. **Candas D, Li JJ**. MnSOD in Oxidative Stress Response-Potential Regulation Via Mitochondrial Protein Influx. *Antioxid. Redox Signal.* (June 8, 2013). doi: 10.1089/ars.2013.5305.
22. **Cardenas ME, Cutler NS, Lorenz MC, Di Como CJ, Heitman J**. The TOR signaling cascade regulates gene expression in response to nutrients. *Genes Dev.* 13: 3271–3279, 1999.
23. **Carew JS, Zhou Y, Albitar M, Carew JD, Keating MJ, Huang P**. Mitochondrial DNA mutations in primary leukemia cells after chemotherapy: clinical significance and therapeutic implications. *Leukemia* 17: 1437–47, 2003.
24. **Carter HN, Hood DA**. Contractile activity-induced mitochondrial biogenesis and mTORC1. *Am. J. Physiol. Cell Physiol.* 303: C540–7, 2012.
25. **Castillo K, Valenzuela V, Matus S, Nassif M, Oñate M, Fuentealba Y, Encina G, Irrazabal T, Parsons G, Court FA, Schneider BL, Armentano D, Hetz C**. Measurement of autophagy flux in the nervous system in vivo. *Cell Death Dis.* 4: e917, 2013.
26. **Chan NC, Salazar AM, Pham AH, Sweredoski MJ, Kolawa NJ, Graham RLJ, Hess S, Chan DC**. Broad activation of the ubiquitin-proteasome system by Parkin is critical for mitophagy. *Hum. Mol. Genet.* 20: 1726–37, 2011.
27. **CHANCE B, WILLIAMS GR**. A simple and rapid assay of oxidative phosphorylation. *Nature* 175: 1120–1, 1955.
28. **Chen G**. Nix and Nip3 Form a Subfamily of Pro-apoptotic Mitochondrial Proteins. *J. Biol. Chem.* 274: 7–10, 1999.
29. **Chen L, Xu B, Liu L, Luo Y, Yin J, Zhou H, Chen W, Shen T, Han X, Huang S**. Hydrogen peroxide inhibits mTOR signaling by activation of AMPKalpha leading to apoptosis of neuronal cells. *Lab. Invest.* 90: 762–73, 2010.
30. **Chen Q, Vazquez EJ, Moghaddas S, Hoppel CL, Lesnefsky EJ**. Production of reactive oxygen species by mitochondria: central role of complex III. *J. Biol. Chem.* 278: 36027–31, 2003.
31. **Chen Y, Dorn GW**. PINK1-phosphorylated mitofusin 2 is a Parkin receptor for culling damaged mitochondria. *Science* 340: 471–5, 2013.

32. **Chinnery PF, Zwijnenburg PJ, Walker M, Howell N, Taylor RW, Lightowlers RN, Bindoff L, Turnbull DM**. Nonrandom tissue distribution of mutant mtDNA. *Am. J. Med. Genet.* 85: 498–501, 1999.
33. **Chinni SR, Shisheva A**. Arrest of endosome acidification by bafilomycin A1 mimics insulin action on GLUT4 translocation in 3T3-L1 adipocytes. *Biochem. J.* 339 (Pt 3: 599–606, 1999.
34. **Choi SL, Kim SJ, Lee KT, Kim J, Mu J, Birnbaum MJ, Soo Kim S, Ha J**. The regulation of AMP-activated protein kinase by H(2)O(2). *Biochem. Biophys. Res. Commun.* 287: 92–7, 2001.
35. **Chu CT**. A pivotal role for PINK1 and autophagy in mitochondrial quality control: implications for Parkinson disease. *Hum. Mol. Genet.* 19: R28–37, 2010.
36. **Cipolat S, Martins de Brito O, Dal Zilio B, Scorrano L**. OPA1 requires mitofusin 1 to promote mitochondrial fusion. *Proc. Natl. Acad. Sci. U. S. A.* 101: 15927–32, 2004.
37. **DEMPSEY EW**. Variations in the structure of mitochondria. *J. Biophys. Biochem. Cytol.* 2: 305–12, 1956.
38. **Denver DR, Morris K, Lynch M, Thomas WK**. High mutation rate and predominance of insertions in the Caenorhabditis elegans nuclear genome. *Nature* 430: 679–82, 2004.
39. **Dias V, Junn E, Mouradian MM**. The Role of Oxidative Stress in Parkinson's Disease. *J. Parkinsons. Dis.* (November 19, 2013). doi: 10.3233/JPD-130230.
40. **Djavaheri-Mergny M, Amelotti M, Mathieu J, Besançon F, Bauvy C, Souquère S, Pierron G, Codogno P**. NF-kappaB activation represses tumor necrosis factor-alpha-induced autophagy. *J. Biol. Chem.* 281: 30373–82, 2006.
41. **Egan DF, Shackelford DB, Mihaylova MM, Gelino S, Kohnz RA, Mair W, Vasquez DS, Joshi A, Gwinn DM, Taylor R, Asara JM, Fitzpatrick J, Dillin A, Viollet B, Kundu M, Hansen M, Shaw RJ**. Phosphorylation of ULK1 (hATG1) by AMP-activated protein kinase connects energy sensing to mitophagy. *Science* 331: 456–61, 2011.
42. **Eilers M, Oppliger W, Schatz G**. Both ATP and an energized inner membrane are required to import a purified precursor protein into mitochondria. *EMBO J.* 6: 1073–7, 1987.
43. **Ericsson JLE**. Studies on induced cellular autophagy. *Exp. Cell Res.* 56: 393–405, 1969.
44. **Federico A, Cardaioli E, Da Pozzo P, Formichi P, Gallus GN, Radi E**. Mitochondria, oxidative stress and neurodegeneration. *J. Neurol. Sci.* 322: 254–62, 2012.
45. **Fleury C, Mignotte B, Vayssière J-L**. Mitochondrial reactive oxygen species in cell death signaling. *Biochimie* 84: 131–41, 2002.
46. **Frank M, Duvezin-Caubet S, Koob S, Occhipinti A, Jagasia R, Petcherski A, Ruonala MO, Priault M, Salin B, Reichert AS**. Mitophagy is triggered by mild oxidative stress in a mitochondrial fission dependent manner. *Biochim. Biophys. Acta* 1823: 2297–310, 2012.

47. **Frank S, Gaume B, Bergmann-Leitner ES, Leitner WW, Robert EG, Catez F, Smith CL, Youle RJ**. The role of dynamin-related protein 1, a mediator of mitochondrial fission, in apoptosis. *Dev. Cell* 1: 515–25, 2001.
48. **Gerasimenko J V, Gerasimenko O V, Palejwala A, Tepikin A V, Petersen OH, Watson AJM**. Menadione-induced apoptosis: roles of cytosolic Ca(2+) elevations and the mitochondrial permeability transition pore. *J. Cell Sci.* 115: 485–97, 2002.
49. **Gispert S, Ricciardi F, Kurz A, Azizov M, Hoepken H-H, Becker D, Voos W, Leuner K, Müller WE, Kudin AP, Kunz WS, Zimmermann A, Roeper J, Wenzel D, Jendrach M, García-Arencíbia M, Fernández-Ruiz J, Huber L, Rohrer H, Barrera M, Reichert AS, Rüb U, Chen A, Nussbaum RL, Auburger G**. Parkinson phenotype in aged PINK1-deficient mice is accompanied by progressive mitochondrial dysfunction in absence of neurodegeneration. *PLoS One* 4: e5777, 2009.
50. **Greenamyre JT, Sherer TB, Betarbet R, Panov A V**. Complex I and Parkinson's disease. *IUBMB Life* 52: 135–41, 2001.
51. **Grumati P, Coletto L, Schiavinato A, Castagnaro S, Bertaggia E, Sandri M, Bonaldo P**. Physical exercise stimulates autophagy in normal skeletal muscles but is detrimental for collagen VI-deficient muscles. *Autophagy* 7: 1415–23, 2011.
52. **Grünewald A, Gegg ME, Taanman J-W, King RH, Kock N, Klein C, Schapira AH V**. Differential effects of PINK1 nonsense and missense mutations on mitochondrial function and morphology. *Exp. Neurol.* 219: 266–73, 2009.
53. **Haag-Liautard C, Coffey N, Houle D, Lynch M, Charlesworth B, Keightley PD**. Direct estimation of the mitochondrial DNA mutation rate in Drosophila melanogaster. *PLoS Biol.* 6: e204, 2008.
54. **Halestrap AP, Clarke SJ, Javadov SA**. Mitochondrial permeability transition pore opening during myocardial reperfusion--a target for cardioprotection. *Cardiovasc. Res.* 61: 372–85, 2004.
55. **Hayman J**. Charles Darwin's mitochondria. *Genetics* 194: 21–5, 2013.
56. **Holian A, Wilson DF**. Relationship of transmembrane pH and electrical gradients with respiration and adenosine 5'-triphosphate synthesis in mitochondria. *Biochemistry* 19: 4213–21, 1980.
57. **Holloszy JO, Booth FW**. Biochemical adaptations to endurance exercise in muscle. *Annu. Rev. Physiol.* 38: 273–91, 1976.
58. **Hong J, Nakano Y, Yokomakura A, Ishihara K, Kim S, Kang Y-S, Ohuchi K**. Nitric oxide production by the vacuolar-type (H+)-ATPase inhibitors bafilomycin A1 and concanamycin A and its possible role in apoptosis in RAW 264.7 cells. *J. Pharmacol. Exp. Ther.* 319: 672–81, 2006.
59. **Hood DA**. Mechanisms of exercise-induced mitochondrial biogenesis in skeletal muscle. *Appl. Physiol. Nutr. Metab.* 34: 465–72, 2009.
60. **Hoshino A, Mita Y, Okawa Y, Ariyoshi M, Iwai-Kanai E, Ueyama T, Ikeda K, Ogata T, Matoba S**. Cytosolic p53 inhibits Parkin-mediated mitophagy and promotes mitochondrial dysfunction in the mouse heart. *Nat. Commun.* 4: 2308, 2013.

61. **Hough R, Pratt G, Rechsteiner M**. Purification of two high molecular weight proteases from rabbit reticulocyte lysate. *J. Biol. Chem.* 262: 8303–13, 1987.
62. **Hunt J V, Wolff SP**. Oxidative glycation and free radical production: a causal mechanism of diabetic complications. *Free Radic. Res. Commun.* 12-13 Pt 1: 115–23, 1991.
63. **Huss JM, Kopp RP, Kelly DP**. Peroxisome proliferator-activated receptor coactivator-1alpha (PGC-1alpha) coactivates the cardiac-enriched nuclear receptors estrogen-related receptor-alpha and -gamma. Identification of novel leucine-rich interaction motif within PGC-1alpha. *J. Biol. Chem.* 277: 40265–74, 2002.
64. **Hutson NJ, Mortimore GE**. Suppression of cytoplasmic protein uptake by lysosomes as the mechanism of protein regain in livers of starved-refed mice. *J. Biol. Chem.* 257: 9548–54, 1982.
65. **Ichiki T**. Deficiency of subunits of complex I and mitochondrial encephalomyopathy. *Ann. Neurol.* 23: 287 – 294, 1988.
66. **Ide T, Tsutsui H, Hayashidani S, Kang D, Suematsu N, Nakamura K, Utsumi H, Hamasaki N, Takeshita A**. Mitochondrial DNA damage and dysfunction associated with oxidative stress in failing hearts after myocardial infarction. *Circ. Res.* 88: 529–35, 2001.
67. **Iqbal S, Ostojic O, Singh K, Joseph A-M, Hood DA**. Expression of mitochondrial fission and fusion regulatory proteins in skeletal muscle during chronic use and disuse. *Muscle Nerve* 48: 963–70, 2013.
68. **Irrcher I, Ljubicic V, Hood DA**. Interactions between ROS and AMP kinase activity in the regulation of PGC-1alpha transcription in skeletal muscle cells. *Am. J. Physiol. Cell Physiol.* 296: C116–23, 2009.
69. **Ishikawa K, Takenaga K, Akimoto M, Koshikawa N, Yamaguchi A, Imanishi H, Nakada K, Honma Y, Hayashi J-I**. ROS-generating mitochondrial DNA mutations can regulate tumor cell metastasis. *Science* 320: 661–4, 2008.
70. **Jaber N, Dou Z, Lin RZ, Zhang J, Zong W-X**. Mammalian PIK3C3/VPS34: the key to autophagic processing in liver and heart. *Autophagy* 8: 707–8, 2012.
71. **Jamart C, Naslain D, Gilson H, Francaux M**. Higher activation of autophagy in skeletal muscle of mice during endurance exercise in the fasted state. *Am. J. Physiol. Endocrinol. Metab.* 305: E964–74, 2013.
72. **Jang S, Kang HT, Hwang ES**. Nicotinamide-induced mitophagy: event mediated by high NAD+/NADH ratio and SIRT1 protein activation. *J. Biol. Chem.* 287: 19304–14, 2012.
73. **Janué A, Olivé M, Ferrer I**. Oxidative stress in desminopathies and myotilinopathies: a link between oxidative damage and abnormal protein aggregation. *Brain Pathol.* 17: 377–88, 2007.
74. **Jin H, Kanthasamy A, Ghosh A, Anantharam V, Kalyanaraman B, Kanthasamy AG**. Mitochondria-targeted antioxidants for treatment of Parkinson's disease: Preclinical and clinical outcomes. *Biochim. Biophys. Acta* (September 20, 2013). doi: 10.1016/j.bbadis.2013.09.007.

75. **Jin SM, Lazarou M, Wang C, Kane LA, Narendra DP, Youle RJ**. Mitochondrial membrane potential regulates PINK1 import and proteolytic destabilization by PARL. *J. Cell Biol.* 191: 933–42, 2010.
76. **Jin SM, Youle RJ**. The accumulation of misfolded proteins in the mitochondrial matrix is sensed by PINK1 to induce PARK2/Parkin-mediated mitophagy of polarized mitochondria. *Autophagy* 9: 1750–7, 2013.
77. **Kabeya Y, Mizushima N, Ueno T, Yamamoto A, Kirisako T, Noda T, Kominami E, Ohsumi Y, Yoshimori T**. LC3, a mammalian homologue of yeast Apg8p, is localized in autophagosome membranes after processing. *EMBO J.* 19: 5720–8, 2000.
78. **Kabeya Y, Mizushima N, Yamamoto A, Oshitani-Okamoto S, Ohsumi Y, Yoshimori T**. LC3, GABARAP and GATE16 localize to autophagosomal membrane depending on form-II formation. *J. Cell Sci.* 117: 2805–12, 2004.
79. **Kang C, Ji LL**. Muscle immobilization and remobilization downregulates PGC-1α signaling and the mitochondrial biogenesis pathway. *J. Appl. Physiol.* 115: 1618–25, 2013.
80. **Kawai A, Uchiyama H, Takano S, Nakamura N, Ohkuma S**. Autophagosome-Lysosome Fusion Depends on the pH in Acidic Compartments in CHO Cells. *Autophagy* 3: 154–157, 2007.
81. **Keller CW, Fokken C, Turville SG, Lünemann A, Schmidt J, Münz C, Lünemann JD**. TNF-alpha induces macroautophagy and regulates MHC class II expression in human skeletal muscle cells. *J. Biol. Chem.* 286: 3970–80, 2011.
82. **Kim J, Kundu M, Viollet B, Guan K-L**. AMPK and mTOR regulate autophagy through direct phosphorylation of Ulk1. *Nat. Cell Biol.* 13: 132–41, 2011.
83. **Kirisako T, Baba M, Ishihara N, Miyazawa K, Ohsumi M, Yoshimori T, Noda T, Ohsumi Y**. Formation process of autophagosome is traced with Apg8/Aut7p in yeast. *J. Cell Biol.* 147: 435–46, 1999.
84. **Kirkwood SP, Packer L, Brooks GA**. Effects of endurance training on a mitochondrial reticulum in limb skeletal muscle. *Arch. Biochem. Biophys.* 255: 80–8, 1987.
85. **Kondapalli C, Kazlauskaite A, Zhang N, Woodroof HI, Campbell DG, Gourlay R, Burchell L, Walden H, Macartney TJ, Deak M, Knebel A, Alessi DR, Muqit MMK**. PINK1 is activated by mitochondrial membrane potential depolarization and stimulates Parkin E3 ligase activity by phosphorylating Serine 65. *Open Biol.* 2: 120080, 2012.
86. **Kuznetsov A V, Kehrer I, Kozlov A V, Haller M, Redl H, Hermann M, Grimm M, Troppmair J**. Mitochondrial ROS production under cellular stress: comparison of different detection methods. *Anal. Bioanal. Chem.* 400: 2383–90, 2011.
87. **Kwon K-Y, Viollet B, Yoo OJ**. CCCP induces autophagy in an AMPK-independent manner. *Biochem. Biophys. Res. Commun.* 416: 343–8, 2011.
88. **Lagouge M, Argmann C, Gerhart-Hines Z, Meziane H, Lerin C, Daussin F, Messadeq N, Milne J, Lambert P, Elliott P, Geny B, Laakso M, Puigserver P,**

Auwerx J. Resveratrol improves mitochondrial function and protects against metabolic disease by activating SIRT1 and PGC-1alpha. *Cell* 127: 1109–22, 2006.
89. **Lamperti C, Diodato D, Lamantea E, Carrara F, Ghezzi D, Mereghetti P, Rizzi R, Zeviani M**. MELAS-like encephalomyopathy caused by a new pathogenic mutation in the mitochondrial DNA encoded cytochrome c oxidase subunit I. *Neuromuscul. Disord.* 22: 990–4, 2012.
90. **Lazarou M, Jin SM, Kane LA, Youle RJ**. Role of PINK1 binding to the TOM complex and alternate intracellular membranes in recruitment and activation of the E3 ligase Parkin. *Dev. Cell* 22: 320–33, 2012.
91. **Ledenev AN, Ruuge EK**. [Generation of superoxide radicals by ischemic heart mitochondria]. *Biull. Eksp. Biol. Med.* 100: 303–5, 1985.
92. **Lee YJ, Kim N-Y, Suh Y-A, Lee C**. Involvement of ROS in Curcumin-induced Autophagic Cell Death. *Korean J. Physiol. Pharmacol.* 15: 1–7, 2011.
93. **Lehman JJ, Barger PM, Kovacs A, Saffitz JE, Medeiros DM, Kelly DP**. Peroxisome proliferator-activated receptor gamma coactivator-1 promotes cardiac mitochondrial biogenesis. *J. Clin. Invest.* 106: 847–56, 2000.
94. **Lenzi P, Marongiu R, Falleni A, Gelmetti V, Busceti CL, Michiorri S, Valente EM, Fornai F**. A subcellular analysis of genetic modulation of PINK1 on mitochondrial alterations, autophagy and cell death. *Arch. Ital. Biol.* 150: 194–217, 2012.
95. **Levine B, Deretic V**. Unveiling the roles of autophagy in innate and adaptive immunity. *Nat. Rev. Immunol.* 7: 767–77, 2007.
96. **Li L, Chen Y, Gibson SB**. Starvation-induced autophagy is regulated by mitochondrial reactive oxygen species leading to AMPK activation. *Cell. Signal.* 25: 50–65, 2013.
97. **Li LH, Kang T, Chen L, Zhang W, Liao Y, Chen J, Shi Y**. Detection of mitochondrial DNA mutations by high-throughput sequencing in the blood of breast cancer patients. *Int. J. Mol. Med.* 33: 77–82, 2013.
98. **Li X, Fang P, Mai J, Choi ET, Wang H, Yang X**. Targeting mitochondrial reactive oxygen species as novel therapy for inflammatory diseases and cancers. *J. Hematol. Oncol.* 6: 19, 2013.
99. **Lill R, Neupert W**. Mechanisms of protein import across the mitochondrial outer membrane. *Trends Cell Biol.* 6: 56–61, 1996.
100. **Lim JH, Martin F, Guiard B, Pfanner N, Voos W**. The mitochondrial Hsp70-dependent import system actively unfolds preproteins and shortens the lag phase of translocation. *EMBO J.* 20: 941–50, 2001.
101. **Lin J, Handschin C, Spiegelman BM**. Metabolic control through the PGC-1 family of transcription coactivators. *Cell Metab.* 1: 361–370, 2005.
102. **Lin J, Wu H, Tarr PT, Zhang C-Y, Wu Z, Boss O, Michael LF, Puigserver P, Isotani E, Olson EN, Lowell BB, Bassel-Duby R, Spiegelman BM**. Transcriptional co-activator PGC-1 alpha drives the formation of slow-twitch muscle fibres. *Nature* 418: 797–801, 2002.
103. **Lin W, Kang UJ**. Characterization of PINK1 processing, stability, and subcellular localization. *J. Neurochem.* 106: 464–74, 2008.

104. **Lipsky NG, Pedersen PL**. Mitochondrial turnover in animal cells. Half-lives of mitochondria and mitochondrial subfractions of rat liver based on [14C]bicarbonate incorporation. *J. Biol. Chem.* 256: 8652–7, 1981.
105. **Lira VA, Okutsu M, Zhang M, Greene NP, Laker RC, Breen DS, Hoehn KL, Yan Z**. Autophagy is required for exercise training-induced skeletal muscle adaptation and improvement of physical performance. *FASEB J.* 27: 4184–93, 2013.
106. **Liu L, Feng D, Chen G, Chen M, Zheng Q, Song P, Ma Q, Zhu C, Wang R, Qi W, Huang L, Xue P, Li B, Wang X, Jin H, Wang J, Yang F, Liu P, Zhu Y, Sui S, Chen Q**. Mitochondrial outer-membrane protein FUNDC1 mediates hypoxia-induced mitophagy in mammalian cells. *Nat. Cell Biol.* 14: 177–85, 2012.
107. **Ljubicic V, Menzies KJ, Hood DA**. Mitochondrial dysfunction is associated with a pro-apoptotic cellular environment in senescent cardiac muscle. *Mech. Ageing Dev.* 131: 79–88, 2010.
108. **Lluis JM, Buricchi F, Chiarugi P, Morales A, Fernandez-Checa JC**. Dual role of mitochondrial reactive oxygen species in hypoxia signaling: activation of nuclear factor-{kappa}B via c-SRC and oxidant-dependent cell death. *Cancer Res.* 67: 7368–77, 2007.
109. **Loeffler M, Kroemer G**. The Mitochondrion in Cell Death Control: Certainties and Incognita. *Exp. Cell Res.* 256: 19–26, 2000.
110. **Lokireddy S, Wijesoma IW, Teng S, Bonala S, Gluckman PD, McFarlane C, Sharma M, Kambadur R**. The ubiquitin ligase Mul1 induces mitophagy in skeletal muscle in response to muscle-wasting stimuli. *Cell Metab.* 16: 613–24, 2012.
111. **Longley MJ, Prasad R, Srivastava DK, Wilson SH, Copeland WC**. Identification of 5'-deoxyribose phosphate lyase activity in human DNA polymerase and its role in mitochondrial base excision repair in vitro. *Proc. Natl. Acad. Sci. U. S. A.* 95: 12244–8, 1998.
112. **Luo Y, Hu Y, Zhang M, Xiao Y, Song Z, Xu Y**. EtBr-induced selective degradation of mitochondria occurs via autophagy. *Oncol. Rep.* 30: 1201–8, 2013.
113. **MacManus JP, Linnik MD**. Gene expression induced by cerebral ischemia: an apoptotic perspective. *J. Cereb. Blood Flow Metab.* 17: 815–32, 1997.
114. **Madamanchi NR, Runge MS**. Mitochondrial dysfunction in atherosclerosis. *Circ. Res.* 100: 460–73, 2007.
115. **Marchi S, Giorgi C, Suski JM, Agnoletto C, Bononi A, Bonora M, De Marchi E, Missiroli S, Patergnani S, Poletti F, Rimessi A, Duszynski J, Wieckowski MR, Pinton P**. Mitochondria-ros crosstalk in the control of cell death and aging. *J. Signal Transduct.* 2012: 329635, 2012.
116. **Mariño G, López-Otín C**. Autophagy: molecular mechanisms, physiological functions and relevance in human pathology. *Cell. Mol. Life Sci.* 61: 1439–54, 2004.
117. **Matthews W, Driscoll J, Tanaka K, Ichihara A, Goldberg AL**. Involvement of the proteasome in various degradative processes in mammalian cells. *Proc. Natl. Acad. Sci. U. S. A.* 86: 2597–601, 1989.

118. **McLester JR**. Muscle contraction and fatigue. The role of adenosine 5'-diphosphate and inorganic phosphate. *Sports Med.* 23: 287–305, 1997.
119. **Menzies KJ, Singh K, Saleem A, Hood DA**. Sirtuin 1-mediated effects of exercise and resveratrol on mitochondrial biogenesis. *J. Biol. Chem.* 288: 6968–79, 2013.
120. **Miledi R, Slater CR**. Some mitochondrial changes in denervated muscle. *J. Cell Sci.* 3: 49–54, 1968.
121. **Miwa S, Lawless C, von Zglinicki T**. Mitochondrial turnover in liver is fast in vivo and is accelerated by dietary restriction: application of a simple dynamic model. *Aging Cell* 7: 920–3, 2008.
122. **Mizushima N, Yoshimori T, Levine B**. Methods in mammalian autophagy research. *Cell* 140: 313–26, 2010.
123. **Nassif M, Hetz C**. Targeting autophagy in ALS: a complex mission. *Autophagy* 7: 450–3, 2011.
124. **Naviaux RK**. Mitochondrial DNA disorders. *Eur. J. Pediatr.* 159 Suppl: S219–26, 2000.
125. **Nedachi T, Fujita H, Kanzaki M**. Contractile C2C12 myotube model for studying exercise-inducible responses in skeletal muscle. *Am. J. Physiol. Endocrinol. Metab.* 295: E1191–204, 2008.
126. **Nishino I**. New congenital muscular dystrophy due to CHKB mutations. *Rinsho Shinkeigaku* 53: 1112–3, 2013.
127. **Nomikos IN, Wang Y, Lafferty KJ**. Involvement of O2 radicals in "autoimmune" diabetes. *Immunol. Cell Biol.* 67 (Pt 1): 85–7, 1989.
128. **Novak I, Kirkin V, McEwan DG, Zhang J, Wild P, Rozenknop A, Rogov V, Löhr F, Popovic D, Occhipinti A, Reichert AS, Terzic J, Dötsch V, Ney PA, Dikic I**. Nix is a selective autophagy receptor for mitochondrial clearance. *EMBO Rep.* 11: 45–51, 2010.
129. **O'Donnell VB, Spycher S, Azzi A**. Involvement of oxidants and oxidant-generating enzyme(s) in tumour-necrosis-factor-alpha-mediated apoptosis: role for lipoxygenase pathway but not mitochondrial respiratory chain. *Biochem. J.* 310 (Pt 1: 133–41, 1995.
130. **O'Leary MF, Vainshtein A, Iqbal S, Ostojic O, Hood DA**. Adaptive plasticity of autophagic proteins to denervation in aging skeletal muscle. *Am. J. Physiol. Cell Physiol.* 304: C422–30, 2013.
131. **Ondrovicová G, Liu T, Singh K, Tian B, Li H, Gakh O, Perecko D, Janata J, Granot Z, Orly J, Kutejová E, Suzuki CK**. Cleavage site selection within a folded substrate by the ATP-dependent lon protease. *J. Biol. Chem.* 280: 25103–10, 2005.
132. **Otomo C, Metlagel Z, Takaesu G, Otomo T**. Structure of the human ATG12~ATG5 conjugate required for LC3 lipidation in autophagy. *Nat. Struct. Mol. Biol.* 20: 59–66, 2013.
133. **Van den Ouweland JM, Maechler P, Wollheim CB, Attardi G, Maassen JA**. Functional and morphological abnormalities of mitochondria harbouring the tRNA(Leu)(UUR) mutation in mitochondrial DNA derived from patients with

maternally inherited diabetes and deafness (MIDD) and progressive kidney disease. *Diabetologia* 42: 485–92, 1999.

134. **Parajuli N, MacMillan-Crow LA**. Role of reduced manganese superoxide dismutase in ischemia-reperfusion injury: a possible trigger for autophagy and mitochondrial biogenesis? *Am. J. Physiol. Renal Physiol.* 304: F257–67, 2013.
135. **Park J, Lee SB, Lee S, Kim Y, Song S, Kim S, Bae E, Kim J, Shong M, Kim J-M, Chung J**. Mitochondrial dysfunction in Drosophila PINK1 mutants is complemented by parkin. *Nature* 441: 1157–61, 2006.
136. **Pavlakis SG, Phillips PC, DiMauro S, De Vivo DC, Rowland LP**. Mitochondrial myopathy, encephalopathy, lactic acidosis, and strokelike episodes: a distinctive clinical syndrome. *Ann. Neurol.* 16: 481–8, 1984.
137. **Pfanner N, Meijer M**. The Tom and Tim machine. *Curr. Biol.* 7: R100–3, 1997.
138. **Pilegaard H, Saltin B, Neufer PD**. Exercise induces transient transcriptional activation of the PGC-1alpha gene in human skeletal muscle. *J. Physiol.* 546: 851–8, 2003.
139. **Pridgeon JW, Olzmann JA, Chin L-S, Li L**. PINK1 protects against oxidative stress by phosphorylating mitochondrial chaperone TRAP1. *PLoS Biol.* 5: e172, 2007.
140. **Puigserver P, Wu Z, Park CW, Graves R, Wright M, Spiegelman BM**. A cold-inducible coactivator of nuclear receptors linked to adaptive thermogenesis. *Cell* 92: 829–39, 1998.
141. **Qi Z, Zhang Y, Guo W, Ji L, Ding S**. Increased Insulin Sensitivity and Distorted Mitochondrial Adaptations during Muscle Unloading. *Int. J. Mol. Sci.* 13: 16971–85, 2012.
142. **Quinlan CL, Orr AL, Perevoshchikova I V, Treberg JR, Ackrell BA, Brand MD**. Mitochondrial complex II can generate reactive oxygen species at high rates in both the forward and reverse reactions. *J. Biol. Chem.* 287: 27255–64, 2012.
143. **Rahman M, Mofarrahi M, Kristof AS, Nkengfac B, Harel S, Hussain S**. REACTIVE OXYGEN SPECIES REGULATION OF AUTOPHAGY IN SKELETAL MUSCLES. *Antioxid. Redox Signal.* (November 1, 2013). doi: 10.1089/ars.2013.5410.
144. **Rambold AS, Kostelecky B, Elia N, Lippincott-Schwartz J**. Tubular network formation protects mitochondria from autophagosomal degradation during nutrient starvation. *Proc. Natl. Acad. Sci. U. S. A.* 108: 10190–5, 2011.
145. **Redout EM, Wagner MJ, Zuidwijk MJ, Boer C, Musters RJP, van Hardeveld C, Paulus WJ, Simonides WS**. Right-ventricular failure is associated with increased mitochondrial complex II activity and production of reactive oxygen species. *Cardiovasc. Res.* 75: 770–81, 2007.
146. **Van Remmen H, Ikeno Y, Hamilton M, Pahlavani M, Wolf N, Thorpe SR, Alderson NL, Baynes JW, Epstein CJ, Huang T-T, Nelson J, Strong R, Richardson A**. Life-long reduction in MnSOD activity results in increased DNA damage and higher incidence of cancer but does not accelerate aging. *Physiol. Genomics* 16: 29–37, 2003.

147. **Samjoo IA, Safdar A, Hamadeh MJ, Raha S, Tarnopolsky MA**. The effect of endurance exercise on both skeletal muscle and systemic oxidative stress in previously sedentary obese men. *Nutr. Diabetes* 3: e88, 2013.
148. **Santel A, Frank S, Gaume B, Herrler M, Youle RJ, Fuller MT**. Mitofusin-1 protein is a generally expressed mediator of mitochondrial fusion in mammalian cells. *J. Cell Sci.* 116: 2763–74, 2003.
149. **Santidrian AF, Matsuno-Yagi A, Ritland M, Seo BB, LeBoeuf SE, Gay LJ, Yagi T, Felding-Habermann B**. Mitochondrial complex I activity and NAD+/NADH balance regulate breast cancer progression. *J. Clin. Invest.* 123: 1068–81, 2013.
150. **El Sayed SM, Mahmoud AA, El Sawy SA, Abdelaal EA, Fouad AM, Yousif RS, Hashim MS, Hemdan SB, Kadry ZM, Abdelmoaty MA, Gabr AG, Omran FM, Nabo MMH, Ahmed NS**. Warburg effect increases steady-state ROS condition in cancer cells through decreasing their antioxidant capacities (Anticancer effects of 3-bromopyruvate through antagonizing Warburg effect). *Med. Hypotheses* 81: 866–70, 2013.
151. **Schapira AH, Cooper JM, Dexter D, Clark JB, Jenner P, Marsden CD**. Mitochondrial complex I deficiency in Parkinson's disease. *J. Neurochem.* 54: 823–7, 1990.
152. **Schlesinger DH, Goldstein G, Niall HD**. The complete amino acid sequence of ubiquitin, an adenylate cyclase stimulating polypeptide probably universal in living cells. *Biochemistry* 14: 2214–8, 1975.
153. **Schweers RL, Zhang J, Randall MS, Loyd MR, Li W, Dorsey FC, Kundu M, Opferman JT, Cleveland JL, Miller JL, Ney PA**. NIX is required for programmed mitochondrial clearance during reticulocyte maturation. *Proc. Natl. Acad. Sci. U. S. A.* 104: 19500–5, 2007.
154. **Shacka JJ, Klocke BJ, Roth KA**. Autophagy, bafilomycin and cell death: the "a-B-cs" of plecomacrolide-induced neuroprotection. *Autophagy* 2: 228–30, 2006.
155. **Shiba-Fukushima K, Imai Y, Yoshida S, Ishihama Y, Kanao T, Sato S, Hattori N**. PINK1-mediated phosphorylation of the Parkin ubiquitin-like domain primes mitochondrial translocation of Parkin and regulates mitophagy. *Sci. Rep.* 2: 1002, 2012.
156. **Shokolenko IN, Wilson GL, Alexeyev MF**. Persistent damage induces mitochondrial DNA degradation. *DNA Repair (Amst).* 12: 488–99, 2013.
157. **Singh K, Hood DA**. Effect of denervation-induced muscle disuse on mitochondrial protein import. *Am. J. Physiol. Cell Physiol.* 300: C138–45, 2011.
158. **Skulachev VP**. [Mechanism of oxidative phosphorylation and general principles of bioenergetics]. *Usp. Sovrem. Biol.* 77: 125–54, 1974.
159. **Sun Y, Vashisht AA, Tchieu J, Wohlschlegel JA, Dreier L**. Voltage-dependent anion channels (VDACs) recruit Parkin to defective mitochondria to promote mitochondrial autophagy. *J. Biol. Chem.* 287: 40652–60, 2012.
160. **Susin SA, Zamzami N, Castedo M, Hirsch T, Marchetti P, Macho A, Daugas E, Geuskens M, Kroemer G**. Bcl-2 inhibits the mitochondrial release of an apoptogenic protease. *J. Exp. Med.* 184: 1331–41, 1996.

161. **Takahashi M, Hood DA**. Chronic stimulation-induced changes in mitochondria and performance in rat skeletal muscle. *J. Appl. Physiol.* 74: 934–41, 1993.
162. **Talbert EE, Smuder AJ, Min K, Kwon OS, Szeto HH, Powers SK**. Immobilization-induced activation of key proteolytic systems in skeletal muscles is prevented by a mitochondria-targeted antioxidant. *J. Appl. Physiol.* 115: 529–38, 2013.
163. **Tao R, Coleman MC, Pennington JD, Ozden O, Park S-H, Jiang H, Kim H-S, Flynn CR, Hill S, Hayes McDonald W, Olivier AK, Spitz DR, Gius D**. Sirt3-mediated deacetylation of evolutionarily conserved lysine 122 regulates MnSOD activity in response to stress. *Mol. Cell* 40: 893–904, 2010.
164. **Tarnopolsky MA, Raha S**. Mitochondrial myopathies: diagnosis, exercise intolerance, and treatment options. *Med. Sci. Sports Exerc.* 37: 2086–93, 2005.
165. **Taymans J-M, Van den Haute C, Baekelandt V**. Distribution of PINK1 and LRRK2 in rat and mouse brain. *J. Neurochem.* 98: 951–61, 2006.
166. **Teplova V V, Tonshin AA, Grigoriev PA, Saris N-EL, Salkinoja-Salonen MS**. Bafilomycin A1 is a potassium ionophore that impairs mitochondrial functions. *J. Bioenerg. Biomembr.* 39: 321–9, 2007.
167. **Thomas C, Mackey MM, Diaz AA, Cox DP**. Hydroxyl radical is produced via the Fenton reaction in submitochondrial particles under oxidative stress: implications for diseases associated with iron accumulation. *Redox Rep.* 14: 102–8, 2009.
168. **Toyoda T, Hayashi T, Miyamoto L, Yonemitsu S, Nakano M, Tanaka S, Ebihara K, Masuzaki H, Hosoda K, Inoue G, Otaka A, Sato K, Fushiki T, Nakao K**. Possible involvement of the alpha1 isoform of 5'AMP-activated protein kinase in oxidative stress-stimulated glucose transport in skeletal muscle. *Am. J. Physiol. Endocrinol. Metab.* 287: E166–73, 2004.
169. **Trocoli A, Djavaheri-Mergny M**. The complex interplay between autophagy and NF-κB signaling pathways in cancer cells. *Am. J. Cancer Res.* 1: 629–49, 2011.
170. **Tsukada M, Ohsumi Y**. Isolation and characterization of autophagy-defective mutants of Saccharomyces cerevisiae. *FEBS Lett.* 333: 169–74, 1993.
171. **Uguccioni G, Hood DA**. The importance of PGC-1α in contractile activity-induced mitochondrial adaptations. *Am. J. Physiol. Endocrinol. Metab.* 300: E361–71, 2011.
172. **Underwood BR, Imarisio S, Fleming A, Rose C, Krishna G, Heard P, Quick M, Korolchuk VI, Renna M, Sarkar S, García-Arencibia M, O'Kane CJ, Murphy MP, Rubinsztein DC**. Antioxidants can inhibit basal autophagy and enhance neurodegeneration in models of polyglutamine disease. *Hum. Mol. Genet.* 19: 3413–29, 2010.
173. **Unoki M, Nakamura Y**. Growth-suppressive effects of BPOZ and EGR2, two genes involved in the PTEN signaling pathway. *Oncogene* 20: 4457–65, 2001.
174. **Vadlamudi RK, Shin J**. Genomic structure and promoter analysis of the p62 gene encoding a non-proteasomal multiubiquitin chain binding protein. *FEBS Lett.* 435: 138–42, 1998.

175. **Valente EM, Abou-Sleiman PM, Caputo V, Muqit MMK, Harvey K, Gispert S, Ali Z, Del Turco D, Bentivoglio AR, Healy DG, Albanese A, Nussbaum R, González-Maldonado R, Deller T, Salvi S, Cortelli P, Gilks WP, Latchman DS, Harvey RJ, Dallapiccola B, Auburger G, Wood NW**. Hereditary early-onset Parkinson's disease caused by mutations in PINK1. *Science* 304: 1158–60, 2004.
176. **Vincow ES, Merrihew G, Thomas RE, Shulman NJ, Beyer RP, MacCoss MJ, Pallanck LJ**. The PINK1-Parkin pathway promotes both mitophagy and selective respiratory chain turnover in vivo. *Proc. Natl. Acad. Sci. U. S. A.* 110: 6400–5, 2013.
177. **Wang K, Long B, Jiao J-Q, Wang J-X, Liu J-P, Li Q, Li P-F**. miR-484 regulates mitochondrial network through targeting Fis1. *Nat. Commun.* 3: 781, 2012.
178. **Wang Y, Nartiss Y, Steipe B, McQuibban GA, Kim PK**. ROS-induced mitochondrial depolarization initiates PARK2/PARKIN-dependent mitochondrial degradation by autophagy. *Autophagy* 8: 1462–76, 2012.
179. **Wilkinson KD, Urban MK, Haas AL**. Ubiquitin is the ATP-dependent proteolysis factor I of rabbit reticulocytes. *J. Biol. Chem.* 255: 7529–32, 1980.
180. **Winge DR**. Sealing the mitochondrial respirasome. *Mol. Cell. Biol.* 32: 2647–52, 2012.
181. **Wu C-A, Chao Y, Shiah S-G, Lin W-W**. Nutrient deprivation induces the Warburg effect through ROS/AMPK-dependent activation of pyruvate dehydrogenase kinase. *Biochim. Biophys. Acta* 1833: 1147–56, 2013.
182. **Wu D, Cederbaum AI**. Inhibition of autophagy promotes CYP2E1-dependent toxicity in HepG2 cells via elevated oxidative stress, mitochondria dysfunction and activation of p38 and JNK MAPK. *Redox Biol.* 1: 552–565, 2013.
183. **Wu Z, Puigserver P, Andersson U, Zhang C, Adelmant G, Mootha V, Troy A, Cinti S, Lowell B, Scarpulla RC, Spiegelman BM**. Mechanisms Controlling Mitochondrial Biogenesis and Respiration through the Thermogenic Coactivator PGC-1. *Cell* 98: 115–124, 1999.
184. **Yamamoto A, Tagawa Y, Yoshimori T, Moriyama Y, Masaki R, Tashiro Y**. Bafilomycin A1 prevents maturation of autophagic vacuoles by inhibiting fusion between autophagosomes and lysosomes in rat hepatoma cell line, H-4-II-E cells. *Cell Struct. Funct.* 23: 33–42, 1998.
185. **Yan G, Shen X, Jiang Y**. Rapamycin activates Tap42-associated phosphatases by abrogating their association with Tor complex 1. *EMBO J.* 25: 3546–55, 2006.
186. **Yoneda M, Tanaka M, Nishikimi M, Suzuki H, Tanaka K, Nishizawa M, Atsumi T, Ohama E, Horai S, Ikuta F**. Pleiotropic molecular defects in energy-transducing complexes in mitochondrial encephalomyopathy (MELAS). *J. Neurol. Sci.* 92: 143–58, 1989.
187. **Yorimitsu T, He C, Wang K, Klionsky DJ**. Tap42-associated protein phosphatase type 2A negatively regulates induction of autophagy. *Autophagy* 5: 616–24, 2009.

188. **Zatloukal K, Stumptner C, Fuchsbichler A, Heid H, Schnoelzer M, Kenner L, Kleinert R, Prinz M, Aguzzi A, Denk H**. p62 Is a common component of cytoplasmic inclusions in protein aggregation diseases. *Am. J. Pathol.* 160: 255–63, 2002.
189. **Zhang Y, Dawson VL, Dawson TM**. Oxidative stress and genetics in the pathogenesis of Parkinson's disease. *Neurobiol. Dis.* 7: 240–50, 2000.
190. **Zimmerman MC, Zucker IH**. Mitochondrial dysfunction and mitochondrial-produced reactive oxygen species: new targets for neurogenic hypertension? *Hypertension* 53: 112–4, 2009.
191. **Ziviani E, Tao RN, Whitworth AJ**. Drosophila parkin requires PINK1 for mitochondrial translocation and ubiquitinates mitofusin. *Proc. Natl. Acad. Sci. U. S. A.* 107: 5018–23, 2010.

The Role of Autophagy in the Maintenance of Mitochondrial Quality and Adaptations to Contractile Activity

Alexa Parousis and David A. Hood

Muscle Health Research Centre, School of Kinesiology and Health Science

York University, Toronto, Ontario, M3J 1P3, Canada

Keywords: C2C12, Autophagy, Bafilomycin, Contractile Activity, LC3

Address for correspondence: Dr. David A Hood

School of Kinesiology and Health Science

York University, Toronto, ON

M3J 1P3, Canada

Tel: (416) 736-2100 ext. 66640

Fax: (416) 736-5698

Email: dhood@yorku.ca

Abstract

Autophagy is a critical survival mechanism facilitating protein turnover and pathogen defense in post-mitotic cells in a lysosomal-dependent process. More recently, mitophagy has been identified for arbitrating the selective recognition and targeting of aberrant mitochondria for degradation. Mitochondrial availability is the net result of mitochondrial catabolism via mitophagy and organelle biogenesis. Although the latter process has been well described, mitophagy in skeletal muscle is less understood, and it is currently unknown how these two opposing mechanisms converge during contractile activity. We have previously reported that chronic contractile activity (CCA) of C2C12 myotubes in cell culture, reduced mTORC1 activation, a negative regulator of autophagy, suggesting enhanced autophagy activation with CCA. In the presence of a specific autophagy inhibitor Bafilomycin A1 (BafA), mitochondria exhibited severely compromised state 3 and state 4 respiration, along with increases in reactive oxygen species (ROS) production, LC3-II levels and mitochondrial p62. As previously demonstrated, CCA resulted in an approximately 2-fold increase in mitochondrial COX activity and COXIV protein. In the current study, CCA enhanced mitophagy gene expression, and ameliorated BafA-induced mitochondrial dysfunction, recovering respiration and ROS levels back toward control levels. CCA led to a 50% decline to LC3-II in the presence of BafA, which precisely emulated the reduction observed with N-acetylcysteine (NAC), antioxidant administration. Thus, we reason the CCA-induced

normalization of autophagy occurred through a reduction in oxidant-stress. These findings indicate that contractile activity stabilizes autophagy flux through a reduction in oxidative stress and an amelioration of mitochondrial dysfunction, and may represent a therapeutic intervention to autophagy deregulation by improving mitochondrial and muscle health.

Introduction

Endurance exercise has long been known to evoke favorable molecular adaptations, including an increased inclination for aerobic metabolism in skeletal muscle (18), and conveys a potential therapeutic intervention to muscle wasting (12) and myopathy (56). Chronic contractile-activity (CCA) in skeletal muscle activates a collective transcriptional program of oxidative relevant genes mediated via the PPARγ co-activator 1α (PGC-1α) (52), upregulating features of antioxidant defense (54) and imparts resistance to catabolic stimuli in muscle (11).

Autophagy mediates a pro-survival mechanism via the catabolism of intracellular proteins and pathogens in long-lived post-mitotic cells. Substrates are sequestered in double membranous structures eventually fusing with the lysosome for hydrolytic digestion of autophagic cargo. Selective autophagy is a newly implicated branch of the catabolic process, involving the discrimination of substrates, usually membrane-bound organelles, and in the case of mitophagy, a series of events that identify and localize the mitochondria to the autophagosome. Recently, dysregulation of selective autophagy has sparked interest for its role in the pathophysiology of Parkinson's disease (57), cardiomyopathies (1), and cancer (22, 26, 53). Beyond their bioenergetic role of oxidative phosphorylation (OXPHOS) in eukaryotic cells, mitochondria can radically modulate cellular homeostasis. Aberrant mitochondria participate in cell fate decisions by initiating apoptotic pathways (43), facilitate proinflammatory signaling (40) and

disrupt cellular redox status by elevating reactive species (ROS) production (19, 25, 35). Thus, mitophagy mitigates apoptotic signaling (48) and tempers cellular stress responses by evoking indispensable quality control. Since mtDNA is transmitted through binary fission and is estimated to be 15-fold more vulnerable to oxidant insult and mutations than nuclear DNA (8, 15), the selective degradation of perturbed organelles ensures fitness of the mitochondrial progeny. Mitophagy stimuli include ETC abnormalities (42), mtDNA damage (47), hypoxia (30), and dissipation of the membrane potential ($\Delta\Psi m$) (55).

PTEN-induced putative kinase I (PINK1), is a conserved serine/threonine kinase, possessing an N-terminal mitochondrial targeting sequence (59), with a dense expressional profile in brain, muscle and testes (49). The kinase is believed to function as a mitophagy sensor, arbitrating multi-tiered mitochondrial quality control mechanisms, through import, mitophagy, and fission (6). PINK1 recruits the E3-ubiquitin (Ub) ligase Parkin in a $\Delta\Psi m$-dependent manner, in association with Fbxo7 (4), during depolarization events. Parkin-mediated ubiquitin modification provides a binding scaffold for the autophagy adaptor SQSTM1/p62 (37), and primes mitochondria for degradation independently of the canonical Ub-proteasome system. The microtubule-associated protein 1 light chain 3 beta (LC3b) undergoes post-translational modifications to produce two distinct isoforms LC3-I and LC3-II (24). Cytosolic LC3-I is covalently bound to phosphotidylethanolamine (PE) converting it to LC3-II, a critical lipidation event

involving Atg7/Atg3 conjugation events, permitting the maturation of the autophagosome (41). Targeted substrates are tethered to the autophagosome by means of an LC3-II binding motif on the p62 adaptor protein (27). Localization of the mitochondria to the autophagosome is conditional on the Bcl-2 associated protein NIX, a specific inducer of mitophagy (39).

Mitochondrial ROS (44) and exercise (45) are potent activators of AMPK in skeletal muscle, an energy sensing kinase, shown to induce autophagy in skeletal muscle with activation (44). Several studies have demonstrated an upregulation in bulk-autophagy concomitant to the physiological adaptations to exercise (10, 14, 21, 36) in muscle. Mitochondrial availability is a function of the balance of organelle synthesis and mitophagy. Surprisingly, understanding of how these two mechanisms converge to regulate organelle content remains obscure. Emerging evidence in humans suggests that mitophagy is downregulated with ageing and inactivity, and modified with acute activity (9). A decrement in this process may underlie functional deficits of muscle function with age. We have previously demonstrated that mitophagy markers are upregulated in response to acute exercise (46), but little is known about the implications of autophagy suppression on mitochondrial function and in response to contractile-activity. In this study, we sought to investigate whether contractile activity could offset the mitochondrial insults induced by defective clearance, and hypothesized that mitophagy activation would

be elicited concomitantly with the adaptions to contractile activity to enhance mitochondrial turnover, and improve mitochondrial function.

Methods

Cell culture - C_2C_{12} murine myoblasts (ATCC, Manassas, VA) were proliferated on six-well and 10 cm culture dishes coated with 0.1% gelatin in Dulbecco's modified Eagle's medium (DMEM) (Wisent, St-Bruno, QC) supplemented with 10% FBS (Thermo Scientific, Waltham, MA) and 1% penicillin-streptomycin (P/S). At 90–95% confluency, differentiation into myotubes was induced by replacing growth medium with DMEM supplemented with differentiation media (DM) containing 5% heat-inactivated horse serum (Invitrogen) and 1% P/S. DM was replenished daily for 4 days until fully differentiated myotubes were observed.

Stimulation of muscle cells to induce chronic contractile activity - Lids from plastic six-well and 10 cm dishes were fitted with two platinum wire electrodes such that lengths ran parallel to each other at opposite ends, and when placed in the dish become submerged in media. Fully differentiated myotubes were subjected to electrical stimulation-induced contractile activity in a parallel circuit attached to a stimulator unit at a frequency of 5 Hz and an intensity of 9 V, chronically for 3 h/day over 4 successive

days beginning on *day 4* of differentiation. This stimulation protocol has been previously described in detail (7). Differentiation medium was replenished 1 h prior to stimulation, containing vehicle (anhydrous ethanol) or 3 nM Bafilomycin A1 (BioShop, ON, Canada). Stimulation was performed at 37° C and 5% CO_2, and the media was replenished following stimulation across all conditions.

NAC treatment- C2C12 myoblasts were differentiated as described above. On day four of differentiation, media was supplemented with one of four conditions, vehicle, 10 mM N-Acetyl-L-cysteine (NAC; Sigma-Aldrich), 3 nM BafilomycinA1 (BafA), or 10 mM NAC plus 3 nM BafA. Media containing the indicated concentrations was replenished daily. Following 24 and 72 hours of treatment, cells were lysed as described and the supernatant fraction was used for immunoblotting analysis.

Mitochondrial isolation- Mitochondria were isolated from myotubes in tissue culture using an adapted protocol (32) via differential centrifugation. Briefly, myotubes grown in 10cm plates were washed 2x in ice-cold PBS and scraped on ice using rubber policemen in mitochondrial isolation buffer (MIB; 10% 0.1 M Tris-MOPS, 1% EGTA-Tris, and 20% 1 M sucrose, pH 7.4). Cells were pelleted at a centrifugation speed of 600 g (Beckman JA25.5) for 10 minutes at 4ºC and pellets were resuspended in 3 ml of MIB on ice. Suspensions were transferred to chilled 15ml glass potters and subjected to

homogenization with an Elvehjem PTFE Tissue Grinder (Wheaton, NJ, USA) at 800 rpm for 35 strokes. Homogenates were transferred to fresh isolation tubes and recentrifuged at 600 g. The supernatant fractions containing mitochondria and cytosol were collected and passed through a 40 μm filter (BD Falcon) and the pellet discarded. Filtered homogenates were centrifuged at 9,000 g for 10 min and the resulting mitochondrial fractions were resuspended in 500 μl of MIB and transferred to 1.5 ml Eppendorf tubes. The mitochondrial pellets were subject to a final wash-spin in a microcentrifuge at 9,000 g for 10 min, the supernatants were discarded and the pellets were resuspended in a final volume of 120 μl of MIB. Fresh mitochondria were used immediately for respiration and ROS assays.

Mitochondrial Oxygen Consumption – Fresh mitochondria (100 μl) were incubated with 200 μl of VO_2 buffer (250 mM sucrose, 50 mM KCl, 25 mM Tris base, and 10 mM K_2HPO_4, pH 7.4), and oxygen consumption was measured at 30°C with continuous stirring in a Clark electrode respiratory chamber (Strathkelvin Instruments, North Lanarkshire, Scotland) in the presence of 10 mM glutamate to assess state 4 respiration, followed by glutamate plus 0.44 mM ADP to elicit state 3 respiration. NADH addition during state 3 respiration was used to evaluate the integrity of the inner mitochondrial membrane.

ROS detection- Mitochondrial levels of ROS were quantified using 2',7' dichlorodihydrofluorescein diacetate (D_2DCFDA; Sigma-Aldrich, St. Louis, MO). When oxidized, the compound is converted to the highly fluorescent DCF, with an emission spectrum between 480-520 nm, proportional to levels of ROS. Mitochondria (75 μg) were isolated as described and incubated in VO_2 buffer and D_2DCFDA for 45 min at 37℃, with glutamate (state 4) or glutamate and ADP (state 3). Fluorescence was assessed in a microplate reader using KC4 software and corrected for oxygen consumption for the corresponding state of respiration.

RNA isolation and mRNA expression analysis- Total RNA was isolated from cultured C2C12 myotubes using TRIzol reagent (Invitrogen) according to manufacturer's instructions. RNA concentration and quality was assessed using spectrophotometry (Ultrospec 2100; Biochrom, UK) and further verified with RNA gels. The mRNA expression of PINK1, Parkin, and BNIP3L/NIX was quantified using StepONE Plus PCR System (Applied Biosystems, California, USA) and SYBR® Green Supermix (Quanta Biociences, MD, USA). First-strand cDNA synthesis from 2 μg of total RNA was performed with primers using Superscript III reverse transcriptase and Oligo$(dt)_{20}$ (Invitrogen) according to manufacturer's instructions. Forward and reverse primers were optimized to verify primer efficiency and dissociation melt curves were analyzed for primer specificity. All samples were run in duplicate, simultaneously with negative

controls that contained no cDNA. Final primers were as follows: *LC3b* (FOR: 5'-GCTTGCAGCTCAATGCTAAC-3', REV: 5'-CCTGCGAGGCATAAACCATGT-3'), *PINK1* (FOR: 5'-GCTTGCCAATCCCTTCTATG-3', REV: 5'-CTCTCGCTGGAGCAGTGAC-3'), *Parkin* (FOR: 5'-TGTGACCTGGAACAACAGAGTA-3', REV: 5'-TCAGGTCCACTCGTGTCAA-3'), *Bnip3L* (FOR: 5'-TGAGTGACAGACAGGAAACAGA-3', REV: 5'-GGCCTGAAACATTCCTTACAA-3'), *GAPDH* (FOR: 5'-AACACTGAGCATCTCCCTCA-3', REV: 5'-GTGGGTGCAGCGAACTTTAT-3') and *β2-microglogulin* (FOR: 5'-GCCAAACCCTCTGTACTTCTCA, REV: 5'-TTGGGCACAGTGACAGACTT-3').

Transcript levels were normalized to two housekeeping genes, GAPDH and β_2-microglobulin, and analyzed using the $2^{-\Delta\Delta^{Ct}}$ method. Statistical significance was calculated on Δct values using two-way ANOVA and Boneferroni's post hoc tests.

Fluorescence microscopy- C2C12 cells were plated on glass-bottom 6 well dishes (3.5 mm wells) coated with 0.1% gelatin. When cells reached a confluency of ~80%, they were co-transfected with pBABE GFP-LC3 (Addgene; (23) encoding LC3, which is localized to autophagosome membranes after processing, and pDsRed2-Mito (Clontech, CA, USA), an expression vector that encodes a fusion of red fluorescence protein and the mitochondrial targeting sequence from COX subunit VIII, using Lipofectamine 2000

(Life Technologies, CA, USA). Fluorescence was visualized using an inverted Nikon Eclipse TE2000-U fluorescent microscope equipped with 100x oil objective lens, with a custom designed chamber designed to maintain a constant temperature of 37^{o}C with 5% CO_2. All images were taken at the same exposure and representative images reflect a minimum of 30 images per condition, as well as repeated experiments.

Cytochrome c oxidase (COX) activity assay- Cells were harvested 21 h after the last stimulation period and measurement of COX activity was performed as previously described (52). Briefly, cells were resuspended in 120 µl of enzyme extraction buffer (100 mM Na-K-phosphate, 2 mM EDTA, pH 7.2), sonicated 3 × 3 sec on ice, and subjected to repeated freeze-thaw cycles in liquid N_2. The supernatant fraction containing the enzyme extracts was removed and used to measure COX enzyme activity. COX activity was measured over time as a reduction in absorbance at 550 nm of reduced equine cytochrome c, and activity was quantified using a 96-well plate in a microplate reader (Bio-Tek Synergy HT, Winooski, VT) at 30°C. The data were compiled using KC4 software and corrected for protein concentration to determine COX activity.

Immunoblotting and Protein Extraction- Cultured myotubes were washed 2x with ice-cold PBS and scraped in Passive Lysis Buffer (Promega, Madison WI) supplemented with cOmplete Protease Inhibitor Cocktail Tablets (Roche, Basel, Switzerland). Following extractions, protein

was quantified using the Bradford method. Whole cell and mitochondrial fraction extracts (20–40 μg of protein) were separated using 8-15% SDS-PAGE and then transferred to nitrocellulose membranes. Membranes were blocked in 5% skim milk in TBST buffer for 1 h, and then incubated overnight at 4°C with primary antibodies directed against COXIV (1:1000; Calbiochem), MnSOD (1:000; Upstate Biotechnology), Bnip3L/NIX (1:500; Abcam ab109414), LC3B (1:1000; Cell Signaling #2775), p62/SQSTM1 (1:40,0000; Sigma-Aldrich P0067), aciculin (1:500; in house), VDAC 1:5000 (Abcam). Secondary antibodies were used as per manufacturer's suggestions (Santa-Cruz Biotechnologies).

Statistical analysis- The means and standard errors were calculated for all measured values, and statistical significance between groups was determined by ANOVA with Boneferroni *post-hoc* tests (Graphpad, La Jolla, CA). Results were considered statistically significant when $P \leq 0.05$. Graph bars represent the means and S.E.M.

Results

Mitochondrial dysfunction with autophagy inhibition is ameliorated by chronic contractile activity.

CCA successfully induced mitochondrial biogenesis, resulting in a 1.6-fold increase in cytochrome c oxidase (COX) activity (Fig *2A*). This was corroborated by a significant 2.8-fold increase in cytochrome c oxidase subunit IV (COXIV) protein levels (Figs.

2B,2C). This effect of contractile activity was not observed when autophagy was inhibited by BafA. However, sustained autophagy inhibition invoked the accretion of mitochondria that presumably escape degradation as demonstrated by an increase in mitochondrial enzyme activity. Significant elevations of both COX activity and COXIV protein were observed with BafA treatment alone ($P<0.05$). The combination of BafA treatment with CCA did not lead to an additive response in the quantity of mitochondria.

To assess changes in organelle function, we quantified oxygen consumption in isolated mitochondrial fractions across conditions. As expected state 3 respiration was 3-4-fold greater than state 4 respiration in mitochondria from control cells. BafA treatment produced mitochondria with severe 2.5-3-fold depressions in both state 4 and state 3 respiration (Fig *3A*). CCA did not alter the rates of oxygen consumption observed under control conditions, but successfully reversed the respiratory dysfunction induced by BafA, resulting in a 2-3-fold improvement over the BafA-treated cells, back toward control conditions. Mitochondrial reactive oxygen species (ROS) production was elevated in response to autophagic disruption in state 3 (2.3-fold) and state 4 (1.6-fold) respiration (Fig *3B*). CCA had no effect on ROS production in control, vehicle-treated cells, but ameliorated BafA-induced ROS production and reversed the increase in ROS production by 55% to levels that matched untreated controls. These results indicate that CCA can positively regulate mitochondrial function under conditions of cellular stress, and attenuate the increase in ROS production resulting from autophagic defects. The

effects of CCA on ROS levels in isolated mitochondria were independent of changes in MnSOD, since levels of the protein were unaffected by CCA, but increased by BafA (Fig *3C*,*3D*).

CCA and autophagy suppression induce mitophagy gene expression.

In order to explain some of the molecular mechanisms regulating mitophagy during contractile-activity, relative changes in gene expression of PINK1, Parkin and BNIP3L/NIX were quantified. CCA led to a 2-fold increase in PINK1 mRNA levels (Fig *4*), but had no effect on the ubiquitin E3-Ligase Parkin, or the mitophagy targeting molecule Bnip3L/NIX. In contrast, autophagy suppression with BafA led to a large increase in PINK1 gene expression, as well as more modest changes in Parkin and Bnip3L/NIX ($P < 0.05$).

In vitro fluorescent characterization of autophagy.

To further characterize whether CCA potentiates autophagy and mitochondrial clearance, we employed live-cell imaging of cells transfected with expression vectors encoding GFP-LC3 (23) and DsRed2-Mito. In vehicle-treated control cells, GFP-LC3 exhibited diffuse fluorescence (Fig *5*). Autophagic suppression with BafA considerably upregulated the accretion of autophagosomes observed. CCA appeared to induce a greater frequency of LC3-punctae compared to vehicle, control conditions, indicative of

autophagy induction. However, when CCA was coupled to autophagy disruption, LC3 appeared to be more diffusely redistributed within the cytosol as compared to BafA treatment alone. Co-localization of mitochondria to LC3 did appear to be enhanced in the CCA + BafA group, suggestive of enhanced mitophagy.

LC3-II accretion is reduced following contractile-activity with autophagy inhibition.

We next assessed autophagic flux by examining the levels of autophagy proteins LC3-I and LC3-II, as well as the autophagy substrate p62 using immunobloting. Bafilomycin effectively inhibited flux in C2C12 myotubes (Fig *6A-C*), as shown by a 24-fold accrual in LC3-II protein levels, as well as a 15-fold increase in the LC3-II/LC3-I ratio. CCA had no effect on the very low levels of LC3-II, or on the LC3-II/LC3-I ratio. However, CCA produced a 50% reduction in LC3-II levels ($P<0.001$) with BafA treatment, with a similar significant downregulation in the LC3-II/LC3-I ratio, indicating a reduction in LC3-II formation when autophagy was inhibited. Whole cell p62 levels were also significantly enhanced following BafA treatment (Fig *7A,7C*), accompanied by a dramatic 30-fold increase in p62 levels associated with the isolated mitochondria (Fig *7B,7D*). CCA tended to reduce p62 levels in whole cell lysates ($P=0.06$), and significantly decreased the localization of p62 to mitochondria, indicating a lower drive for mitophagy in the presence of enhanced mitochondrial quality.

N-Acetyl-L-cysteine treatment

In view of the fact that CCA attenuated mitochondrial defects and enhanced autophagy flux, accompanied by a reversal in ROS production in BafA treated groups, we sought to investigate whether these alterations could be mediated by the reduced ROS production. Thus, we treated myotubes with N-Acetyl-L-cysteine (NAC), a thiol antioxidant, to assess the role of ROS in modulating autophagy flux with BafA treatment. NAC reduced LC3-II levels by 50% in myotubes treated with BafA for 72 hrs (Fig *8A*), similar to our observations with CCA (Fig *6*). Further NAC attenuated autophagic flux by 2.4-fold (Fig *8B*). The reductions to LC3-II observed with NAC treatment were independent of alterations in p62 (Fig *8A*), indicating that antioxidant treatment did not affect protein aggregate clearance. These results indicate ROS are key modulators of cellular autophagy flux and directly contribute to autophagy induction in muscle cells.

Discussion

Autophagy is a critical survival mechanism facilitating protein turnover and pathogen defense in post-mitotic cells. The process was first recognized for its cytoprotective role in the re-mobilization of cellular nutrients in response to nutrient duress (50) via inhibition of TOR (38). Failure of autophagy has been linked to congenital muscular dystrophies, and the reinstatement of normal autophagy flux has been shown to ameliorate the dystrophic phenotype and myofibrillar degeneration (13). Muscle-specific

autophagy knockouts, $Atg7^{-/-}$ mice display a loss of fiber-integrity and muscle mass, and the accumulation of abnormal mitochondria (33). Autophagy disruption has been noted in a variety of myopathologies, including sporadic inclusion body myositis (IBM), and polymyositis with mitochondrial pathology (PM-mito) (17), characterized by protein aggregation and progressive muscle weakness. Inefficient clearance of toxic protein aggregates may facilitate decrements in muscle function with pathology or age. In healthy cells, autophagy is a tightly regulated process, and it has consistently been shown to be transiently upregulated in response to exercise in skeletal muscle (14, 20, 28). This is likely because contractile activity induces a host of transcriptional and metabolic alterations that may account for an enhanced autophagy drive. Moreover, the process has been suggested to necessitate the adaptation to a more oxidative phenotype in muscle (29).

Mitochondria are both key mediators of cellular bioenergetics and robust initiators of cellular apoptotic signaling (58), thus mitochondrial quality control is both integral to energy production and cytoprotection (31). Organelle availability reflects a dynamic relationship between catabolism (i.e. mitophagy), and the anabolic process of biogenesis in response to enhanced metabolic demands. Chronic contractile activity (CCA) has been established as an effective model of mitochondrial biogenesis (52), which activates a transcriptional profile resembling the response to chronic treadmill training in mice (3). Muscle contraction results in bursts of ROS (16), as well as 5'AMP-activated kinase

(AMPK) activation, and can mediate the cross-talk between exercise and autophagy through a convergence on mTOR signaling. Downstream AMPK phosphorylation targets include the autophagy-initiator kinase ULK1 (34), along with PGC-1α which positively regulates TFEB (51), a transcription factor important for lysosomal biogenesis. However, the mechanism by which exercise modulates selective autophagy are far from clear cut, and the effects of autophagy suppression on mitochondrial function and content have yet to be investigated. Thus, the purpose of our study was to examine the role of autophagy in the mitochondrial adaptations to contractile activity, and the implications of autophagy suppression on mitochondrial quality, function and content in muscle cells. Our expectation was that a block in autophagy would inhibit mitochondrial turnover via impaired mitophagy, leading to the accumulation of aberrant organelles, and that CCA would counterbalance mitochondrial dysfunction by providing nascent, functional organelles.

To evaluate the effects of autophagy inhibition on the molecular adaptations to chronic contractile activity (CCA), we treated differentiated C2C12 myotubes with a specific inhibitor of the lysosomal V-ATPase Bafilomycin A1 (BafA) for the duration of the CCA protocol to monitor the effects of sustained autophagy deficit on the function and quality of the mitochondria, in order to model the prolonged defects characteristic of pathological states. As previously reported (5, 52), CCA effectively increased mitochondrial content as observed by approximately 2-fold increases in COXIV protein

expression and COX activity. In the absence of CCA, BafA led to severe deficits to mitochondrial respiration. This effect was completely reversed following CCA, indicating that contractile activity led to the production of nascent, functional organelles. This evidence also establishes selective autophagy as an integral mechanism which maintains organelle fitness and function. We demonstrate that contractile activity can rescue the oxidative respiration insult induced by defective mitochondrial turnover. BafA treatment also upregulated the mitophagy-specific genes PINK1, Parkin and BNIP3L, suggesting that defective organelle clearance induces the expression of genes responsible for mitophagy signaling. CCA alone resulted in enhanced PINK1 expression, indicating a heightened reliance on mitochondrial quality-control pathways during contractile activity-induced mitochondrial biogenesis. These findings are in agreement with our recent work which demonstrated a greater mitophagy drive post-exercise in skeletal muscle (46).

Reactive oxygen species are a normal by-product of oxidative phosphorylation, escaping complexes I and III in the process of oxidative phosphorylation. Mitochondrial matrix antioxidants such as manganese superoxide dismutase (MnSOD) efficiently quench superoxide anion radicals, however with mitochondrial dysfunction, free-radicals out-live internal defense systems and this exacerbates the production of intracellular ROS. Excessive ROS levels are known to trigger apoptotic signaling and potentiate muscle wasting stimuli (2). Our results indicate ROS were upregulated with autophagic

inhibition, despite the marked elevation in MnSOD protein with BafA treatment. CCA reversed this increase in ROS production, thereby restoring levels back toward control values. Interestingly, our data reveal that CCA overturned the dysfunctional phenotype induced by aberrant organelle elimination.

To investigate the effects of CCA on autophagy flux, we assessed LC3-II/LC3-I protein levels in the presence of autophagy inhibition. BafA drastically disrupted autophagic flux, resulting in a 25-fold increase in LC3-II accretion. Although CCA alone resulted in an increase in the population of cells with observable GFP-LC3 fluorescent punctae, we did not observe a significant increase in LC3-II protein, or in the ratio of LC3-II/LC3-I. Indeed, the decrease in LC3-II/LC3- ratio with CCA likely indicates a reduced mitophagic requirement, given the higher quality of mitochondria produced with CCA. Consistent with this is the modest reduction in mitochondrial-associated p62 with CCA. A similar phenomenon was recently illustrated by Jiang and colleagues, who found a reduction of flux with exercise following chloroquine treatment (21). The alternate explanation is that CCA enhanced cargo clearance via an increase in lysosomal capacity. This possibility remains to be explored.

We postulated that the observed CCA-associated decrement in ROS could mediate the ability of CCA to re-establish autophagic flux with BafA treatment. To examine this possibility, we co-treated differentiated myotubes with the non-specific antioxidant NAC, along with BafA. Our results indicate that NAC reduced LC3-II

accretion in BafA treated cells to an equivalent extent as CCA, by about 50%. The ability of NAC to reduce autophagosome accretion in this model of autophagy suppression suggests that CCA modulates ROS production to restore autophagy flux. Thus, we speculate that in models of suppressed autophagy, approximately 50% of autophagy flux can be attributed to disruptions in cellular redox status.

In conclusion, our results indicate that CCA mediates a reversal of mitochondrial deficits induced by aberrant autophagy. Thus, contractile activity represents a potential therapeutic intervention against mitochondrial dysfunction in muscle, since it stimulates the production of healthier mitochondria, and therefore normalizes mitophagy flux. These results support the view that mitophagy mediates an indispensable mitochondrial quality control pathway in muscle cells, and that contractile activity can reverse mitophagy defects and contribute to muscle health.

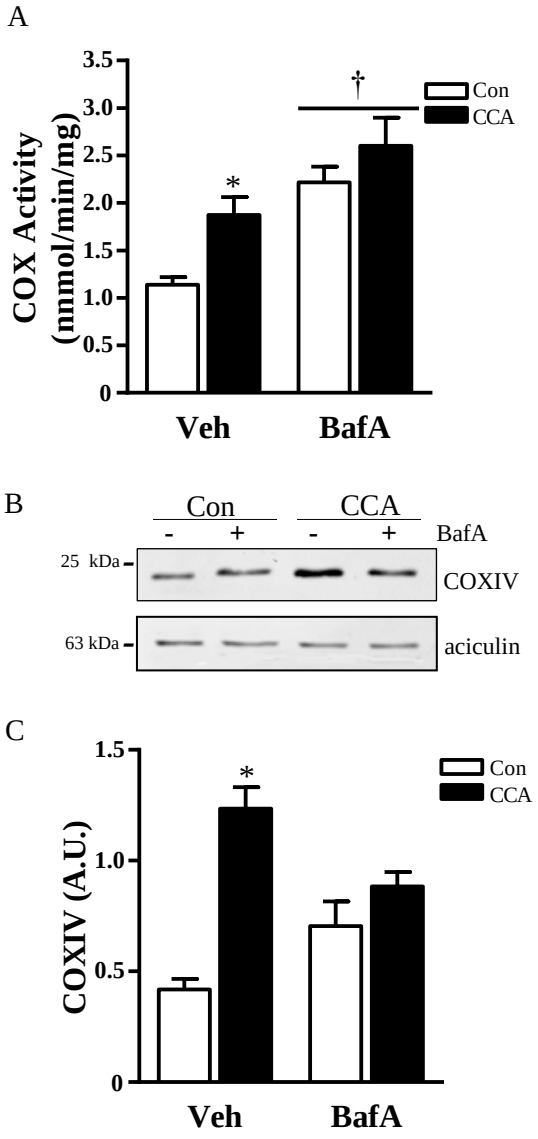

Figure 2: CCA-induced mitochondrial biogenesis. Differentiated myotubes were chronically stimulated to induce mitochondrial biogenesis in the presence of vehicle or Bafilomycin A1 (BafA). *A*: Cytochrome oxidase (COX) activity (**P* < 0.05, vs. vehicle Con; †*P* < 0.05, Main effect of BafA vs. vehicle; n=6) *B*: Representative western-blot of whole cell extracts probed for COXIV and aciculin protein. *C*: Graphical densitometric quantification, COXIV normalized to aciculin. (**P* < 0.001 vs. vehicle Con; *n* = 8). A.U. arbitrary units.

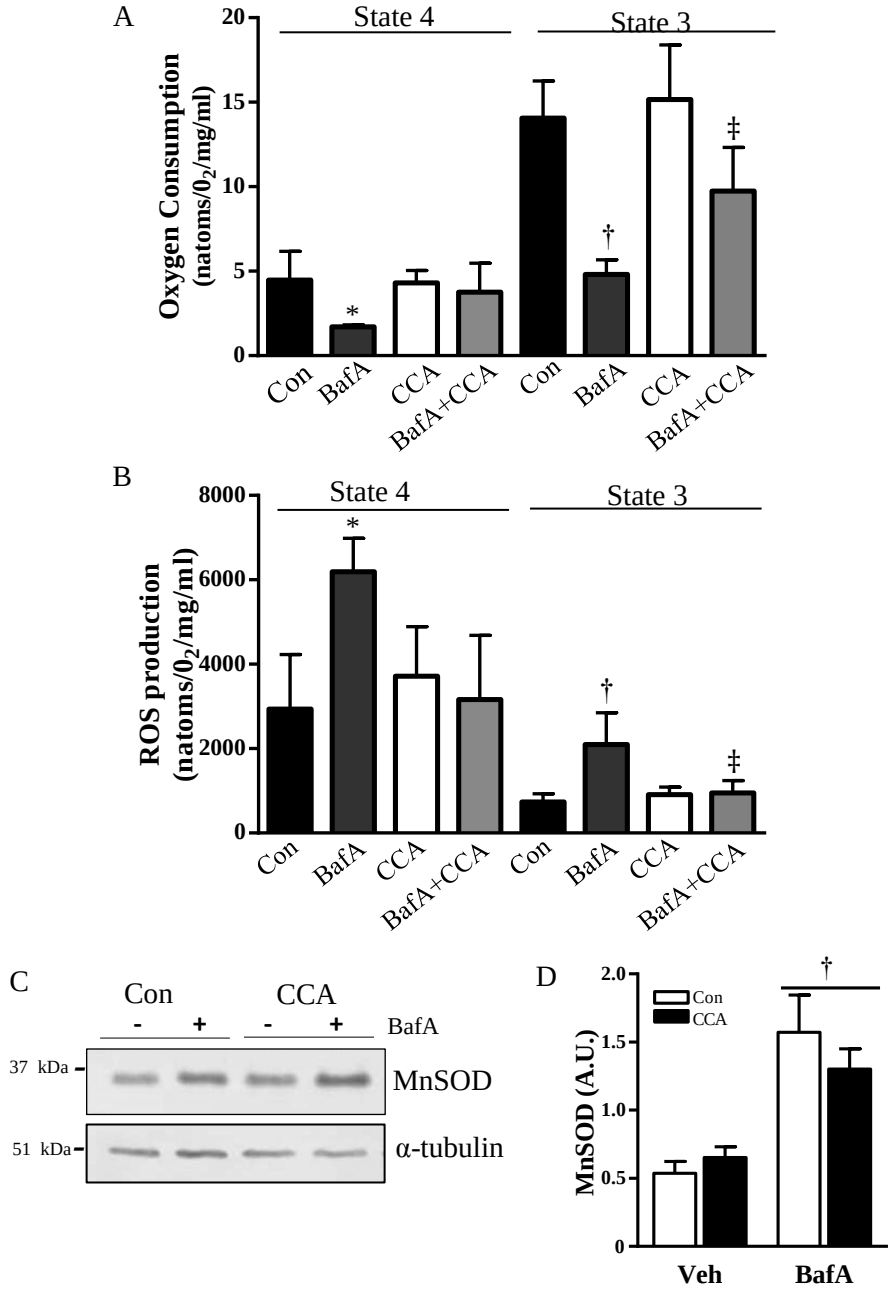

Figure 3: Mitochondrial respiration and ROS production. Mitochondria were isolated from myotube tissue culture by differential centrifugation. State 4 and state 3 respiration were measured and normalized to protein concentration. ROS production was determined on isolated mitochondria and normalized to respiration. *A*: State 4 and state 3 respiration (*$P < 0.05$, vs. Con State 4; †$P < 0.001$, vs. Con State 3; ‡$P < 0.05$,BafA+CCA vs. BafA Con; $n = 4$). *B*: Mitochondrial ROS production (*$P < 0.05$, vs. Con State 4; †$P < 0.001$, vs. Con State 3; ‡$P < 0.05$,BafA+CCA vs. BafA Con; $n = 4$). *C:* Representative western blot of MnSOD protein expression. *D:* Graphical quantification († $P < 0.001$, Main effect of BafA vs. vehicle; $n = 6$). A.U. arbitrary units.

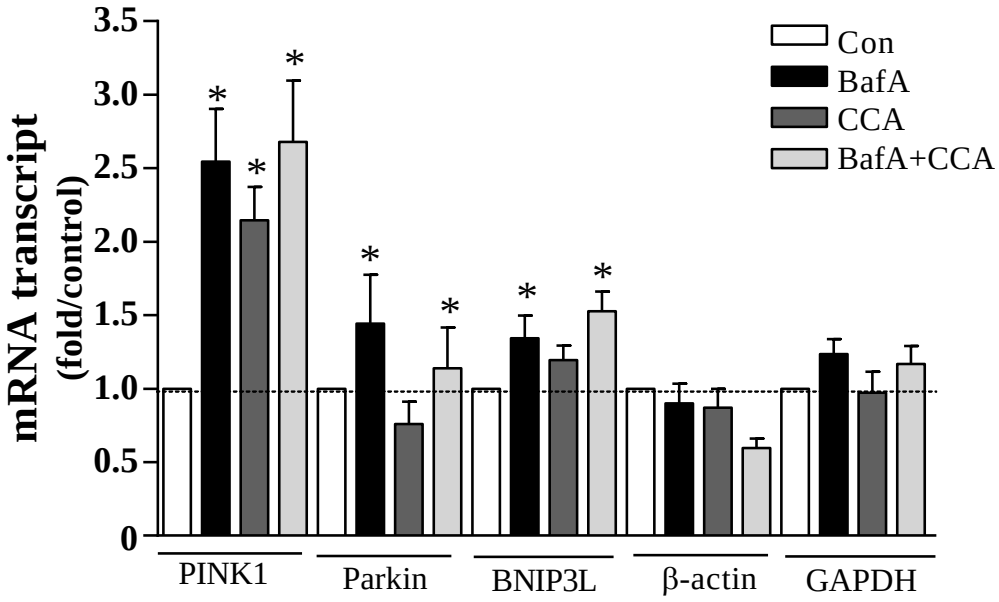

Figure 4: Real-time PCR analysis of mitophagy mRNA expression in control and CCA myotubes, treated with vehicle (Veh) or Bafilomycin A1 (BafA). Transcript levels were normalized to both β-actin and GAPDH (*P < 0.05, vs. control levels of the same transcript).

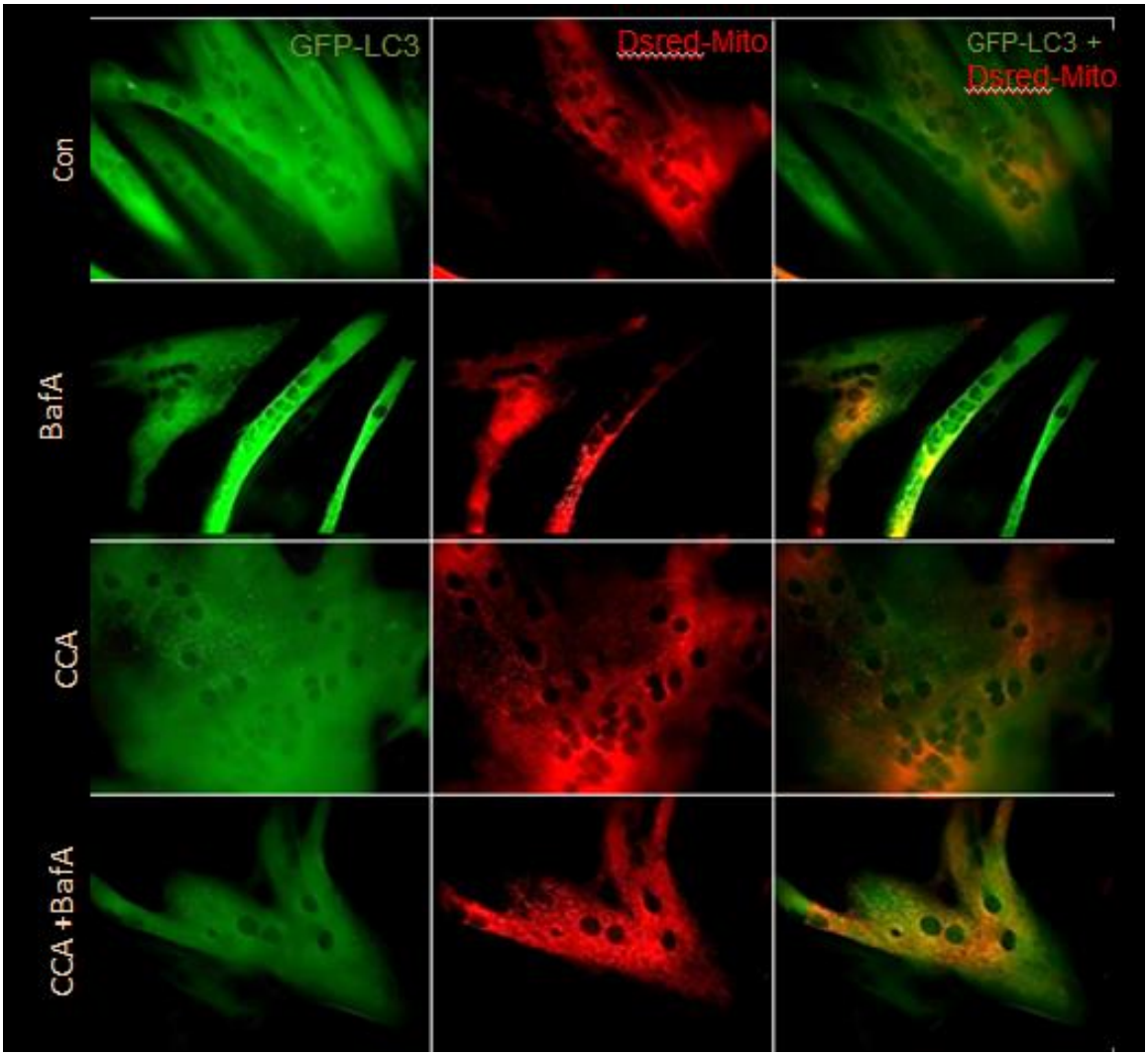

Figure 5: Live-cell fluorescence microscopy of C2C12 myotubes co-expressing GFP-LC3 and mitoDSred at 100x magnification. Fully differentiated myotubes were chronically stimulated to induce mitochondrial biogenesis in the presence of vehicle or Bafilomycin A1.

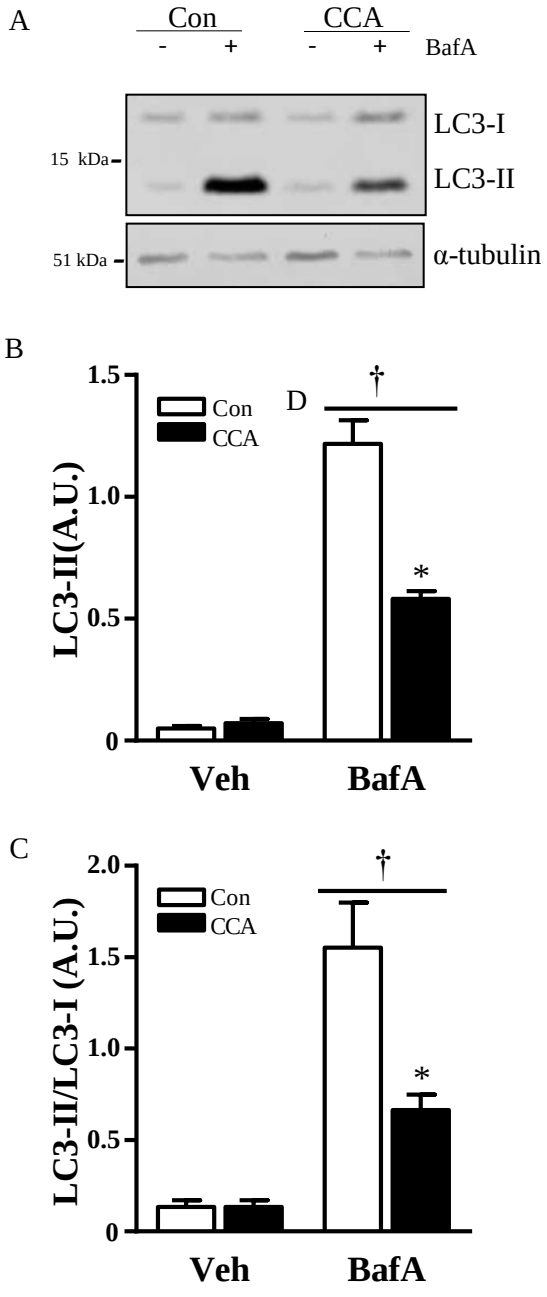

Figure 6: Expression of autophagy proteins in response to CCA in C2C12 myotubes, treated with Bafilomycin A1 (BafA). *A*: Representative western-blot. *B:* Graphical densitometric quantification*;* LC3-II normalized to α-tubulin protein (**P* < 0.001, BafA CCA vs. BafA Con; †*P* < 0.001, Main effect of BafA vs. vehicle *n* = 8). *C*: LC3-II normalized to LC3-I protein (**P* < 0.001, BafA CCA vs. BafA Con; †*P* < 0.001, Main effect of BafA vs. vehicle *n* = 8). A.U. arbitrary units.

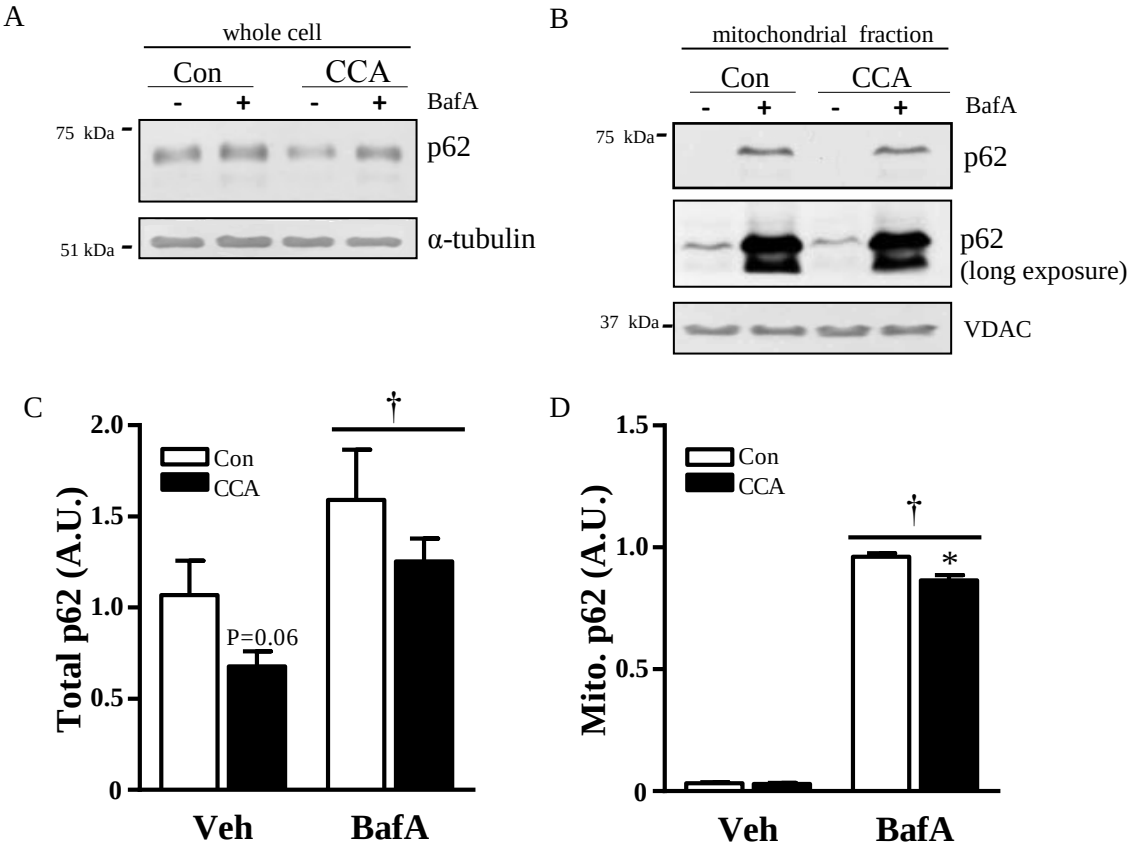

Figure 7: Expression of autophagy proteins in response to CCA in C2C12 myotubes treated with Bafilomycin A1 (BafA). Representative western-blots; *A*: Whole cell extracts and *B:* mitochondrial fractions were probed for p62, VDAC and α-tubulin. Graphical densitometric quantification *C*: Total p62 normalized to α-tubulin (†$P < 0.01$, Main effect of BafA vs. vehicle; P=0.06 vehicle CCA vs. vehicle Con; $n = 5$). *D*: Mitochondrial p62 (†$P < 0.001$, Main effect of BafA vs. vehicle; *$P < 0.01$, BafA Con vs. BafA +CCA; $n = 3$). A.U. arbitrary units.

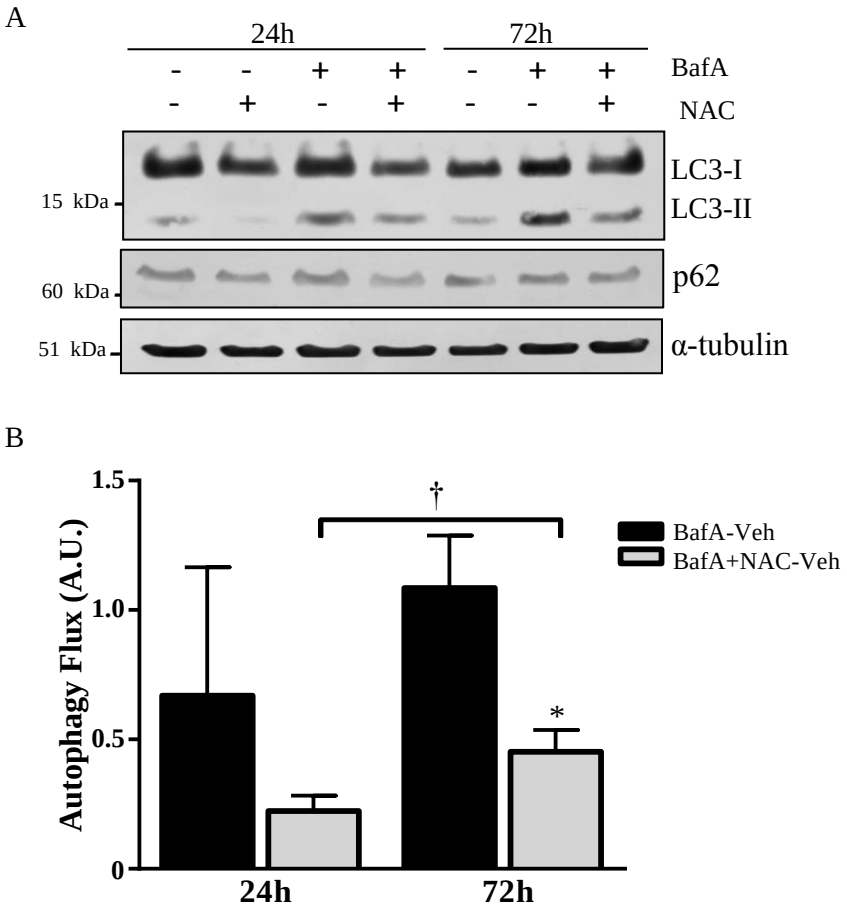

Figure 8: Autophagy flux with co-incubation of NAC (N-Acetylcysteine) and BafA in muscle cells, *A*: Representative western-blots of whole cell extracts probed with LC3, p62 and α-tubulin. *B:* Graphical representation of Autophagy Flux, LC3-II/α-tubulin flux was determined by deducting control levels from BafA/BafA+NAC treated conditions, (†$P < 0.01$, Main effect of NAC treatment; *$P < 0.05$, 72h BafA+NAC vs. 24h BafA; n=3). A.U. arbitrary units.

References

1. **Albin R, Dowell RT, Zak R, Rabinowitz M**. Synthesis and degradation of mitochondrial components in hypertrophied rat heart. *Biochem. J.* 136: 629–37, 1973.

2. **Aucello M, Dobrowolny G, Musarò A**. Localized accumulation of oxidative stress causes muscle atrophy through activation of an autophagic pathway. [Online]. *Autophagy* 5: 527–9, 2009.

3. **Burch N, Arnold A-S, Item F, Summermatter S, Brochmann Santana Santos G, Christe M, Boutellier U, Toigo M, Handschin C**. Electric pulse stimulation of cultured murine muscle cells reproduces gene expression changes of trained mouse muscle. *PLoS One* 5: e10970, 2010.

4. **Burchell VS, Nelson DE, Sanchez-Martinez A, Delgado-Camprubi M, Ivatt RM, Pogson JH, Randle SJ, Wray S, Lewis PA, Houlden H, Abramov AY, Hardy J, Wood NW, Whitworth AJ, Laman H, Plun-Favreau H**. The Parkinson's disease-linked proteins Fbxo7 and Parkin interact to mediate mitophagy. *Nat. Neurosci.* 16: 1257–65, 2013.

5. **Carter HN, Hood DA**. Contractile activity-induced mitochondrial biogenesis and mTORC1. *Am. J. Physiol. Cell Physiol.* 303: C540–7, 2012.

6. **Chu CT**. A pivotal role for PINK1 and autophagy in mitochondrial quality control: implications for Parkinson disease. *Hum. Mol. Genet.* 19: R28–37, 2010.

7. **Connor MK, Irrcher I, Hood DA**. Contractile activity-induced transcriptional activation of cytochrome C involves Sp1 and is proportional to mitochondrial ATP synthesis in C2C12 muscle cells. *J. Biol. Chem.* 276: 15898–904, 2001.

8. **Denver DR, Morris K, Lynch M, Thomas WK**. High mutation rate and predominance of insertions in the Caenorhabditis elegans nuclear genome. *Nature* 430: 679–82, 2004.

9. **Drummond MJ, Addison O, Brunker L, Hopkins PN, McClain DA, Lastayo PC, Marcus RL**. Downregulation of E3 Ubiquitin Ligases and Mitophagy-Related Genes in Skeletal Muscle of Physically Inactive, Frail Older Women: A Cross-

Sectional Comparison. *J. Gerontol. A. Biol. Sci. Med. Sci.* (February 13, 2014). doi: 10.1093/gerona/glu004.

10. **Ferraro E, Giammarioli AM, Chiandotto S, Spoletini I, Rosano G**. Exercise-induced skeletal muscle remodeling and metabolic adaptation: redox signaling and role of autophagy. *Antioxid. Redox Signal.* (January 22, 2014). doi: 10.1089/ars.2013.5773.

11. **Geng T, Li P, Yin X, Yan Z**. PGC-1α promotes nitric oxide antioxidant defenses and inhibits FOXO signaling against cardiac cachexia in mice. *Am. J. Pathol.* 178: 1738–48, 2011.

12. **Gielen S, Sandri M, Kozarez I, Kratzsch J, Teupser D, Thiery J, Erbs S, Mangner N, Lenk K, Hambrecht R, Schuler G, Adams V**. Exercise training attenuates MuRF-1 expression in the skeletal muscle of patients with chronic heart failure independent of age: the randomized Leipzig Exercise Intervention in Chronic Heart Failure and Aging catabolism study. *Circulation* 125: 2716–27, 2012.

13. **Grumati P, Coletto L, Sabatelli P, Cescon M, Angelin A, Bertaggia E, Blaauw B, Urciuolo A, Tiepolo T, Merlini L, Maraldi NM, Bernardi P, Sandri M, Bonaldo P**. Autophagy is defective in collagen VI muscular dystrophies, and its reactivation rescues myofiber degeneration. *Nat. Med.* 16: 1313–20, 2010.

14. **Grumati P, Coletto L, Schiavinato A, Castagnaro S, Bertaggia E, Sandri M, Bonaldo P**. Physical exercise stimulates autophagy in normal skeletal muscles but is detrimental for collagen VI-deficient muscles. *Autophagy* 7: 1415–23, 2011.

15. **Haag-Liautard C, Coffey N, Houle D, Lynch M, Charlesworth B, Keightley PD**. Direct estimation of the mitochondrial DNA mutation rate in Drosophila melanogaster. *PLoS Biol.* 6: e204, 2008.

16. **Heinzel FR, Luo Y, Dodoni G, Boengler K, Petrat F, Di Lisa F, de Groot H, Schulz R, Heusch G**. Formation of reactive oxygen species at increased contraction frequency in rat cardiomyocytes. *Cardiovasc. Res.* 71: 374–82, 2006.

17. **Hiniker A, Daniels BH, Lee HS, Margeta M**. Comparative utility of LC3, p62 and TDP-43 immunohistochemistry in differentiation of inclusion body myositis

from polymyositis and related inflammatory myopathies. *Acta Neuropathol. Commun.* 1: 29, 2013.

18. **Holloszy JO**. Adaptation of skeletal muscle to endurance exercise. *Med. Sci. Sports* 7: 155–64, 1975.

19. **Ishikawa K, Kimura S, Kobayashi A, Sato T, Matsumoto H, Ujiie Y, Nakazato K, Mitsugi M, Maruyama Y**. Increased reactive oxygen species and anti-oxidative response in mitochondrial cardiomyopathy. [Online]. *Circ. J.* 69: 617–20, 2005. http://www.ncbi.nlm.nih.gov/pubmed/15849452 [23 Feb. 2014].

20. **Jamart C, Naslain D, Gilson H, Francaux M**. Higher activation of autophagy in skeletal muscle of mice during endurance exercise in the fasted state. *Am. J. Physiol. Endocrinol. Metab.* 305: E964–74, 2013.

21. **Jiang D, Chen K, Lu X, Gao H, Qin Z, Lin F**. Exercise ameliorates the detrimental effect of chloroquine on skeletal muscles in mice via restoring autophagy flux. *Acta Pharmacol. Sin.* 35: 135–42, 2014.

22. **Jiang X, Li X, Huang H, Jiang F, Lin Z, He H, Chen Y, Yue F, Zou J, He Y, You P, Wang W, Yang W, Zhao H, Lai Y, Wang F, Zhong W, Liu L**. Elevated levels of mitochondrion-associated autophagy inhibitor LRPPRC are associated with poor prognosis in patients with prostate cancer. *Cancer* (January 3, 2014). doi: 10.1002/cncr.28551.

23. **Kabeya Y, Mizushima N, Ueno T, Yamamoto A, Kirisako T, Noda T, Kominami E, Ohsumi Y, Yoshimori T**. LC3, a mammalian homologue of yeast Apg8p, is localized in autophagosome membranes after processing. *EMBO J.* 19: 5720–8, 2000.

24. **Kabeya Y, Mizushima N, Yamamoto A, Oshitani-Okamoto S, Ohsumi Y, Yoshimori T**. LC3, GABARAP and GATE16 localize to autophagosomal membrane depending on form-II formation. *J. Cell Sci.* 117: 2805–12, 2004.

25. **Kumari U, Ya Jun W, Huat Bay B, Lyakhovich A**. Evidence of mitochondrial dysfunction and impaired ROS detoxifying machinery in Fanconi Anemia cells. *Oncogene* 33: 165–72, 2014.

26. **Lehman JJ, Barger PM, Kovacs A, Saffitz JE, Medeiros DM, Kelly DP**. Peroxisome proliferator-activated receptor gamma coactivator-1 promotes cardiac mitochondrial biogenesis. *J. Clin. Invest.* 106: 847–56, 2000.

27. **Lim J, Kim H-W, Youdim MBH, Rhyu IJ, Choe K-M, Oh YJ**. Binding preference of p62 towards LC3-ll during dopaminergic neurotoxin-induced impairment of autophagic flux. [Online]. *Autophagy* 7: 51–60, 2011. http://www.ncbi.nlm.nih.gov/pubmed/21045561 [25 Feb. 2014].

28. **Lira VA, Okutsu M, Zhang M, Greene NP, Laker RC, Breen DS, Hoehn KL, Yan Z**. Autophagy is required for exercise training-induced skeletal muscle adaptation and improvement of physical performance. *FASEB J.* 27: 4184–93, 2013.

29. **Lira VA, Okutsu M, Zhang M, Greene NP, Laker RC, Breen DS, Hoehn KL, Yan Z**. Autophagy is required for exercise training-induced skeletal muscle adaptation and improvement of physical performance. *FASEB J.* 27: 4184–93, 2013.

30. **Liu L, Feng D, Chen G, Chen M, Zheng Q, Song P, Ma Q, Zhu C, Wang R, Qi W, Huang L, Xue P, Li B, Wang X, Jin H, Wang J, Yang F, Liu P, Zhu Y, Sui S, Chen Q**. Mitochondrial outer-membrane protein FUNDC1 mediates hypoxia-induced mitophagy in mammalian cells. *Nat. Cell Biol.* 14: 177–85, 2012.

31. **Lokireddy S, Wijesoma IW, Teng S, Bonala S, Gluckman PD, McFarlane C, Sharma M, Kambadur R**. The ubiquitin ligase Mul1 induces mitophagy in skeletal muscle in response to muscle-wasting stimuli. *Cell Metab.* 16: 613–24, 2012.

32. **Maitra PK, Estabrook RW**. Studies of baker's yeast metabolism. II. The role of adenine nucleotides and inorganic phosphate in the control of respiration during alcohol oxidation. [Online]. *Arch. Biochem. Biophys.* 121: 129–39, 1967.

33. **Masiero E, Agatea L, Mammucari C, Blaauw B, Loro E, Komatsu M, Metzger D, Reggiani C, Schiaffino S, Sandri M**. Autophagy is required to maintain muscle mass. *Cell Metab.* 10: 507–15, 2009.

34. **Mihaylova MM, Shaw RJ**. The AMPK signalling pathway coordinates cell growth, autophagy and metabolism. *Nat. Cell Biol.* 13: 1016–23, 2011.

35. **Murphy MP**. Mitochondrial dysfunction indirectly elevates ROS production by the endoplasmic reticulum. *Cell Metab.* 18: 145–6, 2013.

36. **Nair U, Klionsky DJ**. Activation of autophagy is required for muscle homeostasis during physical exercise. *Autophagy* 7: 1405–6, 2011.

37. **Narendra D, Tanaka A, Suen D-F, Youle RJ**. Parkin is recruited selectively to impaired mitochondria and promotes their autophagy. *J. Cell Biol.* 183: 795–803, 2008.

38. **Noda T**. Tor, a Phosphatidylinositol Kinase Homologue, Controls Autophagy in Yeast. *J. Biol. Chem.* 273: 3963–3966, 1998.

39. **Novak I, Kirkin V, McEwan DG, Zhang J, Wild P, Rozenknop A, Rogov V, Löhr F, Popovic D, Occhipinti A, Reichert AS, Terzic J, Dötsch V, Ney PA, Dikic I**. Nix is a selective autophagy receptor for mitochondrial clearance. *EMBO Rep.* 11: 45–51, 2010.

40. **Oka T, Hikoso S, Yamaguchi O, Taneike M, Takeda T, Tamai T, Oyabu J, Murakawa T, Nakayama H, Nishida K, Akira S, Yamamoto A, Komuro I, Otsu K**. Mitochondrial DNA that escapes from autophagy causes inflammation and heart failure. *Nature* 485: 251–5, 2012.

41. **Otomo C, Metlagel Z, Takaesu G, Otomo T**. Structure of the human ATG12~ATG5 conjugate required for LC3 lipidation in autophagy. *Nat. Struct. Mol. Biol.* 20: 59–66, 2013.

42. **Palikaras K, Tavernarakis N**. Mitophagy in neurodegeneration and aging. *Front. Genet.* 3: 297, 2012.

43. **Petrosillo G, Ruggiero FM, Paradies G**. Role of reactive oxygen species and cardiolipin in the release of cytochrome c from mitochondria. *FASEB J.* 17: 2202–8, 2003.

44. **Rahman M, Mofarrahi M, Kristof AS, Nkengfac B, Harel S, Hussain S**. REACTIVE OXYGEN SPECIES REGULATION OF AUTOPHAGY IN SKELETAL MUSCLES. *Antioxid. Redox Signal.* (November 1, 2013).

45. **Richter EA, Ruderman NB**. AMPK and the biochemistry of exercise: implications for human health and disease. *Biochem. J.* 418: 261–75, 2009.

46. **Saleem A, Carter HN, Hood DA**. p53 is necessary for the adaptive changes in cellular milieu subsequent to an acute bout of endurance exercise. *Am. J. Physiol. Cell Physiol.* 306: C241–9, 2014.

47. **Shokolenko IN, Wilson GL, Alexeyev MF**. Persistent damage induces mitochondrial DNA degradation. *DNA Repair (Amst).* 12: 488–99, 2013.

48. **Tatsuta T, Langer T**. Quality control of mitochondria: protection against neurodegeneration and ageing. *EMBO J.* 27: 306–14, 2008.

49. **Taymans J-M, Van den Haute C, Baekelandt V**. Distribution of PINK1 and LRRK2 in rat and mouse brain. *J. Neurochem.* 98: 951–61, 2006.

50. **Tsukada M, Ohsumi Y**. Isolation and characterization of autophagy-defective mutants of Saccharomyces cerevisiae. *FEBS Lett.* 333: 169–74, 1993.

51. **Tsunemi T, Ashe TD, Morrison BE, Soriano KR, Au J, Roque RAV, Lazarowski ER, Damian VA, Masliah E, La Spada AR**. PGC-1α rescues Huntington's disease proteotoxicity by preventing oxidative stress and promoting TFEB function. *Sci. Transl. Med.* 4: 142ra97, 2012.

52. **Uguccioni G, Hood DA**. The importance of PGC-1α in contractile activity-induced mitochondrial adaptations. *Am. J. Physiol. Endocrinol. Metab.* 300: E361–71, 2011.

53. **Unoki M, Nakamura Y**. Growth-suppressive effects of BPOZ and EGR2, two genes involved in the PTEN signaling pathway. *Oncogene* 20: 4457–65, 2001.

54. **Valle I, Alvarez-Barrientos A, Arza E, Lamas S, Monsalve M**. PGC-1alpha regulates the mitochondrial antioxidant defense system in vascular endothelial cells. *Cardiovasc. Res.* 66: 562–73, 2005.

55. **Wang Y, Nartiss Y, Steipe B, McQuibban GA, Kim PK**. ROS-induced mitochondrial depolarization initiates PARK2/PARKIN-dependent mitochondrial degradation by autophagy. *Autophagy* 8: 1462–76, 2012.

56. **Wenz T, Diaz F, Hernandez D, Moraes CT**. Endurance exercise is protective for mice with mitochondrial myopathy. *J. Appl. Physiol.* 106: 1712–9, 2009.

57. **Yang Q, Mao Z**. Dysregulation of autophagy and Parkinson's disease: the MEF2D link. *Apoptosis* 15: 1410–4, 2010.

58. **Yang Y, Xing D, Zhou F, Chen Q**. Mitochondrial autophagy protects against heat shock-induced apoptosis through reducing cytosolic cytochrome c release and downstream caspase-3 activation. *Biochem. Biophys. Res. Commun.* 395: 190–5, 2010.

59. **Zhou C, Huang Y, Shao Y, May J, Prou D, Perier C, Dauer W, Schon EA, Przedborski S**. The kinase domain of mitochondrial PINK1 faces the cytoplasm. *Proc. Natl. Acad. Sci. U. S. A.* 105: 12022–7, 2008.

Future Work

1. We document that autophagy is an integral process mediating mitochondrial homeostasis in muscle cells. Future work could involve in-depth assessment of the response of mitophagy to exercise, and the response of lysosomal biogenesis and enzymes in response to CCA. Further, we could apply a combination of genetic and pharmacological interventions of inducing and inhibiting autophagy to assess the role of this process in regulating muscle mass and mitochondrial content in models of use, disuse and pathology.

2. Since PINK1 mRNA levels were found to be upregulated in response to contractile activity in muscle cells, to further elucidate the role of PINK1 in contractile activity we could use siRNA-mediated knockdown and visualize mitochondrial dynamics in myoblasts and myotubes to assess the role of the kinase in muscle mitochondria. Further, we could knockdown key autophagy proteins such as ULK1 or ATG7 in muscle cells in culture as a genetic approach to autophagy suppression, in order to gauge the implications for muscle homeostasis. Inflammatory cytokines (TNF-α, IL-6, IL-1) could be used as indices of muscle health, and can be measured in response to autophagy protein abrogation in conjunction with indices of mitochondrial health. The same chronic contractile activity protocol (3h x 4d) could be utilized to assess the effects of

such knockdown on the mitochondrial adaptations to contractile activity. TUNEL assays may be performed to measure the implications of mitophagy on whole cell viability, and apoptotic markers such as cytosolic AIF and cytochrome c, could be all measured in response to CCA in order to determine if contractile activity could mediate a cytoprotective response.

Conversely, cells could be treated with autophagy inducing agents such as mTOR-dependent Rapamycin, or mTOR-independent inducers such as Clonadine and Trehalose and mitochondrial markers and adaptations could be assessed in response to CCA. Mitochondrial turnover could be visually assessed (fluorescence microscopy) in response to CCA in vitro using DsRed1-E5/Mito-timer, a fluorescent probe that gradually transitions from red to green over time and allows for ratio-metric calculations to examine organelle turnover. This will provide novel insights on the influence of contractile activity on rates of mitochondrial turnover.

2. To further elucidate the role of autophagy in skeletal muscle and mitochondrial quality, we could confirm our present findings in animal models. Autophagy-activators could be administered to mouse models undergoing models of use (exercise) and disuse (denervation) to monitor whether there is any effect on skeletal muscle mass (attenuation or preservation) in response to elevated autophagy. PINK1 immunohistochemistry can be performed on muscle-cross-sections to determine the localization and prevalence of

the protein in muscle. Immunohistochemistry of muscle cross-sections during conditions of use and disuse can be similarly assessed for several mitochondrial targeted proteins, such as BNIP3L, Parkin, Trap1 and the mitochondrial anti-apototic protein Bcl-2.

Appendix A: Data and Statistical Analyses

Table 2A. Individual values and Statistical analysis for COX Activity Assay

N	Vehicle		3 nM BafA	
	Control	**CCA**	**Control**	**CCA**
1	1.382	1.794	2.738	2.792
2	1.267	1.768	2.494	3.425
3	0.845	1.179	1.663	2.283
4	1.223	2.013	2.342	1.347
5	1.228	1.873	2.355	3.061
6	1.187	2.61	2.366	2.707
Average	1.188	1.872	2.326	2.602
Std. Dev	0.165	0.420	0.326	0.659
Std. Error	0.074	0.188	0.146	0.295

Two Way ANOVA- Control vs. CCA		
Source of Variation	P value summary	Significant?
Interaction	ns	No
CCA	**	Yes
Drug	***	Yes

Bonferroni post tests- Control vs. CCA				
Treatment	Difference	t	P Value	Summary
Vehicle	0.735	2.749	P < 0.05	*
Bafilomycin A1	0.385	1.44	P > 0.05	ns

Table 2B. Individual values and Statistical analysis for COXIV protein

N	Vehicle		3 nM BafA	
	Control	CCA	Control	CCA
1	0.476	1.650	0.506	1.047
2	0.502	1.176	0.845	1.000
3	0.459	1.231	0.310	0.582
4	0.405	1.364	0.716	0.918
5	0.400	0.660	0.645	1.040
6	0.385	1.304	0.415	0.869
7	0.587	1.295	0.906	0.726
8	0.131	1.200	1.291	
Average	0.437	1.230	0.572	0.909
Std. Dev	0.125	0.257	0.296	0.161
Std. Error	0.019	0.132	0.081	0.071

Two Way ANOVA- Control vs. CCA		
Source of Variation	P value summary	Significant?
Interaction	***	Yes
CCA	***	Yes
Drug	ns	No

Bonferroni post tests- Control vs. CCA				
Treatment	Difference	t	P Value	Summary
Vehicle	0.816	6.869	P<0.001	***
Bafilomycin A1	0.179	1.454	P > 0.05	ns

Table 3Ai. Individual values and Statistical analysis for State 4 Respiration

N	Vehicle		3 nM BafA	
	Control	CCA	Control	CCA
1	4.730	5.220	1.590	4.610
2	3.950	3.620	1.820	5.760
3	6.650	4.580	1.810	2.260
4	2.551	3.811	1.614	2.386
Average	4.470	4.308	1.708	3.754
Std. Dev	1.481	0.638	0.107	1.488
Std. Error	0.855	0.368	0.062	0.859

Two Way ANOVA- Control vs. CCA		
Source of Variation	P value summary	Significant?
Interaction	ns	No
CCA	ns	No
Drug	*	Yes

Bonferroni post tests- Control vs. CCA				
Treatment	Difference	t	P Value	Summary
Vehicle	-0.163	0.181	P > 0.05	ns
Bafilomycin A1	2.046	2.281	P > 0.05	ns

Table 3A ii. Individual values and Statistical analysis for State 3 Respiration

N	Vehicle		3 nM BafA	
	Control	CCA	Control	CCA
1	16.810	18.520	3.900	13.180
2	14.480	14.770	5.730	9.080
3	11.540	10.890	4.300	6.960
4	13.399	16.476	5.328	9.743
Average	14.057	15.164	4.814	9.741
Std. Dev	1.906	2.802	0.742	2.236
Std. Error	1.100	1.618	0.428	1.291

Two Way ANOVA- Control vs. CCA		
Source of Variation	P value summary	Significant?
Interaction	ns	No
CCA	*	Yes
Drug	***	Yes

Bonferroni post tests- Control vs. CCA				
Treatment	Difference	t	P Value	Summary
Vehicle	1.107	0.657	P > 0.05	ns
Bafilomycin A1	4.926	2.924	P < 0.05	*

Table 3B i. Individual values and Statistical analysis for State 4 ROS

N	Vehicle		3 nM BafA	
	Control	CCA	Control	CCA
1	1844.54	4239.62	6847.00	2047.15
2	3689.90	5113.48	5266.83	1674.78
3	1838.43	2583.27	5794.59	4362.09
4	4372.54	2920.55	6855.11	4576.16
Average	2936.35	3714.23	6190.88	3165.05
Std. Dev	1121.16	1017.71	686.04	1312.89
Std. Error	647.30	587.57	396.09	758.00

Two Way ANOVA- Control vs. CCA		
Source of Variation	P value summary	Significant?
Interaction	**	Yes
CCA	ns	No
Drug	*	Yes

Bonferroni post tests- Control vs. CCA				
Treatment	Difference	t	P Value	Summary
Vehicle	777.9	0.900	P > 0.05	ns
Bafilomycin A1	-3026	3.499	P<0.01	**

Table 3B ii. Individual values and Statistical analysis for State 3 ROS

N	Vehicle		3 nM BafA	
	Control	CCA	Control	CCA
1	452.462	1015.000	3013.154	735.308
2	793.774	974.416	1229.512	696.645
3	883.530	1011.370	2283.880	1320.810
4	821.795	636.270	1872.770	1042.050
Average	737.890	909.264	2099.829	948.703
Std. Dev	167.961	158.411	647.504	253.105
Std. Error	96.972	91.459	373.837	146.130

Two Way ANOVA- Control vs. CCA		
Source of Variation	P value summary	Significant?
Interaction	**	Yes
CCA	*	Yes
Drug	**	Yes

Bonferroni post tests- Control vs. CCA				
Treatment	Difference	t	P Value	Summary
Vehicle	171.4	0.573	P > 0.05	ns
Bafilomycin A1	-1151	3.849	P<0.01	**

Table 3D. Individual values and Statistical analysis for MnSOD protein

N	Vehicle		3 nM BafA	
	Control	CCA	Control	CCA
1	0.602	0.624	1.679	1.240
2	0.805	0.362	2.079	1.137
3	0.105	0.714	0.390	1.495
4	0.397	0.528	1.337	1.188
5	0.656	0.691	1.647	1.134
6	0.505	1.043	2.293	2.078
7	0.683	0.601		0.834
Average	0.512	0.660	1.571	1.379
Std. Dev	0.213	0.193	0.612	0.366
Std. Error	0.099	0.093	0.274	0.150

Two Way ANOVA- Control vs. CCA		
Source of Variation	P value summary	Significant?
Interaction	ns	No
CCA	ns	No
Drug	***	Yes

Bonferroni post-tests- Control vs. CCA				
Treatment	Difference	t	P Value	Summary
Vehicle	0.1157	0.536	P > 0.05	ns
Bafilomycin A1	-0.2701	1.201	P > 0.05	ns

Table 4A i. Individual values and Statistical analysis for PINK1 mRNA normalized to 2 house keeping genes.

N	Vehicle		3 nM BafA	
	Control	CCA	Control	CCA
1	105.702	136.751	202.248	250.936
2	95.022	197.010	275.584	325.643
3	100.380	106.235	265.523	202.215
4	88.802	142.303	154.598	128.969
5	91.507	228.270	222.378	291.564
6	116.528	218.342	307.040	103.588
7	81.841	254.281	451.888	440.725
8	101.039	161.530	250.683	210.388
9	87.905	206.753	284.408	343.610
10	90.581	154.297	203.386	187.575
Average	99.657	171.485	237.895	217.152
Std. Dev	9.701	44.866	77.163	98.639
Std. Error	4.193	20.320	22.668	36.215

Two Way ANOVA- Control vs. CCA		
Source of Variation	P value summary	Significant?
Interaction	*	Yes
CCA	ns	No
Drug	***	Yes

Bonferroni post-tests- Control vs. CCA				
Treatment	Difference	t	P Value	Summary
Vehicle	84.65	2.704	P < 0.05	*
Bafilomycin A1	-13.25	0.423	P > 0.05	ns

Table 4A ii. Individual values and Statistical analysis for Parkin mRNA normalized to 2 house keeping genes.

N	Vehicle		3 nM BafA	
	Control	CCA	Control	CCA
1	11.021	9.603	21.533	17.735
2	11.045	15.004	38.184	34.705
3	12.504	5.892	27.176	17.753
4	12.159	20.789	21.516	8.673
5	11.325	9.213	17.039	9.640
6	10.687	7.848	21.442	14.283
7	9.264	1.806	6.246	4.598
8	9.225	2.109	4.753	2.687
9	9.016	5.152	6.967	12.816
10	11.168	12.061	15.480	6.525
Average	11.457	11.391	24.482	17.131
Std. Dev	1.172	5.615	10.044	8.846
Std. Error	0.292	2.252	3.039	3.853

Two Way ANOVA- Control vs. CCA		
Source of Variation	P value summary	Significant?
Interaction	ns	No
CCA	ns	No
Drug	*	Yes

Bonferroni post-tests- Control vs. CCA				
Treatment	Difference	t	P Value	Summary
Vehicle	-1.794	0.530	P > 0.05	ns
Bafilomycin A1	-5.092	1.505	P > 0.05	ns

Table 4A iii. Individual values and Statistical analysis for Bnip3L mRNA normalized to 2 house keeping genes.

N	Vehicle		3 nM BafA	
	Control	CCA	Control	CCA
1	318.540	559.680	515.070	695.031
2	336.193	370.173	443.701	624.447
3	347.229	334.286	500.443	509.594
4	394.969	366.214	463.230	398.808
5	348.628	460.699	506.872	648.878
6	304.579	467.252	642.918	532.337
7	239.452	196.273	461.043	423.882
8	333.742	197.555	373.908	333.776
9	348.429	397.631	511.082	487.193
10	375.320	249.804	347.029	368.682
Average	341.689	426.384	512.039	568.182
Std. Dev	40.137	115.362	78.612	119.079
Std. Error	12.729	34.582	28.491	44.412

Two Way ANOVA- Control vs. CCA		
Source of Variation	P value summary	Significant?
Interaction	ns	No
CCA	ns	No
Drug	***	Yes

Bonferroni post-tests- Control vs. CCA				
Treatment	Difference	t	P Value	Summary
Vehicle	25.25	0.578	P > 0.05	ns
Bafilomycin A1	25.73	0.589	P > 0.05	ns

Table 6B. Individual values and Statistical analysis for LC3-II protein

N	Vehicle		3 nM BafA	
	Control	CCA	Control	CCA
1	0.021	0.024	1.000	0.571
2	0.030	0.039	1.761	0.517
3	0.084	0.038	1.395	0.436
4	0.023	0.027	1.390	0.707
5	0.088	0.056	1.000	0.566
6	0.024	0.145	1.000	0.686
7	0.080	0.118	1.092	0.637
8	0.050	0.122	1.100	0.535
Average	0.045	0.055	1.258	0.580
Std. Dev	0.028	0.046	0.257	0.085
Std. Error	0.013	0.019	0.128	0.042

Two Way ANOVA- Control vs. CCA		
Source of Variation	P value summary	Significant?
Interaction	***	Yes
CCA	***	Yes
Drug	***	Yes

Bonferroni post-tests- Control vs. CCA				
Treatment	Difference	t	P Value	Summary
Vehicle	0.021	0.288	P > 0.05	ns
Bafilomycin A1	-0.635	8.619	P<0.001	***

Table 6C. Individual values and Statistical analysis for LC3-II:LC3I protein ratio

N	Vehicle		3 nM BafA	
	Control	CCA	Control	CCA
1	0.023	0.029	1.000	0.976
2	0.154	0.248	1.632	0.472
3	0.159	0.276	1.650	0.502
4	0.061	0.180	1.423	0.486
5	0.092	0.055	1.042	0.382
6	0.030	0.125	1.000	0.863
7	0.231	0.168	1.560	0.653
8	0.318	0.505	3.119	0.969
Average	0.086	0.152	1.291	0.614
Std. Dev	0.098	0.142	0.654	0.225
Std. Error	0.024	0.041	0.128	0.099

Two Way ANOVA- Control vs. CCA		
Source of Variation	P value summary	Significant?
Interaction	**	Yes
CCA	**	Yes
Drug	***	Yes

Bonferroni post-tests- Control vs. CCA				
Treatment	Difference	t	P Value	Summary
Vehicle	0.064	0.343	P > 0.05	ns
Bafilomycin A1	-0.890	4.714	P<0.001	***

Table 7C. Individual values and Statistical analysis for whole cell p62 protein

N	Vehicle		3 nM BafA	
	Control	CCA	Control	CCA
1	0.929	0.648	0.959	1.470
2	1.185	0.674	2.011	1.401
3	0.702	0.613	1.639	0.811
4	1.093	0.597	1.482	1.302
5	0.615	1.061	2.637	1.593
6	1.892	0.477	0.817	0.941
Average	1.069	0.678	1.591	1.253
Std. Dev	0.419	0.182	0.617	0.283
Std. Error	0.187	0.081	0.276	0.126

Two Way ANOVA- Control vs. CCA		
Source of Variation	P value summary	Significant?
Interaction	ns	p<0.06
CCA	ns	No
Drug	**	Yes

Bonferroni post-tests- Control vs. CCA				
Treatment	Difference	t	P Value	Summary
Vehicle	-0.391	1.512	P > 0.05	ns
Bafilomycin A1	-0.338	1.307	P > 0.05	ns

Table 7D. Individual values and Statistical analysis for mitochondrial-associated p62 protein

N	Vehicle		3 nM BafA	
	Control	CCA	Control	CCA
1	0.037	0.038	0.949	0.847
2	0.024	0.023	0.991	0.839
3	0.035	0.026	0.943	0.909
Average	0.032	0.029	0.961	0.865
Std. Dev	0.006	0.007	0.021	0.031
Std. Error	0.004	0.005	0.015	0.022

Two Way ANOVA- Control vs. CCA		
Source of Variation	P value summary	Significant?
Interaction	**	Yes
CCA	**	Yes
Drug	***	Yes

Bonferroni post-tests- Control vs. CCA				
Treatment	Difference	t	P Value	Summary
Vehicle	-0.003	0.146	P > 0.05	ns
Bafilomycin A1	-0.096	4.946	P<0.01	**

Table 8B. Individual values and Statistical analysis for NAC + BafA treated myotubes

N	24 Hours				72 Hours		
	Vehicle	**NAC**	**BafA**	**BafA + NAC**	**Vehicle**	**BafA**	**BafA + NAC**
1	0.229	0.034	0.812	0.488	0.243	1.200	0.604
2	0.187	0.010	0.410	0.443	0.161	1.479	0.630
3	0.048	0.010	1.250	0.203	0.091	1.072	0.618
Average	0.155	0.018	0.824	0.378	0.165	1.251	0.617
Std. Dev	0.077	0.012	0.343	0.125	0.062	0.170	0.010
Std. Error	0.055	0.008	0.243	0.088	0.044	0.120	0.007

Bonferroni's Multiple Comparison Test	**Mean Diff.**	**t**	**P value**	**95% CI of diff**
Vehicle vs BafA	-0.669	4.267	P < 0.05	-1.250 to -0.089
Vehicle vs BafA	-1.096	6.986	P < 0.001	-1.676 to -0.515
NAC vs BafA	-0.806	5.138	P < 0.01	-1.386 to -0.225
NAC vs BafA	-1.232	7.857	P < 0.001	-1.813 to -0.652
NAC vs BafA + NAC	-0.599	3.820	P < 0.05	-1.179 to -0.018
BafA vs Vehicle	0.659	4.201	P < 0.05	0.078 to 1.239
BafA + NAC vs BafA	-0.872	5.561	P < 0.01	-1.452 to -0.292
Vehicle vs BafA	-1.085	6.920	P < 0.001	-1.666 to -0.505
BafA vs BafA + NAC	0.633	4.038	P < 0.05	0.053 to 1.214

Table 8B. contd.

Autophagy Flux LC3II

Two Way ANOVA-		
Source of Variation	P value summary	Significant?
Interaction	ns	No
Drug	**	Yes
Time	ns	No

Bonferroni post-tests- Control vs. CCA				
Treatment	Difference	t	P Value	Summary
24h	-0.445	2.003	P > 0.05	ns
72h	-0.633	2.847	P < 0.05	*

Appendix B: Additional Data

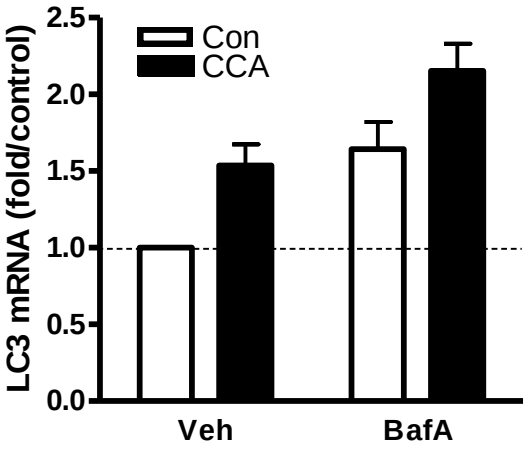

Supp. Figure 1: Real-time PCR analysis of LC3 mRNA expression in control and CCA myotubes, treated with vehicle (Veh) or Bafilomycin A1 (BafA). Transcript levels were normalized to both β-actin and GAPDH.

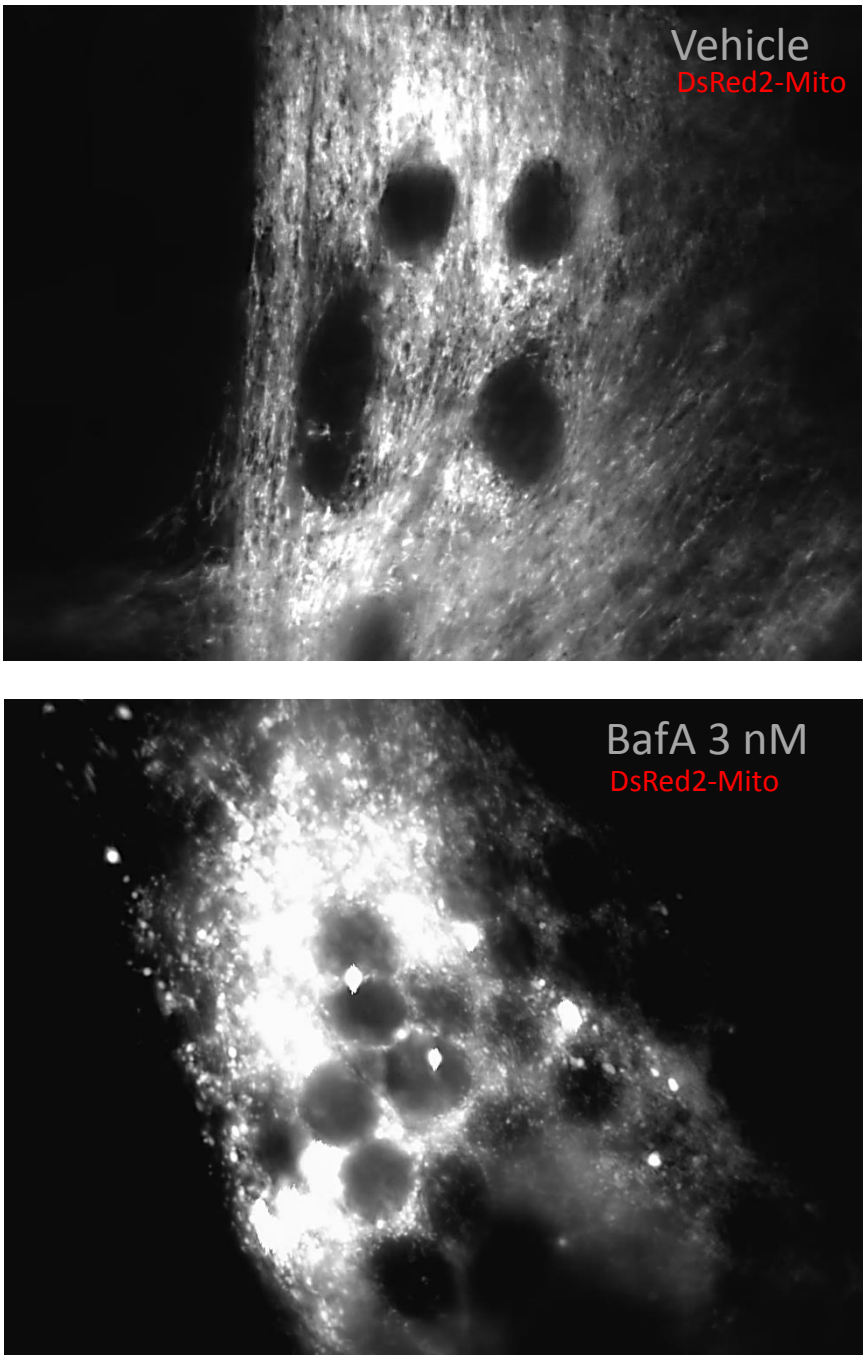

Supp. Figure 2: Mitochondrial morphology with autophagy suppression. Live-cell fluorescent mitochondrial visualization in C2C12 myotubes transfected with mitoDSred at 100x magnification in the presence of vehicle or Bafilomycin A1.

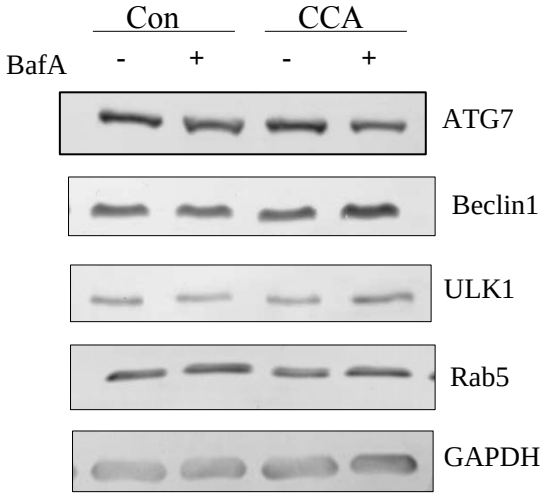

Supp. Figure 3: Representative western-blot of whole cell extracts probed for ATG7, Beclin1, ULK1, Rab5 and GAPDH protein.

Appendix C: Laboratory Methods and Protocols

Cell Culture

Cells

1. C2C12 murine skeletal muscle cells (ATCC, CRL-1772)

Materials

1. Dulbecco's Modified Eagle's Medium (DMEM; Sigma D-5796/500ml)
2. Fetal Bovine Serum (FBS; Fisher Scientifitc SH3039603C/500ml)
    a. Aliquoted into 50ml sterile conical tubes and stored at -20°C
3. Penicillin/Streptomycin (P/S; Invitrogen 15140-122/100ml)
    a. Sterile aliquots of 6mls and stored at -20°C)
4. Horse Serum (HS; Invitrogen 16050-114/1000ml)
    a. Aliquoted into 50ml sterile conical tubes and stored at -20°C
    b. Heat-inactivated for 30 minutes at 56.0°C
5. 0.25% Trypsin-EDTA (1x), phenol red (Invitrogen 25200-072/500ml)
    a. Sterile aliquots of 30mls stored at -20°C
6. Dulbecco's Phosphate Buffered Saline (PBS; Sigma D-8537/500ml)
7. 15ml conical tubes, sterile (BD Falcon 352097)
8. 50ml conical tubes, sterile (BD Falcon 352098)
9. 175cm^2 canted/vented tissue cultured flasks (BD Falcon 353112)
10. 6-well sterile tissue culture dish (Sarstedt 83.1839.300)
11. Gelatin (Sigma G1890)
    a. 0.1% solution autoclaved for sterilization

Procedure

1. Allow myoblasts to proliferate in 175cm^2 flask with growth medium (GM; DMEM supplemented with 10% FBS and 1% P/S) until 70% confluent.
2. Prepare six 6-well dishes for plating by coating the bottom surface with 0.1% gelatin and allow to fully dry in laminar flow hood.
3. Pre-heat GM, trypsin and PBS in 37°C water bath for 30 minutes prior to use.

4. Discard old GM from tissue culture flask and wash with 10mL of PBS to rinse off remaining GM.
5. Apply 5mL of trypsin in the flask and place in the incubator at 37°C for 3 minutes.
6. Remove flask from incubator and gently knock sides of the flask to ensure cells are lifted from flask bottom. Remove trypsin with cells and place into a sterile 15mL conical tube.
7. Rinse flask with 5mls GM and add to sterile 15mL conical tube containing the cells.
8. Spin tube for 3 minutes at 1400rpm at room temperature.
9. Discard the supernatant and add 1mL of GM for resuspension with 1ml pipette.
10. Add 3mL of GM to resuspended cell mixture for a total volume of 4mL.
11. Fill each well of tissue culture dishes with 2mls of GM and add 100µl of cell mixture to each well.
12. Rotate plate in a circular motion for 30 sec and subsequently place into 37°C incubator overnight.
13. The following day remove GM from cells and replace with differentiation medium (DM; DMEM supplemented with 5% heat-inactivated HS and 1% P/S) once myoblasts are 90-95% confluent.
14. Refresh DM every other day. Mature myotubes will form after five days and be ready for contractile activity.

Cell Harvesting From Plates for Enzyme Assays

1. Grow cells up in two 10 cm dishes.
2. Pour off the medium. Wash each plate twice with 5 ml cold Dulbecco's Phosphate Buffered Saline (DPBS; Sigma D-5527) without EDTA. Discard and keep the plates on ice during the entire procedure. Remove all of the DPBS the second time to avoid excessive volume at the end.
3. Add 0.8 ml of cold DPBS to plate A. Scrape with rubber policeman and transfer to plate B. Scrape and add to a pre-labelled eppendorf tube with a hole on the top.
4. Spin the cells at 4 ^{o}C for 3 min at 13.0 rpm in a microcentrifuge. Discard the supernate with a Pasteur pipette.
5. Add 100 µl enzyme extraction buffer and vortex vigorously to disperse the pellet.
6. Sonicate 3 x 3 sec on ice, make sure that the sonicator is set to 30.
7. Freeze in liq N_2 and thaw 5 min at 37 ^{o}C. Vortex vigorously for 5 sec.
8. Spin in microcentrifuge at 4 ^{o}C for 5 min at 13.0 rpm.
9. Remove the supernate and add it to a new labelled eppendorf tube with a hole on the top.
10. Add 100 µl enzyme extraction buffer to the pellet and vortex vigorously.
11. Repeat steps 5 to 7. For the last spin in the microcentrifuge spin the samples for 5 minutes at 13.0 rpm.
12. Combine the supernates and use immediately for enzyme assays, or freeze in liq N_2.
13. Measure the total protein concentration using Bradford protein assays.
14. Set aside 40µl to measure the total protein concentration using Bradford protein assays.
15. Set up plate reader according to the protocol for COX Assay for the microplate reader.
16. Your sample should add up to 50 µl. For C2C12 cells take 40 µl of extraction buffer and add to the bottom of three wells. Then add 10 µl of the sample to each well and mix by shaking the bottom of the plate.
17. Use the multipipette to add 250 µl of test solution to the wells and quickly place the plate onto the tray of the plate reader to measure rates of oxidation.
18. For differentiated C2C12 cells you can dilute your samples by half with extraction buffer. For example, 25 µl of sample plus 25 µl of extraction buffer. Then take 10 µl of your sample to do your COX assay and use the remainder to measure protein concentration.

Chronic Contractile Activity of C2C12 Myotubes in Culture

Stimulation of muscle cells to induce CCA: Lids from plastic six-well dishes (3.5-mm wells) were fitted with two platinum wire electrodes such that 2-cm lengths ran parallel to each other at opposite ends of the dish 2 cm apart. Myotubes were subjected to electrical stimulation-induced contractile activity in a parallel circuit (4 six-well dishes at a time/protocol) at a frequency of 5 Hz and an intensity of 9 V chronically for 3 h/day over 4 successive days beginning on day 4 of differentiation, as described previously (7, 17, 18). Differentiation medium (3 ml) was replenished 1 h prior to stimulation. Following this time, custom-made lids with implanted electrodes replaced typical lids, and dishes were attached to the electrical stimulator unit. Each well was carefully inspected to ensure electrodes were submerged in the medium prior to the stimulation. Myotubes were quiescent for 21 h after each bout of contractile activity, and the medium was changed 1h prior to stimulation each day. The total stimulation protocol lasts for 4 days, and cells were collected for enzyme, protein, or RNA extractions 21 h after the fourth stimulation period. We define this treatment CCA in this cell culture model to differentiate it from the responses observed under more acute stimulation conditions.

Cells

1. C_2C_{12} murine myocytes (ATCC)

Materials

1. Electrical Stimulator
   Gange bipolar output (+ /- amplitude adjustable using one knob)

   Output voltage range = 0 to +/- 30V

   Maximum Output current = 1A

   Adjustable output pulse duration from 0.001 to 0.1 seconds (10-1 kHz)

   Adjustable output pulse repetition from 0.0005 to 0.01 seconds (100-2 kHz)

   Adjustable polarity duration range from 1 to 100 seconds (0.01 to 1 Hz)

Polarity duration range = time duration for the output "pulse burst" to be positive before switching to a similar negative (amplitude) pulse burst. Positive and negative duration are of equal value except for the amplitude.

2. 6-well sterile plastic culture dishes with modified covers for electrical stimulation (see below). Coat 6-well plates with 0.1% gelatin and leave to dry in the hood.

Procedures

1: Differentiate C2C12 Myotubes, preferably cells under 15 passages as described in the Differentiation of C2C12 cells protocol.

2: Replace media with (15mL for 10 -cm plates; 3 ml for 3.5-mm well) of fresh DM 1 hour prior to onset of stimulation. Mark condition on side of bottom plate.

3: Spray stimulator lids with ethanol and place under UV light until dry.

4: Replace lids with custom fitted wire electrode lids and attached probes making sure that each wire is fully immersed in media and lids sit flat on dishes and allow cells to equilibrate for 10 min.

5: Turn on stimulator unit to 9 V and a frequency of 5 Hz, continue stimulating for 3 hrs.

6: Once the 3 h of stimulation is complete, replace lids and media for fresh DM.

7: Wash stimulator lids with warm water, using a gentle-gloved hand to remove residue from platinum wire, perform a final rinse with dH_2O and spray with ethanol before storing for the next session.

-----Repeat previous steps for 4 days------

8: After a 21 hour recovery period, harvest the cells for the various assays.

Before each stimulation protocol, electrodes are rinsed with ddH_2O, sprayed and wiped with 70% ethanol and UV light sterilized for a minimum of 20 min.

2. Myotubes (80-90% confluence) are stimulated in a parallel circuit (up to 3 6-well dishes at a time/protocol) at 5Hz, 12V for the acute stimulation protocol and at 5Hz, 10V for the chronic or continuous stimulation protocols.

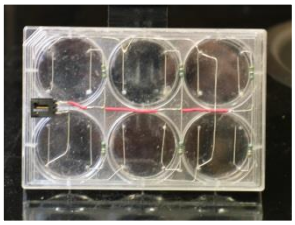

Electrical Stimulation of myocytes in culture.
(Left: picture of electrical stimulator; Right: Modified cover of a 6-well dish for stimulation)

Specifications of the Muscle Cell Stimulator on Mar 4th, 2008

Voltage

Voltage is constant and accurate in the 6-well plates. When set at 9v the true output is 8.5v.

There is a positive train and negative train consisting of 5 repetitions each at a frequency of 5Hz.

Current

The current across a 6-well plate with 3mL and 2mL of media is 37mA and 20mA respectively.

When 6 plates (3mL) are attached to the stimulator the current is 130mA.
When 5 plates (3mL) are attached to the stimulator the current is 105mA.

The current in a 10cm plate with 15mL is 7mA.

When there is more contact between the wires and the media there is more current, therefore if the wires are pushed down it makes a considerable difference than if they are up or just touching the media.

Resistance

The resistance across a 6-well plate with 3mL and 2mL of media is 12 KΩ and 350KΩ respectively (direction of measurement makes no difference, see below).

The resistance in a 10cm plate with 15mL seems to be more confusing in one direction it is 1.6MΩ and the other direction it is 700KΩ. Both of these are not constant and seem to change with time in an opposite manner… Jim says it seems to act as a semiconductor … needs to be measured again.

Cytochrome C Oxidase Assay for Microplate Reader

J. Biol. Chem. 189:665, 1951,
Meth. Biochem. Anal. 2:427, 1955,
Meth. Enzymol. 10:245, 1967.

THEORY:

Tissue extract containing cytochrome c oxidase is added to the test solution containing fully reduced cytochrome c. The rate of cytochrome c oxidation is measured over time as a reduction in absorbance at 550 nm. The reaction is carried out at 30^{o} C.

REAGENTS:

1. 20 mM KCN; MW= 65.12, 13.02 mg/10 ml dH_2O

2. 100 mM K-Phosphate Buffer

- make up 0.1 M KH_2PO_4; MW= 136.09
  = 13.6 g/1000 ml
  (pH approx. 5)
  (rm. temp)
- make up 0.1 M $K_2HPO_4.3H_2O$; MW= 174.18
  = 17.4 g/1000 ml
  (pH approx. 8)
  (rm. temp)
- mix in equal proportions, pH to 7.0

3. 10 mM K-Phosphate Buffer

- dilute 0.1 M KPO_4 Buffer prepared above 1:10 with ddH_2O (eg. 10 ml buffer + 90 ml ddH_2O)

4. Extraction Buffer (100 mM Na-K-Phosphate, 2 mM EDTA; pH 7.2)

- 500 ml 0.1 M $Na_2HPO_4.2H_2O$;

Combine 8.9 g sodium phosphate with 0.372 g EDTA up to 500 ml.

- 200 ml 0.1 M KH_2PO_4;

Combine 2.7 g potassium phosphate with 0.149 g EDTA up to 200 ml.

- combine both solutions and pH to 7.2

5. Test Solution (reduced cytochrome c, 2 mg/ml), for 10 ml (enough for 36 microplate wells);

- weigh out 20 mg of horse heart cytochrome c (Sigma, C-2506) in a scintillation vial

- add 1 ml of 10 mM KPO_4 buffer and dissolve cytochrome c

- make up a small volume of 10 mg/ml sodium dithionite-10 mM KPO_4 stock solution (make fresh each experiment and use within twenty minutes)

- add 40 μl of the dithionite stock solution to the test solution and observe red-orange colour change

- add 8 ml of ddH_2O

- add 1 ml of 100 mM KPO_4 buffer.

PROCEDURE:

1: Wash 10 cm plates 2x with chilled PBS.
2: Add 500 µl of PBS per plate and scrape with a rubber policeman. Combine supernatant from 2- 10cm plates and transfer to Eppendorf.
3: Place whole cell lysate samples in liquid N_2. Thaw in a 37°C water bath for 5 min. Repeat freeze-thaw cycle.
4: Place the Eppendorf tubes in the aluminium block on ice and Sonicate each tube 3 x 3 seconds, cleaning the probe between samples.

8. Add 200 μl of Test Solution into 4-8 wells of 96-well microplate and incubate at 30°C for 10 minutes to stabilize the temperature and absorbance.

9. Open KC4 plate reader program (on Triton). Select CONTROL icon, then PRE-

HEATING tab, enter 30°C and select ON. (Do not run assay until KC4 temperature has reached 30°C.)

10. Select WIZARD icon, then READING PARAMETERS icon.

- Select Kinetic for Reading Type.
- Select Absorbance for Reader and 550 nm for wavelength (drop-down menu).
- Select Sweep for Read Mode.
- Select 96 Well Plate (default) for Plate Type.
- Enter first and last well to be read (eg. A1 and A4 if reading 4 samples simultaneously).
- Select Yes and Pre-heating and enter 30 for Temperature Control.
- For Shaking enter 0 for both intensity and duration (shaking is not necessary and it will delay the first reading).
- Do not select either of the two options for Pre-reading.
- Click on the KINETIC… rectangular tile to open the Kinetic window.
- Enter run time (1 minute is recommended) and select MINIMUM for Interval time (under these conditions the minimum Interval time should be 3 seconds).
- Select Allow Well Zoom During Read to see data in real time (optional).
- Under Scales, checkmarks should appear for both Auto check boxes. Do not select Individual Well Auto Scaling.
- Press OK to return to Reading Parameters window. Press OK to return to Wizard window. Press OK. Do not save the protocol.

11. Set the multipipette to 250 μl and secure 4-8 yellow tips on the white projections (make sure they are on tight and all at the same height).

12. In a second, clean 96 well plate, pipette samples into 4-8 empty wells (start with A1). Recommended volumes: 30 μl of 80-fold extract for Mixed Gastroc, 10 μl for Heart. Adjust volumes according to oxidative capacity of the tissue. (eg. 25 μl for Red Gastrocnemius and 35 μl for White Gastrocnemius).

13. Remove microplate with Test Solution in 4-8 wells from the incubator (as long as it has been incubating for 10 minutes). Place this plate beside the plate with the sample extracts in it.

14. On KC4 program, select the READ icon and press the START READING icon, then press the READ PLATE button. A box will appear that says, "Insert plate and start reading". Do not press OK yet, but move the mouse so that the cursor hovers over the OK button.

15. Using the multipipette (set to 250 μl) carefully draw up the Test Solution. Make sure the volume is equal in all the pipette tips, and that no significant air bubbles have entered any of the tips.

16. Pipette the Test Solution into the wells with the sample extracts (the second plate). As soon as all the Test Solution has been expelled from the tips (do not wait for the second push from the multipipette), place the plate onto the tray of the plate reader and with the other hand on the mouse, press the OK button. (Speed at this point is paramount, as there is an unavoidable latency period between the time of pressing the OK button and the time of the first reading.)

17. If desired, add 5 μl KCN to one of the wells to measure any absorbance changes in the presence of the CYTOX inhibitor.

18. Once reading is complete, hold the CTRL key on the keyboard, and use the mouse to click once on each of the squares corresponding to a well that had sample in it. Once all the desired wells have been highlighted by a black square (up to a maximum of 8 wells), let go of the CTRL key and a large graph will appear with lines on it representing each sample.

19. To obtain the rate of change of absorbance over different time periods, select Options and enter the amount of time for which you would like a rate of change of absorbance to be calculated. The graph, along with one rate (at whichever time interval is selected) for each sample can be printed on a single sheet of paper, and the results can be saved.

20. The delta absorbance will appear in units of mOD/min and the number given will be negative. Convert this to OD/min by dividing by 1000 and omit the negative sign in the calculation. (eg. if Mean V: -394.8 mOD/mn, then use 0.395 OD/min)

CALCULATION: CYTOX activity (μmole/min/g tissue)

$$= \frac{\text{delta absorbance/min x total volume (ml) x 80 (dilution)}}{\text{18.5 (}\mu\text{mol/ml extinction coeff.) x sample vol (ml)}}$$

Example Calculation:

30 μl of 80-fold sample extract
250 μl of Test Solution
Mean V: -284.2 mOD/mn

$$\text{COX activity} = \frac{(.284)(.280)(80)}{(18.5)(.030)}$$

= 11.5 μmol/min/g tissue

= 11.5 U/g tissue

Tissue	**Heart**	**Mixed Gastroc**
Weight (mg)	5 mg	7.5 mg
Vol. for 20-fold	100 μl	150 μl
Remove, put in new Eppendorf	50 μl	75 μl
Vol. needed for 80-fold	Add 150 μl of extract. buffer	Add 225 μl of extract. buffer
Final Volume of 80-fold	200 μl	300 μl
Vol. of 80-fold per well	10 μl	30 μl

Fluorescence Microscopy

C2C12 myoblasts were plated on custom-made glass bottom 6-well dishes coated with 0.1% gelatin. Upon 80-90% confluency, C2C12 myoblasts were co-transfected with the mitoDSred and pbabe GFP-LC3 construct using Lipofectamine 2000 reagent (Life Technologies). Transfection efficiency was estimated at 40%. Following transfection, media was replaced with DM to induce differentiation. DM was replenished daily and day 4 myotubes were subject to the same CCA protocol described earlier. 21 hours post the final bout of chronic contractile activity (CCA), live-cell fluorescence microscopy was performed to visualize mitochondria and LC3. Fluorescence was visualized using an inverted Nikon Eclipse TE2000-U fluorescent microscope equipped with 100x oil objective lens, with a custom designed chamber designed to maintain a constant temperature of 37^{o}C with 5% CO_2. All images were taken at the same exposure and representative images reflect a minimum of 30 images per condition, as well as repeated experiments.

-For BafA treated myotubes. Cells were exposed to four different treatments, vehicle control, veh CCA, 3 nM BafA control, 3 nM BafA +CCA.

Materials

-pBABE GFP-LC3(Addgene) which is localized to autophagosome membranes after processing.

-pDsRed2-Mito (Clontech, CA, USA), an expression vector that encodes a fusion of red fluorescence protein and the mitochondrial targeting sequence from COX subunit VIII.

-Lipofectamine 2000 (Life Technologies, CA, USA)

- Nikon Eclipse TE2000-U fluorescent microscope equipped with 100x oil objective lens

-C2C12 cells (ATCC, Manassas, VA)

Mitochondrial Isolation from C2C12 Myotubes

REFERENCES: Frezza et al., Nature Protocols 2007; 2(2):287-95.

SOLUTIONS:
Mitochondrial Isolation Buffer (MIB) (*make fresh)

1. 10 ml of 0.1 M Tris-MOPS (store at 0-4°C)
   0.1 M Tris 6.05 g / 500 ml
   pH to 7.4 using MOPS

2. 1 ml of 0.1 M EGTA/Tris (store at 0-4°C)
   0.1 M EGTA 19.05 g / 500 ml
   pH to 7.4 using Tris

3. 20 ml of 1 M sucrose (*make fresh)
   1 M sucrose 34.33 g / 100 ml

ISOLATION PROCEDURE:

This final isolation procedure has been determined to be the optimal method for the isolation of intact mitochondria from the tissue culture of C2C12 myotubes through differential centrifugation. The entire procedure is done at 4°C (everything to be kept on ice).

1: Set out materials (get 2 buckets of ice and chill Teflon pestle and glass potter (15 ml), centrifugation tubes, 15 ml conical tube, 200 ml of MIB and PBS on ice).

2: Remove the 10 cm plates from the incubator, and wash 2x with ice-cold PBS (keep plates on ice).

3: Add ~1.5 ml of MIB per plate, and quickly and gently scrape the plates with a rubber policeman, rotate the plate 45° and re-scrape to ensure all the cells have detached. Transfer the scraped cells into chilled pre-labelled mitochondrial

isolation tube and keep on ice and cap when done. If using for mitochondrial respiration use a minimum of 10 x 10 cm plates.

---- Repeat this step for each sample ----

4: At a centrifuge setting of 600 g, with Beckman JA25.5 ROTOR, centrifuge the samples for 10 min. Discard the supernatant and Resuspend the pellet in 3 ml of ice-cold MIB.

5: Transfer the suspension into a chilled 15 ml Potter-Elvehjem. Homogenize the cells using the PTFE Tissue Grinders at 800 rpm for 35 strokes. Set timer to ensure consistency between samples.

6: Transfer the supernatant to a fresh tube and centrifuge for 10 min at 600g, transfer only the supernatant gently through a falcon tube fitted with a 45 µm filter, being careful to avoid the pellet.

7: Collect the supernatant and (contains mitochondria and cytosol) and transfer to a clean pre-chilled mitochondrial isolation tube. Quick spin at 600 g for 3 min to ensure that any remaining cellular debris is pelleted, now transfer only the supernatant to the last fresh tube.

8: Centrifuge the supernatant at 9,000 x g for 10 min. at 4°C.

9: Discard the supernatant and the resultant pellet is the mitochondria.

10: Gently Resuspend the pellet in 400 µl of MIB and transfer mitochondrial solution to a 1.5 ml Eppendorf.

11: Spin in a microcentrifuge at 9,000 x g for 10 min. at 4°C.

12: Discard the supernatant and re-suspend the mitochondria in 80-120 µl of MIB depending on mitochondrial yield. Record the final volume and perform a Bradford assay to assess total µg of mitochondrial yield.

13: Use fresh mitochondria immediately for respiration and ROS analysis.

Mitochondrial Respiration

(Muscle) Estabrook, R.W., Meth. Enzymol., **10**: 41-47 (1967)

THEORY:

The rate of mitochondrial respiration is an important consideration in the biochemical analysis of mitochondria. There are three phases of interest in analyzing the respiratory ability of mitochondria. Mitochondria produce ATP in the presence of oxygen. The respiratory ability of the freshly isolated mitochondrial fractions and the homogenates can be illustrated by measuring the rate of oxygen consumption using a Clark oxygen electrode in the presence of a) the substrate alone (e.g. glutamate for state 4 or resting respiration); b) ADP, (state 3 or active respiration); and c) $NADH^+$, which is used to measure the amount of damage that has occurred to the mitochondria, since the inner membrane is impermeable to $NADH^+$.

SOLUTIONS:

VO_2 Buffer for **muscle** mitochondria :

250 mM **Sucrose**	(FW=342.30)	42.8 g/500 ml
50 mM **KCl**	(FW=74.55)	1.86 g/500ml
25 mM	**Tris-HCl ***	1.97 g/500ml
10 M **K_2HPO_4**	(FW=174.18)	0.871 g/500ml

*In place of 25mM Tris-HCl you can use 25 mM Tris (aka Tris (hydroxymethylamine). This works out to 1.5125 g/500ml (FW=121.4). Using Tris in place of Tris-HCl means that you will have to add more HCl to get the pH down to 7.4.

Substrate for Muscle

1. **Glutamate** (MW= 147.13 g/mol) final conc. of 11.1 mM

840 mM initial conc. (123.34) mg/ml)

2. **ADP** (MW = 427.2 g/mol) - Final conc of 0.44 mM

80 mM initial conc. (34.1) mg/ml)

3. **NADH** (MW = 709.4 g/mol). Final conc.: 2.8 mM

0.5 M initial conc. (354.7 mg/ml)

Mitochondrial Respiration Procedure

1: Set water bath at 30^{o}C - clean out chambers (Clark oxygen electrode; Yellow Springs Inst. Co., Yellow Springs, OH) and stir bars.

2: Add 200 µl of VO_2 Buffer to the chamber.

3: Remove all bubbles in the chamber and allow it to reach equilibrium temperature (30^{o}C).

4: Put in 100 µl of isolated mitochondria from tissue culture and begin spinning.

5: Allow a steady state oxygen consumption to be reached.

6: Calibrate high to 100% and begin recording, allow sufficient time to calculate drift or basal respiration.

7: Add 5 µl of Glutamate (State IV).

8: Wait for slope to stabilize and add 5µl ADP (State III).

9: Finally add 5 µl of NADH. Prepare the next chamber while the respiration recordings are being made.

10: Clean out the chamber in the following manner: Remove the electrode and aspirate, remove the magnetic stir bar and aspirate, and finally, clean the electrode by rinsing with distilled water and pat dry.

11: Put electrode in the next chamber (which should already have the buffer and sample in it).

12: Prepare the next chamber while measuring the respiration of the current chamber (ie. add 2 ml of VO_2 Buffer and allow to equilibrate).

13: Calculate the state 4, state 3 and $NADH^+$ rates for each sample. Remember that the chart speed is 3 cm/sec and full scale is 100 %. (slope=rate=blocks/min)

14: Calculate the rates of state 3 and state 4 respiration per mg of mitochondrial protein by dividing the state 3 and 4 rates by the amount of protein (mg) added to the VO_2 Buffer.

Western Blot Procedure

Part A: SDS Polyacrylamide Gel Electrophoresis (SDS-PAGE) – Bio-Rad Mini Protein System

Reagents:

- Acrylamide/Bis-Acrylamide, 30% Solution 37.5:1 (BioShop 10.502)
    - Store at 4°C
- Under Tris Buffer
    - 1M Tris-HCl, pH 8.8 (60.5g/500mL)
    - Store at 4°C
- Over Tris Buffer
    - 1M Tris-HCl, pH 6.8 (12.1g/100mL)
    - Bromophenol Blue (for colour)
    - Store at 4°C
- Ammonium Persulfate (APS)
    - 10% (w/v) APS in ddH_20 (1g/10mL)
    - Store at 4°C
- Sodium Dodecyl Sulfate (SDS)
    - 10% (w/v) in ddH_20 (1g/10mL)
    - Store at room temperature
- TEMED (Sigma T-9281)
- Electrophoresis Buffer, pH 8.3 (10L)
    - 25 mM Tris 30.34g, 192mM Glycine 144g, 0.1% SDS 10g
    - Volume to 10L with ddH_20
    - Store at room temperature
- 2 x Lysis Buffer
- *tert*-Amyl alcohol ReagentPlus, 99% (Sigma 152463)

Procedure:

1. Prepare Mini-Protean gel caster system:
    a. Assemble glass plates as shown below:

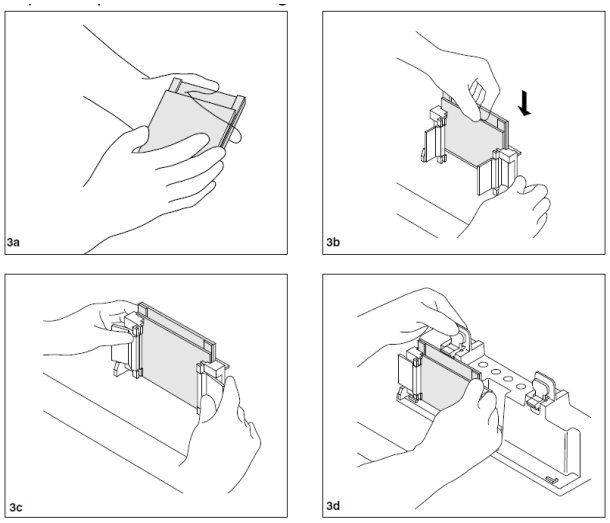

2. Prepare separating gels:

Mini Protean 3 Bio-Rad System volumes

Separating Gel	**8 %**	**10 %**	**12 %**	**15 %**	**18 %**
Acrylamide	2.7 ml	3.3 ml	4.0 ml	5.0 ml	6.0 ml
Water	4.1 ml	3.5 ml	2.8 mL	1.8 ml	0.8 ml
Under Tris	3.0 ml	3.0 ml	3.0 ml	3.0 ml	3.0 ml
SDS	100 µl	100 µl	100 µl	100 µl	100 µl
APS	100 µl	100 µl	100 µl	100 µl	100 µl
TEMED	20 µl	20 µl	20 µl	20 µl	20 µl

a. Mix the contents of the separating gel without TEMED.
b. Add TEMED. Briefly stir. Immediately, pour the contents between the short and spacing plates until the volume reaches 2 cm from the top edge of the short plate
c. Coat the top surface of the gel solution with *tert*-Amyl alcohol to remove any bubbles.
d. Allow 10 - 30 minutes for gel polymerization.
e. Remove *tert*-Amyl alcohol by pouring it off, rinse briefly with ddH20 and remove any remainder by tilting caster to the side and absorbing

fluid with a scrap piece of Whatman paper, being careful not to touch gel.

3. Prepare stacking gel:
    a. For a single mini gel use the following volumes:

Stacking Gel (3% Acrylamide)	1 Mini Gel
Acrylamide	250 µL
Water	1.875 mL
Above Tris buffer	312.5 µL
SDS	25 µL
APS	25 µL
TEMED	8 µL

    b. Mix the contents of the stacking gel without adding TEMED. Stir.
    c. Add TEMED. Stir and pour the stacking gel on top of the polymerized separating gel.
    d. Immediately, add the appropriate comb for desired number of wells and thickness of spacer plate.
    e. Allow 10 - 30 minutes for gel polymerization.
    f. Gels may be used immediately or stored in a wet sealed container at 4ºC.
4. Prepare samples:
    a. Warm block heater to 95ºC.
    b. Pipette the appropriate volume of each sample into a new Eppendorf. *This volume is determined by the protein concentration assessed using the Bradford assay and the required amount of protein required for the detection of the desired protein.*
    c. Add an equal amount of 2X Lysis Buffer supplemented with 5% B-Mercaptoethanol. Add 5 µL of Sample Dye to each sample.
    d. Briefly spin each sample to bring volume to the bottom of the eppendorf.
    e. Incubate each sample at 95ºC for 5 minutes in the heating block to denature the proteins.
    f. Briefly centrifuge again to return volume to the bottom of the Eppendorf.

5. Assemble Mini-Protean electrophoresis rack:
    a. See images below:

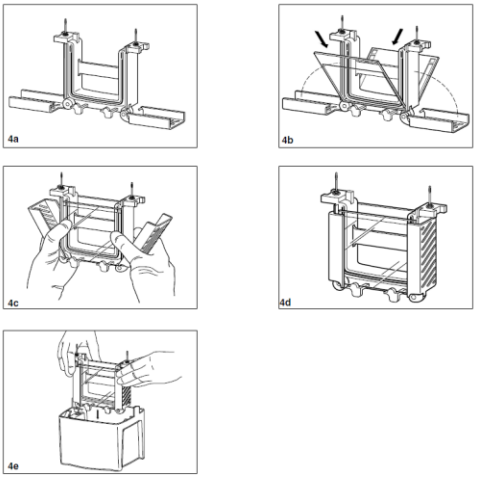

b. If you are only running one gel a plastic rectangular pseudo plate must be clamped on the other side of the caster.
c. Fill the middle chamber of the electrophoresis apparatus with Electrophoresis Buffer. Fill the outer chamber with Electrophoresis Buffer, until the level is approximately 2 cm above the bottom of the gels.
d. Slowly remove the comb using both hands (one on each side) by pulling the comb straight upwards.
e. Fix any wells that are deformed using a pipette tip.
f. Clean out the wells using a pipette tip and Electrophoresis Buffer.
g. Apply 10 μL of protein ladder to the first well.
h. Withdraw the entire volume of the sample using a gel-loading tip. Inject the solution slowly into the bottom of the well.

6. Gel Electrophoresis:
    a. After all samples are loaded, immediately, place the lid on the gel chamber.
    b. Place the positive and negative leads into the power supply.
    c. Use a power supply to apply a constant voltage of 120V across the gel for 60 – 120 minutes, until sufficient separation has been achieved as indicated by the protein ladder.
    d. Prepare for electrotransfer of proteins from the gel to nitrocellulose membrane.

Part B: Western Blotting and Immunodetection

Reagents:

- Transfer Buffer
  - 0.025M Tris-HCl pH 8.3 = 12.14g
  - 0.15M Glycine = 45.05g
  - 20% Methanol = 800mL
  - Make 4L with ddH_20
  - Store at 4°C
- Ponceau S stain
  - 0.1% (w/v) Ponceau S
  - 0.5% (v/v) Acetic Acid
  - Store at room temperature
- Wash Buffer
  - Tris-HCl pH 7.5 12g
  - NaCl 58.5g
  - 0.1% Tween 10mL
  - Store at room temperature
- Blocking Buffer
  - 5% (w/v) skim milk powder in Wash Buffer
- Enhanced Chemiluminescence Fluid (ECL; Santa Cruz - SC-2048)
- Film Developer and Fixer

Procedure:

1. Transfer Procedure
   a. Using a paper cutter and cut 6 pieces of Whatman paper per gel. Each piece should measure 8.5 cm x 6 cm. Wearing gloves cut an 8.5cm x 6 cm piece of nitrocellulose membrane (GE Healthcare RPN303D). Soak Whatman paper and nitrocellulose membrane in Transfer Buffer until use.
   b. Remove electrophoresis plates from chamber and separate the plates.
   c. Remove stacking gel
   d. Assemble Whatman paper, nitrocellulose membrane and gel as shown below, ensuring that the gel and membrane are orientated so that the gel is closer to the black surface and the membrane closer to the white plastic clamp.

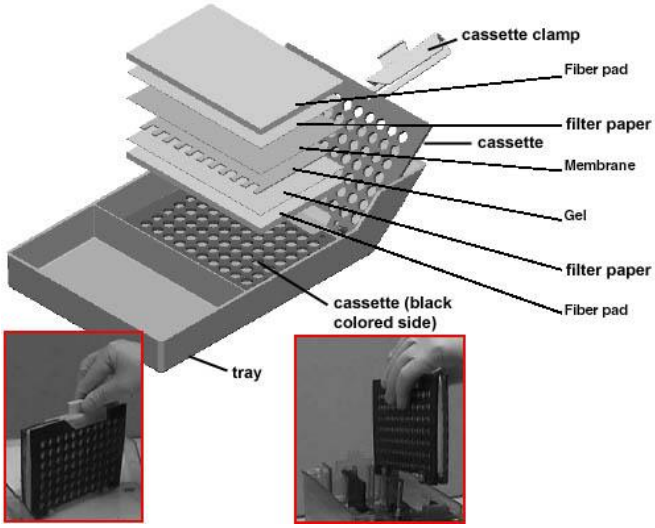

e. Close the cassette and place in the transfer chamber with the black side of the cassette facing the negative electrode (black side) of the chamber.
f. Place an ice pack and magnetic stir bar in the chamber.
g. Place the chamber in a Tupperware container. Place the container on top of a magnetic stir plate. Turn on the stir plate and ensure the magnetic stir bar is spinning.
h. Fill the chamber completely with cold Transfer Buffer. Place lid on the chamber and connect the leads to a power supply.
i. Turn on the power supply and apply a constant voltage of 120V for 1.5 hours. This can vary depending on the size of the protein of interest.

2. Removal of nitrocellulose membrane:
   a. Turn off the power supply and disconnect leads from the power supply.
   b. Remove the cassette from the chamber.
   c. While wearing gloves, carefully dispose of the Whatman paper and gel.
   d. Gently place the nitrocellulose membrane in a plastic dish and apply Ponceau S stain for 2 minutes.
   e. Drain off the remaining Ponceau S and save for reuse.
   f. Rinse the membrane with ddH_2O to reduce the red background. Wrap membrane in saran wrap and scan.
   g. Cut the membrane while protein bands are still visible at the desired molecular weight.
   h. Rotate membrane at room temperature in Wash Buffer until remaining Ponceau S stain has been removed (~5 minutes).
   i. Incubate membrane for 1 hour with rotation in Blocking Buffer at room temperature.

3. Immunodetection
    a. Primary Antibody Incubation
        i. Wrap a flat piece of glass in parafilm. Place the glass in a Pyrex dish. Arrange balls of wet tissue around the dish and cover the entire dish with saran wrap.
        ii. Place the dish in a 4ºC fridge and level.
        iii. Place nitrocellulose membrane strips face up on the flat parafilm surface.
        iv. Dilute the primary antibody raised against the protein of interest in Blocking Buffer. Gently apply ~1-1.5 mL of diluted antibody overtop of the appropriate membrane strip.
    b. Secondary Antibody Incubation
        i. Wash the blots in Wash Buffer with gentle rotation for 5 minutes 3X.
        ii. Incubate the blots as described in step 3.a with the following changes. Incubate the blots for 1 hour with a secondary antibody raised against the species and specific immunoglobulin molecule of the primary antibody. Incubate at room temperature.
    c. Following the incubation, wash the membrane 3X for 5 minutes with Wash Buffer.
4. Enhanced Chemiluminescence Detection

    Note: Complete the following steps in a dark room sufficient for photographic film developing.
    a. Mix ECL fluids "A" and "B" in a 1:1 ratio in small beaker.
    b. Lightly dab off excess moisture by gently laying blot on a clean kim wipe and place blots face up onto plastic wrap surface, tape edges of plastic wrap to ensure smooth working surface. Apply ECL to top surface of blots using a p1000 pipette.
    c. Following 2 minutes, remove blots and lightly dab on clean Kim wipes to remove excess ECL fluid.
    d. Place membrane strips on clean overhead transparency film and remove any bubbles.
    e. Turn off any lights.
    f. Place membrane strips face up in a film cassette and secure with tape.
    g. Prepare the film and apply film overtop of the membrane strips. Do not move the film once it has been placed on top of the membrane.
    h. Close the cassette and expose the film for the desired time.
    i. After a 30 sec exposure time, proceed to step j., use this initial exposure to gauge length required for subsequent exposures.
    j. Attach the film to a film hanger and immerse in the film developing solution for 8 seconds.

k. Hold the film up to a red light briefly, and re-submerse in developer if necessary. When bands become apparent, immediately submerge the film in water and then in the film fixing solution for a minimum of 15 seconds.
l. Following a minimum of 15 seconds in the fixing solution, the film can then be submerged in water and attached to butterfly binder clips to dry. They are no longer light sensitive.

RNA Isolation and qPCR

Reagents:

- TRIZol® Reagent
- 24:1 Chloroform:Isoamylalcohol
    - 24 parts Chlorofom
    - 1 part Isoamylalcohol
- 100% Isopropanol
- 75% Ethanol
- DEPC ddH_2O

Procedure:

5. Cell Culture:
    a. Grow cells in 10cm dish
    b. Pour off the medium. Wash each plate with 5mL of ice-cold Phosphate Buffered Saline (PBS), remove all of the PBS.
    c. Add 400 µl of PBS to plate and gently scrape with a rubber policeman.
    d. Transfer to Eppendorf.
    e. Centrifuge the cells at 14000 rpm for 3 min. Remove all supernate. Resuspend in 2 mL of PBS.
    f. Centrifuge the cells at for 3 min at 14000 rpm in a microcentrifuge. Discard the supernate with a Pasteur pipette.
6. RNA Isolation
    a. Add 1ml TRIZOL. Vortex thoroughly until pellet is completely disrupted.
    b. Add 200 µL of 24:1 chloroform:isoamlyalcohol.
    c. Shake vigorously for 15 seconds and leave @ room temperature for 5 minutes.
    d. Centrifuge at 14000 rpm for 15 minutes at 4^oC.
    e. Transfer the upper phase carefully to a new Eppendorf tube. Add 500 µL of 100% isopropanol and briefly shake.
    f. Incubate at room temperature for 30 minutes.
    g. Spin at 14000 rpm for 10 minutes at 4^oC.
    h. Remove supernatant. Add 500 µL of 75% EtOH and wash the RNA pellet with gentle pipetting.
    i. Centrifuge at 14000 rpm for 1 minute at 4^oC.
    j. Carefully, remove supernatant and air dry the RNA pellet.
    k. Resuspend the pellet in 50 µL of DEPC ddH_2O.
    l. Heat RNA samples at 65^oC for 10 minutes.
7. Quantify RNA
    a. Use a spectrophotometer to measure the absorbance at 260 nm.

b. Freeze and store at -80^{o}C.

Part C: Reverse Transcriptase

Reagents:

- Oligo(dt) 20
- 10 mM dNTP
- DEPC ddH_2O
- Master Mix (per sample)
    - 8 µL of 5x Buffer
    - 2 µL of 0.1 M Dithiothreitol (DTT)
    - 2 µL of RNAse Out
- Superscript III

Procedure:

8. Combine 2 µL of Oligo(dt) 20, 2 µL of 10 mM dNTP, and 4 µg of Sample RNA in a sterile 0.5 mL sterile Eppendorf. Bring the volume to 26 µL with DEPC ddH_2O.
9. Heat the Eppendorf at 65ºC for 5 minutes, followed by 1 minute at 4ºC in a thermocycler.
10. Make the Master Mix.
11. After the Eppendorfs have been heated, add 12 µL of the Master Mix and 2 µL of Supercript III RT.
12. Incubate the Eppendorf for 50 minutes at 55ºC, followed by 15 minutes at 70ºC.
13. Store samples at -20ºC.

Part D: Quantitative Polymerase Chain Reaction (qPCR) Procedure

Reagents:

- DEPC ddtH2O
- Master Mix (per sample and per gene of interest)
    - 12.5 µL of PerfeCTa® SYBR® Green SuperMix with ROX™
    - 2.5 µL of 20 µM Forward Primer
    - 2.5 µL of 20 µM Reverse Primer
    - 5.5 µL of DEPC ddH_2O

Procedure:

14. Biochemical Assay
    a. Autoclave qPCR microtube strips and pipette tips. Sterilize pipettes with EtOH for use.

b. Dilute cDNA samples 1:20 with DEPC ddH_2O.
c.

Create appropriate Master Mixes as determined during optimization. Always use a housekeeping gene to correct for difference in total cDNA amount.

d. Add 2 µL of each diluted cDNA sample in triplicate to microtube strips.
e. Add 23 µL of Master Mix to all wells.
f. Close wells and place in Applied Biosystems StepOne Plus qPCR machine.
g. Set the StepOne Plus application for a reaction volume of 25 µL, SYBR® Green Technology, Normal (~2.5 hour) Reaction Speed, and Include a Melt Curve Analysis.

15. ΔΔCt Analysis
    a. After the run is complete. Confirm that the automatically determined thresholds are in the exponential amplification phase for each gene of interest. Export all data to an Excel spread sheet.
    b. Obtain the cycle number where the sample's amplification plot crosses the defined threshold (i.e. the Ct value).
    c. Average the two closest Ct values.
    d. To determine the ΔCt take the difference between the Ct value of the gene of interest and the Ct value of your housekeeping gene. Raise this to the power of two (i.e. $2^{\Delta Ct}$) and use this to compare differences in gene expression.
    e. To determine find the fold change in the gene expression from your control samples take the ΔCt of each sample and subtract the ΔCt of the control sample. Use these values (ΔΔCt) to generate a graph of gene expression relative to your control condition

ROS Production from Isolated Mitochondria

Background: Mitochondria are the primary source of reactive oxygen species (ROS) to the cell. It is estimated that about 2% of total cellular oxygen is converted to ROS by the inappropriate reduction of molecular oxygen by intermediate members of the electron transport chain (ETC). ROS are damaging molecules that are capable of compromising the integrity of macromolecules within the mitochondria and may lead to overall organelle dysfunction. In particular, mtDNA may be prone to attack by ROS because 1) mtDNA is located in close proximity to the ETC, 2) mtDNA lacks the protective sheath of histones compared to nuclear DNA and, 3) mitochondria have an insufficient repair system for mtDNA mutations. ROS can exist in a variety of molecular permutations such as superoxide (O_2^-), hydroxyl radical (OH^-) and hydrogen peroxide (H_2O_2).

DCF (2,7,-dichloro-fluorescein; Fig.1) is a reagent that is non-fluorescent until the acetate groups are removed by intracellular esterases and oxidation occurs within the mitochondria (Fig.1). DCF is oxidized by all of the different forms of ROS and this can be detected by monitoring the increase in fluorescence with a fluorometric plate reader. The appropriate plate reader filter settings for fluorescein are the following: **Excitation 485/20 and Emission 528/20** (Fig.2).

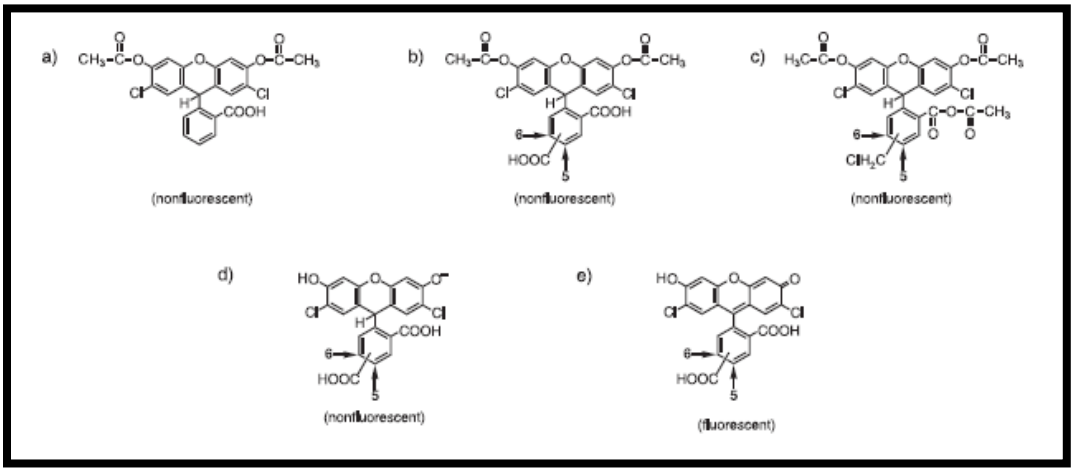

Fig.1-DCF molecule and oxidation of DCF resulting in fluorescence

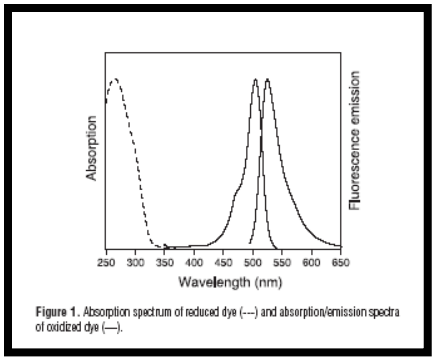

Fig.2-Absorption and Emission Spectra of oxidized dye

KC4 Software Settings: The Settings icon in the upper left corner allows the alteration of various parameters. Once clicked, another window appears, click on the Wizard Icon. In this window there will be a variety of components that can be altered. The following are the parameters that need to be changed in order to utilize the DCF and measure time-dependent ROS production from isolated mitochondria:

1) Top Middle Panel- Absorbance, Fluorescence, Luminescence- choose **Fluorescence**

2) Top Left Panel- End Point, Kinetic, Spectrum- choose **Kinetic**

3) Top Middle Panel- Click on larger box labeled Kinetic to set parameters- **Run Time 1:20:00, Interval 5:00 (takes a measure every 5 minutes),** click on box labeled **Allow Well Zoom during Read,** and also click on box labeled **Individual Well Auto Scaling**- The Well Zoom and Auto scaling allows for monitoring each individual well during the experiment and scales it appropriately.

4) Middle Panel-***Filter Set***- Choose #1, then set the **excitation to 485/20**, and **emission to 528/20** as described above. The optics position should be set to the **TOP** (i.e. readings are taken from the top of the well) and the sensitivity is set at **50** (depending upon the amount and/or nature of the sample).

5) Plate-Type-choose **96-well plate**, choose which wells are to be read i.e. **A1-C12.**

6) Shaking-**Intensity** set at **1, Duration** set at **15s** and then click the box that is labeled **before every reading** (it shakes the samples for 15 s before every reading).

7) Temperature Control- Click on the box indicating **YES ,** also click on box labeled pre-heating, and put 37°C into the temperature box.

DCF Reagent and VO_2 Buffer

DCF (2,7,-dichlorodihydrofluorescein diacetate) reagent MW=487.29 (Molecular Probes D-399/ 100mg)

1°STOCK- Make up **50mM** Stock Solution in EtOH- 24 mg/ml- only make about 500µl i.e. 14 mg per 500µl EtOH. Wrap stock solution in aluminum foil and limit exposure to light since DCF is light-sensitive.

Working Stock Solution-2° STOCK- Dilute 50mM by 100-fold by taking 10µl and adding 990 µl of EtOH to attain a **500uM DCF Stock Solution**. This will be the DCF concentration used to add to the reaction mixture.

VO_2 Buffer- refer to mitochondrial respiration protocol

Procedure

1. Mitochondria are isolated as described in the mitochondrial isolation protocol. Alternatively, frozen mitochondrial extracts can also be used.

2. Determine the volume necessary for 50µg of mitochondria. Typical volumes should range between 5-40µl depending upon concentration of mitochondrial extracts.

3. Final concentration of DCF is 50uM. The total volume of the reaction mixture is 250µl. Thus, 25µl of DCF is used in the reaction mixture since this represents a 10-fold dilution. Set up table (***as shown below***) and determine the amount of VO_2 buffer necessary to make each of the reaction mixtures equal to 250 µl. (Remember to include a ***control*** with only VO2 buffer and DCF reagent as in Well #1 shown below)

	SS			
	Control	Mar.23	Mar.25	Mar.29
	Well #1	Well #2	Well #3	Well #4
µg mito	0	50	50	50
µl mito	0.00	11.77	9.80	17.24
VO2 Buff	225.00	213.23	215.20	207.76
DCF (50uM)	25	25	25	25
Total Volume	250	250	250	250

4. Once table is complete and volumes for all samples have been determined, place the frozen (already thawed) or fresh mitochondria, VO_2 buffer and DCF (500uM) into a 37°C circulating water bath for 5-10 min.

5. Pipette the volume of VO_2 buffer required for each of the samples followed by the mitochondrial samples into the appropriate wells of a 96-well plate. In addition, include a well (usually in the corner well) with only 250 µl of VO_2 buffer to monitor temperature (see below). Place the 96-well plate with the VO_2 buffer and mitochondria into a 37°C incubator. Using the YSI temperature probe, place the recording electrode into the well with buffer only and monitor the temperature until 37°C is reached. During this time, be sure that the KC4 software is set up and that the Biotek plate reader is pre-heating to 37°C.

6. Once mitochondria and buffer have reached temperature (37°C), take the DCF out of the circulating water bath (37°C) and quickly add the DCF to each of the reaction mixtures. Following addition of DCF, promptly place the plate into the Biotek plate reader for fluorescence measurement and start the KC4 program by pressing **READ** plate on the upper left portion of the computer screen. Kinetic program will operate for 1 h and 20 min.

Appendix D: Other Contributions to the Literature

Published Abstracts

1. **A. Parousis**, D. A. Hood, Mitophagy in Skeletal Muscle Cells. *Proc. Muscle Health Awareness Day* **4**, 16 (2013).

Oral Presentations

1. **A. Parousis**, D. A. Hood, Regulators of Mitochondrial Dynamics in Muscle Development and Chronic Contractile Activity. *KAHS Graduate Student Seminar, York University, Toronto, ON (2012).*